



REPUBLIC OF IRAQ  
MINISTRY OF HIGHER EDUCATION AND  
SCIENTIFIC RESEARCH  
AL-FURAT AL-AWSAT TECHNICAL  
UNIVERSITY ENGINEERING TECHNICAL  
COLLEGE - NAJAF

NEW APPROACH OF HIGH-POWER RF  
ENERGY HARVESTING SYSTEM BASED ON  
BEAMFORMING TECHNIQUE

SARAH MOHAMMAD ALIWI

(M. Sc. In Communications Techniques Eng.)

2021





**NEW APPROACH OF HIGH-POWER RF ENERGY HARVESTING  
SYSTEM BASED ON BEAMFORMING TECHNIQUE**

**THESIS  
SUBMITTED TO COMMUNICATION TECHNIQUES  
ENGINEERING DEPARTMENT  
IN PARTIAL FULFILLMENT OF THE REQUIREMENTS FOR  
THE TECHNICAL MASTER DEGREE  
IN  
COMMUNICATION ENGINEERING**

By

**SARAH MOHAMMAD ALIWI**

Supervised by

Asst. Prof. Dr. Hayder Jawad Mohammad

2021

## SUPERVISOR CERTIFICATION

I certify that this thesis titled "**New Approach of High-Power RF Energy Harvesting System Based on Beamforming Technique**" which is being submitted by **Sarah Mohammad Aliwi** was prepared under my supervision at the Communication Techniques Engineering Department, Engineering Technical College-Najaf, AL-Furat Al-Awsat Technical University, as partial fulfillment of the requirements for the degree of Master of Technical in Communication Engineering.

Signature:

Name :**Asst. Prof. Dr. Hayder J. Mohammad**

(Supervisor)

Date:    /    / 2021

In view of the available recommendation, I forward this thesis for debate by the examining committee.

Signature:

Name: **Prof. Dr. Ahmad T. Abdulsadda**

(Head of comm. Tech. Eng. Dept.)

Date:    /    / 2021

## COMMITTEE REPORT

We certify that we have read this thesis titled "**New Approach of High-Power RF Energy Harvesting System Based on Beamforming Technique**" which is being submitted by **Sarah Mohammad Aliwi** and as examining Committee, examined the student in its contents. In our opinion, the thesis is adequate for award of degree of Master.

Signature:

Name:

**Asst. Prof. Dr. Hayder J. Mohammad**

(Supervisor)

Date:    /    / 2021

Signature:

Name:

**Dr. Salim Muhsin Wadi**

(Member)

Date:    /    / 2021

Signature:

Name:

**Asst. Prof. Dr. Ahmed A. Abdullah**

(Member)

Date:    /    / 2021

Signature:

Name:

**Prof. Laith A. Abdulrahim**

(Chairman)

Date:    /    / 2021

### Approval of the Technical Engineering Collage

Signature:

Name: **Asst. Prof. Dr. Hassanain Ghani**

Dean of Technical Engineering Collage

Date:    /    / 2021

## LINGUISTIC CERTIFICATION

This is to certify that this thesis entitled "**New Approach of High-Power RF Energy Harvesting System Based on Beamforming Technique**" was reviewed linguistically. Its language was amended to meet the style of the English language.

Signature:

Name: **Shubbar A. Mousa**

Date:    /    / 2021

## ABSTRACT

Increasing a number of the electronic devices connected to the internet or ones that will be connected in the future impose restriction and challenge, which is how to power all these devices. An energy harvesting system is a promising technique to achieve battery-less devices, which means enabling devices to be more compact when removing the necessity of batteries that must be periodically maintained or replaced. Ambient RF energy harvesting is based on scavenging the energy from environmental (external) RF sources. With this type of the energy, the power density in space is very low, and the energy source location is unknown. These two challenges have to be taken into account. Firstly, this thesis is focused on solving the RF power source location and orientation issue. The multibeam RF (i.e., sort of beamforming) networks (BFNs) are adopted to cover most directions in space, while antennas with circular polarization capabilities are utilized to defeat orientations of the RF power sources. Using several RF energy harvesters in a form of an array called rectenna array is the solution for the second challenge. This increases an amount of the power delivered to each single rectifier, where problems of the nonlinearity will dominate the scene. The author has solved this problem by using the impedance compression network ICN. Rectifiers with ICNs are designed, analyzed, and optimized utilizing the particle swarm optimization PSO algorithm. The proposed rectifier deals with a range of the RF input power and variable load resistance at a resonance frequency of 2.4 GHz. To collect the DC powers from output antenna ports, there are many ways to do so such as DC, RF, Hybrid (RF/DC), and BFN/DC power combining techniques. Each combining technique offers several benefits over others.

## ACKNOWLEDGMENTS

First of all, my thanks and appreciation to my supervisor **Asst. Prof. Dr. Hayder Jawad Mohammad**. Many special thanks and gratitude for **Dr. Nasr Nomas Al-Khafaji** for his valuable guidance, advice, and timely care extended to me during my research period. I am able to successfully complete this research work, and are due deliver this thesis because of their immense patience and constructive feedback.

Many thanks and love to my parents and brothers.

## DECLARATION

I hereby declare that the thesis is my original work except for quotations and citations which have been duly acknowledged.

Date:    /    / 2021

Sarah Mohammad Aliwi

## TABLE OF CONTENTS

<b>SUPERVISOR CERTIFICATION</b>	ii
<b>COMMITTEE REPORT</b>	iii
<b>LINGUISTIC CERTIFICATION</b>	iv
<b>ABSTRACT</b>	v
<b>ACKNOWLEDGMENTS</b>	vi
<b>DECLARATION</b>	vii
<b>LIST OF TABLES</b>	x
<b>LIST OF FIGURES</b>	xiii
<b>LIST OF ABBREVIATIONS</b>	xiv
<b>LIST OF SYMBOLS</b>	xvi
<b>1 GENERAL INTRODUCTION AND LITERATURE REVIEW</b>	<b>1</b>
1.1 Wireless Power Transfer (WPT)	1
1.2 Wireless Energy Harvesting (WEH)	4
1.3 Challenges	8
1.4 Literature Review	8
1.5 Contributions	14
1.6 Organization of Thesis	15
<b>2 THEORETICAL BACKGROUND</b>	<b>16</b>
2.1 RF Energy Harvesting System (RFEH)	16
2.2 Capture Power	17
2.3 Patch Antenna	18
2.3.1 Analysis Square Patch Antenna	19
2.3.2 Circular Polarization	21
2.4 Beam-Forming Network for Energy Harvesting	23
2.4.1 Butler Matrix Structure	23
2.5 Rectifier Circuit and its Principle	26
2.6 Compression networks	27
2.7 Particle Swarm Optimization Algorithm	28
<b>3 ANTENNA ARRAY DESIGN FOR RF ENERGY HARVESTING</b>	<b>31</b>
3.1 Overview	31
3.2 Single Square Patch Antenna Design and Simulation Results	31
3.3 Linear Array Patch Antenna Design and Simulation Results	35
3.4 Simulation and Results for 4X4 Butler Matrix Design	42
3.5 Multi-Beams Antenna Simulation and Results	50
<b>4 RECTIFIER CIRCUIT FOR RF ENERGY HARVESTING</b>	<b>56</b>
4.1 Introduction	56

4.2	Rectifier Selection	56
4.2.1	Diode Selection	57
4.2.2	Diode Topology Selection	61
4.2.3	Mathematical Model for the Voltage Doubler Diode	63
4.3	Matching Circuit	68
4.3.1	Single Branch Impedance Compression Network	68
4.3.2	Mathematical Model for the Single Branch Impedance Compression Network	70
4.4	Implementation of the Single Branch Rectifier Based on ICN	72
4.4.1	Rectifier Design	74
4.4.2	The Proposed ICN Design	74
4.5	Implementation and Results for ICN Optimized by the Particle Swarm Optimization Algorithm	79
<b>5</b>	<b>RECTENNA ARRAY DESIGN FOR RF ENERGY HARVESTING</b>	<b>84</b>
5.1	Overview	84
5.2	DC Power Combining System	86
5.3	RF Power Combining System	87
5.4	Hybrid Power Combining System	89
5.5	BFN/DC Power Combining System	90
5.5.1	Simulation for the Multi-Beam/Multi-Output rectenna	90
5.5.2	Simulation for the Multi-Beam DC Combining System	94
5.6	A comparison between Power Combining Techniques	97
5.7	Discussion the Results of the Effectiveness of the PSO Algorithm in the Rectenna Array Design	100
5.8	A Comparison between Circular and Linear polarization Rectenna Array Design	102
5.9	Related Work	103
<b>6</b>	<b>CONCLUSION AND FUTURE WORK</b>	<b>107</b>
6.1	Conclusion	107
6.2	Future Work	109
	<b>BIBLIOGRAPHY</b>	<b>110</b>
	<b>APPENDIX-A</b>	<b>119</b>
	<b>APPENDIX-B</b>	<b>121</b>
	<b>APPENDIX-C</b>	<b>122</b>
	<b>LIST OF PUBLICATIONS</b>	<b>126</b>

## LIST OF TABLES

1.1	Historical trends in WPT	2
1.2	Comparison of energy sources and harvesting methods,[7]	4
3.1	Calculation and simulation dimensions for the square patch microstripe antenna.	32
3.2	The progressive phase difference and scan beam angle for output ports.	49
3.3	The Comparison of the proposed antenna array single beam and some related designs	55
4.1	A parameters of Schottky diode HSMS-28XX	59
4.2	Dimensions of the proposed rectifier, unit:mm	73
4.3	PSO parameters	81
4.4	The Comparison of the proposed rectifier and some related designs	83
5.1	The Comparison of the proposed rectenna and some related designs	104

## LIST OF FIGURES

1.1	Some feasible applications on wireless power transfer technique	3
1.2	Input power density measured vs frequency [8]	7
1.3	Prototype hardware demonstration of the power over WiFi (PoWiFi) [9]	7
1.4	Sensor update rate [9]	8
1.5	The conventional schematic for compression network	13
2.1	Block diagram of Rectenna model	17
2.2	Microstrip antennas and their feeds	19
2.3	Design of square microstrip patch antenna	21
2.4	Polarization types, rotation of a plane electromagnetic wave [43]	22
2.5	The architecture of a conventional 4 X 4 butler matrix	24
2.6	The architecture of a Hybrid branch-line coupler [46]	25
2.7	I-V (current VS voltage) characteristic curve of Schottky diode	27
2.8	Flow chart of the PSO algorithm	29
3.1	Design of square microstrip patch antenna with truncated corner	32
3.2	Simulated results for a single element square patch antenna	33
3.3	simulated axial ratio	33
3.4	Simulated gain for a single element square patch antenna	34
3.5	Radiation efficiency for single element	34
3.6	The gain of radiation pattern (red line LHCP , blue line RHCP)	35
3.7	The simulated radiation pattern for antenna, radiate at Z direction	35
3.8	Simulated animation results for a single element square patch antenna	36
3.9	A linear patch antenna configuration [52]	36
3.10	A linear patch antenna configuration	37
3.11	The simulated S11 for the linear patch antenna	38
3.12	Simulated results for square patch antenna array	38
3.13	Simulated animation results for square patch antenna array	39
3.14	Simulated axial ratio	39
3.15	The gain of radiation pattern for antenna array (red line LHCP , green line RHCP)	40
3.16	Simulated gain for square patch antenna array	41
3.17	The simulated radiation pattern for antenna, radiate at Z direction	41
3.18	Radiation efficiency for single element	42
3.19	The butler matrix designed designed as a conventional geometry of butler matrix	42
3.20	The optimized butler matrix designed	43
3.21	The Hybrid branch-line coupler designed	44
3.22	Simulated results for the hybrid branch-line coupler designed	44

3.23	The crossover designed	45
3.24	The insertion loss and isolation loss for crossover designed when excite	45
3.25	The insertion loss and isolation loss for a butler matrix designed	46
3.26	The output phases for butler matrix designed	47
3.27	Output power simulated for port1(Red, solid line), port2(Blue, dash line), port3 (Pink, dot dash line), port4 (Yellow, long dash line)	48
3.28	The simulation result for a butler matrix configuration designed in various case for excitation	50
3.29	Multi-beams antenna designed	51
3.30	Simulated results for a multi-beams antenna	52
3.31	The 3D gain pattern simulated at 2.4GHz	52
3.32	The simulated radiation pattern for incorporating design (BFN and antenna) at two plane, solid line for yz plane and dash line for xz plane.	53
3.33	The simulated radiation pattern for incorporating design (BFN and antenna) cuts in main lobe at perpendicular plane	54
3.34	The simulated total gain in dB as function of theta for two case BFN and antenna design and only antenna array design	54
4.1	Schottky diode chip with the equivalent circuit at high frequency	58
4.2	Schematic of the simulation diode in SPICE model at ADS software	59
4.3	The simulation results show some types of diodes	60
4.4	Various RF energy harvesting rectifier topologies	61
4.5	Schematic of the three methods of topologies by using HSMS-286X diode	62
4.6	The comparison between output DC voltage for three methods of topologies by using HSMS-286X diode	62
4.7	The optimization tool in ADS software	63
4.8	Rectifier equivalent circuit	63
4.9	Time domain waveform of output voltage across diodes	65
4.10	Comparison between simulation and calculation results of voltage doubler rectifier	67
4.11	Schematic of single branch impedance compression network (ICN) proposed for RF energy harvesting system	69
4.12	Simulated impedances of the ICN at three reference planes as a function of the wide input range, on the Smith chart	70
4.13	Equivalent circuit design for signal branch impedance compression network	71
4.14	The variation range of input impedance of diode impedance comparing with mathematical compressed impedance results after utilized of single branch ICN proposed	72
4.15	The whole proposed rectifier circuit based on the ICN	73
4.16	Configuration of the single branch rectifier based on (ICN)	73
4.17	Input impedance variations with and without ICN	75
4.18	Comparison of the rectifier efficiency with and without using the proposed ICN	76
4.19	Input impedance as a function of load and frequency for the proposed rectifier circuit	76

4.20	The simulated S11 for rectifier circuit	77
4.21	The simulated output DC voltage versus the variable input power and load	78
4.22	RF-DC conversion efficiency	79
4.23	PSO algorithm impelmention results	80
4.24	Enhanced results by using PSO algorithm	82
4.25	Configuration of rectifier based on single branch (ICN) optimized by using PSO	82
5.1	The combination power methods	85
5.2	The schematic of the rectenna design employing the DC power combining technique	87
5.3	The simulated results (output1(Red, solid line), output2(Blue, dot dot line), output3 (Pink, dot dash line), output4 (Yellow, long dash line), the single output(black, dot line) )	88
5.4	The schematic of the rectenna design employing the RF power combining technique	89
5.5	The simulated results for the RF power combining system	90
5.6	The schematic geometry for rectenna design by the Hybrid power combining	91
5.7	The simulated results for the hybrid power combining system	92
5.8	The simulated results (port1(Red, solid line), port2(Blue, dash line), port3 (Pink, dot dash line), port4 (Yellow, long dash line)) related to antenna scan angle	93
5.9	The simulated results (port1(Red, solid line), port2(Blue, dash line), port3 (Pink, solid line with star symbol), port4 (Yellow, solid line with circle symbol))	94
5.10	The 3D simulation results for BFN and DC combining compact	94
5.11	The schematic geometry for rectenna design by the BFN and DC combining	95
5.12	The simulated results for rectenna with hybrid combining system	96
5.13	The 3D simulation results for rectenna designed explain the rectification efficiency as a function of Theta angle	97
5.14	The simulated results for (DC combining system (Red, solid line), BFN/DC combining system (Blue, dot dot line), for RF combining system (Pink, short dash dot line ), Hybrid combining system (Yellow, long line))	98
5.15	The simulated results for rectenna designed with (Blue, long dash line) and without(Red, solid line) PSO algorithm	101
5.16	The 3D simulation results for rectenna designed RF power (mW) VS mismatch polarization angle (deg) VS DC power (mW)	103

## LIST OF ABBREVIATIONS

Abbreviation	Description
<i>AC</i>	Alternating Current
<i>ADS</i>	Advanced Design System
<i>AM</i>	Amplitude Modulation
<i>AR</i>	Axial Ratio
<i>BFN</i>	Beam Forming Network
<i>BM</i>	Butler Matrix
<i>CDMA</i>	Code Division Multiple Access
<i>CP</i>	Circular Polarization
<i>DC</i>	Direct Current
<i>DE</i>	Differential Evolution
<i>DTV</i>	Digital Television
<i>EH</i>	Energy Harvesting
<i>EM</i>	Electromagnetic Wave
<i>EV</i>	Electrical Vehicle
<i>FM</i>	Frequency Modulation
<i>G</i>	Gain
<i>GA</i>	Genetic algorithm
<i>GSM</i>	Global System Mobile
<i>HB</i>	Harmonic Balanced
<i>HBLC</i>	Hybrid Branch Line Coupler
<i>HFSS</i>	High Frequency EM Simulation Software
<i>HPBW</i>	Half Power Beam Width
<i>HSMS</i>	Hewlett-Packard Surface Mount Schottky
<i>ICN</i>	Impedance Compression Network
<i>IICN</i>	Integrated Impedance Compression Network
<i>IoT</i>	Internet of Things
<i>LHCP</i>	Left Hand Circular Polarization
<i>LPF</i>	Low Pass Filter
<i>LSSP</i>	large-signal S-parameter
<i>LTE</i>	Long Term Evolution
<i>MPT</i>	Microwave Power Transfer
<i>PoWiFi</i>	Power over WiFi
<i>PSO</i>	Particle Swarm Optimization
<i>RCN</i>	Resistance Compression Network
<i>RF</i>	Radio Frequency
<i>RFEH</i>	Radio Frequency Energy Harvesting
<i>RFID</i>	Radio Frequency Identification
<i>RHCP</i>	Right Hand Circular Polarization
<i>RLC</i>	Resistor Inductor Capacitor circuits

## LIST OF ABBREVIATIONS

<b>Abbreviation</b>	<b>Description</b>
<i>SHM</i>	Structural Health Monitoring
<i>SP</i>	Scattering Parameter
<i>SPS</i>	Solar Power Satellite
<i>UMTS</i>	Universal Mobile Telecommunications System
<i>VSWR</i>	Voltage Standing Wave Ratio
<i>WEH</i>	Wireless Energy Harvesting
<i>WPC</i>	Wireless Power Consortium
<i>WPT</i>	Wireless Power Transfer
<i>WSN</i>	Wireless Sensor Network

## LIST OF SYMBOLS

Symbol	Definition
$\epsilon_r$	Relative Permittivity
$\lambda$	Wavelength
$\phi$	Phase delay
$\Gamma$	Reflection Coefficient
$\eta$	Efficiency
$\eta_{rad}$	Radiation Efficiency
$\epsilon_{eff}$	Effective Relative Permittivity
<i>angle</i>	Scan angle
$A_e$	Effective Capture Area
$A_s$	Scattering Area
$AF$	Array Factor
$A_L$	Loss Area
$b_v$	Breakdown Voltage
$C_j$	Junction Capacitance
$I_D$	Diode Current
$I_s$	Saturation Current
$n$	Diode Quality Factor
$ph$	progressive angle
$P_o$	DC output Power
$P_l$	Power loss
$P_{in}$	RF input Power
$S_{11}$	Reflection Coefficient
$R_L$	Load Resistance
$R_s$	Series Resistance
$V_D$	Diode Voltage
$V_f$	Forward Voltage
$V_{br}$	Breakdown Voltage
$V_j$	Junction Voltage
$V_T$	Thermal Voltage
$Z_D$	Diode Impedance
$Z_a$	Antenna Impedance
$Z_o$	Reference Impedance
$Z_{in}$	Input Impedance

# CHAPTER 1

## GENERAL INTRODUCTION AND LITERATURE

### REVIEW

#### 1.1 Wireless Power Transfer (WPT)

Wireless power transfer (WPT) systems have attracted great attention recently where transmission of the electrical energy across space to the receiver devices without using wires (wireless link) becomes fact. The adoption of WPT technology as a substitution employs power electronic devices with self-sustaining energy, thus eliminating the need for batteries from billions or trillions of devices. Accordingly, many benefits can be obtained, such as compact design, low cost, less pollution devices, etc.

In the late 19th century, Nikola Tesla's experiments discovered the short-range transmission of the power between induction coils using inductive and capacitive coupling. Tesla had been enthused to distribute power wirelessly over huge distances, in which relatively high frequency "KHz" had been utilized. Also, he succeeded to generate hundreds of kilowatts [1]. Tesla's experiment had made a lot of inventors, investors, and researchers to think about how to leverage from the electromagnetic to transfer and distribute the power. Since then, the WPT idea was a hot research topic although no commercial work appeared until our current day. Table 1.1 summarizes the most important trends in the WPT technique development [2].

Table 1.1: Historical trends in WPT

Person	Year	Contribution
James C. Maxwell	1860	formulate the first theoretical basis of WPT
John H. Poyntig	1884	describe the energy flux of an EM field
Nikola Tesla	1890	first WPT experiment
William C. Brown	1963	the first microwave power transfer (MPT) system
William C. Brown	1964	rectenna, microwave powered helicopter

In the recent years, the WPT technology has been used in various applications, where several types of energy sources have been exploited. For instance, solar energy coming from Sun light has been converted into the DC power using photovoltaic panels. Some uses of solar energy such as generating electricity for houses and companies to offset the property owner's usage [3], Figure(1.1a). Also, to power all transportation and machinery. A wireless charging pad for mobile phones, based on the Qi standard defined by the Wireless Power Consortium (WPC) as Figure(1.1b).

One stunning application of WPT is the wireless charging of electric vehicles (EVs) that are low-cost and fully autonomous. These attributes can be realized through wireless charging. These are applied by various WPT techniques including inductive coupling, resonant coupling, or microwave power transfer (MPT), as in Figure(1.1c) [4]. Autonomous radio frequency identification (RFID) sensor is the most well-known commercial application. Another innovative WPT application is the batteryless sensor. Wireless sensor networks (WSNs) with advanced technologies are capable of obtaining and collecting relevant information quickly which widely used in many applications requiring monitoring of systems [5], Figure(1.1d).



(a)



(b)



(c)



(d)

Figure 1.1: Some feasible applications on wireless power transfer technique (a) Solar power to charge electric vehicles (b) The simple way to charge mobile devices by WPC (c) The wireless charging of electric vehicles (d) A Batteryless RF-powered wireless sensor system targets building automation

A WPT system can be classified according to the distance between the transmitter and receiver sources into two categories, near-field and far-field wireless power transmission systems. Near field technology or non-radiative energy transfer over short-range distances, this type includes inductive coupling technique where energy is transferred by a magnetic field, and by an electric field in the capacitive coupling technique. Far-field or radiative technology, energy transmission over long distances, includes RF/microwave energy transmission techniques, where energy is transmitted as an electromagnetic wave using electric and magnetic fields, in addition to laser-based optical energy transmission [6].

## 1.2 Wireless Energy Harvesting (WEH)

Energy harvesting (EH) or the energy scavenging of ambient power is a promising technique by which energy is collecting from external environmental sources (e.g. solar energy, kinetic energy, thermal energy, electromagnetic energy), stored or used directly to provide wireless autonomous devices used at numerous applications. The purpose of energy harvesting is to increase the lifetime of field nodes and devices, also to power a sensor network and mobile devices without batteries or to recharging batteries. Thus, EH is potentially attractive to a lot of fields such as the military and commercial sectors. There are several types of ambient environment sources reported as illustrated in Table1.2:

Table 1.2: Comparison of energy sources and harvesting methods,[7]

Energy sources	Power density	Harvesting methods
Solar	100 mW/cm <sup>3</sup>	Solar cells
Vibrations (human motion)	4 μW/cm <sup>3</sup>	Piezoelectric Electrostatic
Vibrations (machine motion)	800 μW/cm <sup>3</sup>	Electromagnetic
Wind	177 mW/cm <sup>2</sup>	Generator
Thermal (human)	60μW/cm <sup>2</sup>	Thermal electric
Thermal (industry)	10 mW/cm <sup>2</sup>	
Radio frequency (RF-GSM)	300μW/cm <sup>2</sup>	Patch antenna
Radio frequency (RF-WiFi)	150μW/cm <sup>2</sup>	
Radio frequency (RF-AM)	2mW/cm <sup>2</sup>	Magnetic coil antenna

### 1. Solar energy

Among all the ambient environmental sources, solar energy has the highest power density. The ambient sun energy uses by thermoelectric to convert temperature differences into equivalent electric current and voltage. Photovoltaic converts solar energy and light energy into electrical current. Energy harvesting systems provide a good amount of fuel savings for cars, lorries and trucks.

## 2. Mechanical energy

Mechanical energy or piezoelectric energy harvesting attached to moving objects or ambient vibrating generating such as a cousin noise, low-frequency vibration, human motion and even motors, and vehicles and machines moving, convert them into an electrical signal by piezoelectric devices. Example of mechanical energy includes piezoelectric floor tiles and batteryless remote control.

## 3. Thermal energy

Heat and temperature variations are the mains sources of thermal energy thermo- electric technique, employed to convert the temperature fluctuations into a usable energy form, as examples as terrestrial and space applications. Pyroelectric device converts waste heat into electrical energy, useful for IoT and wireless sensors.

## 4. Wind energy

Wind energy harvesting system converts wind power into an electric signal, wind turbines micro-wind turbines are techniques that generate electrical power from wind energy.

All the above types mentioned above are used in WSN applications and also structural health monitoring (SHM) [7].

## 5. RF/Electromagnetic energy

Electromagnetic (EM) energy sources are significantly increased in our surrounding environment, for example, WiFi routers are connected every day. Not all power emitted by those devices will be captured by other devices such as our phones. Thus, the local atmospheres are contaminated with the EM energy. Consequently, a lot of researchers have devoted their research to leverage this wasted EM energy regardless where and when the EM energy is. One drawback associated with this type of energy is the low density in space, but it is always available (durability). Despite this deficit, the EM durability was the main reason to make researchers pursuing the research in this field on collecting the wasted RF energy, at a frequency range of (3 KHz - 300 GHz), from ambient environment RF sources. The EM-RF harvester can obtain the energy from various RF sources including mobile phones, WiFi systems, routers, TV towers, radio stations, and mobile base stations. RF sources operate at one of the following bands, AM radio (550 - 1720) kHz, FM (88 - 108) MHz, DTV (400 - 800) MHz, GSM (0.9/1.8) GHz and WiFi (2.4/5/5.8) GHz. Figure(1.2) demonstrates measured input power density [8].

In [7], authors have investigated various RF energy harvesting applications, extracted power from different types of sources. For instance, the 1mW was extracted from the GSM station as well. AM signals, emitted from a 50m far-station, have exploited to power the WSN with a maximum power of 2.39 mW. Furthermore, the WiFi sources extracted power at range (10nW - 0.1 $\mu$ W) away as a maximum as 10m from the harvester. Authors, in [9], have designed PoWiFi harvester

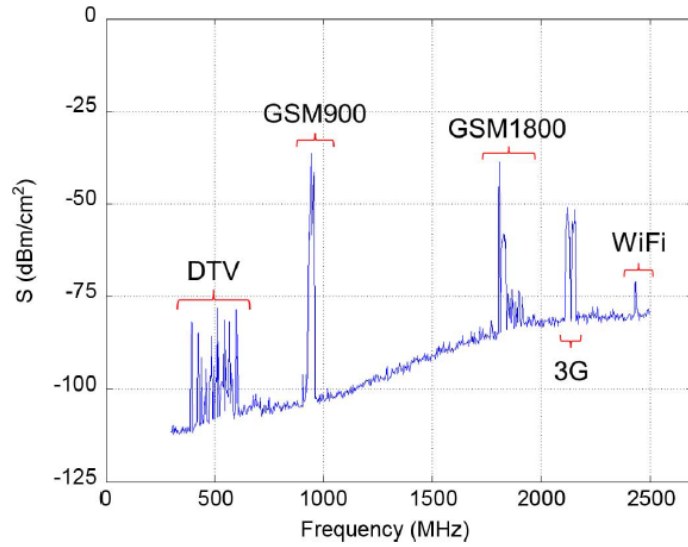
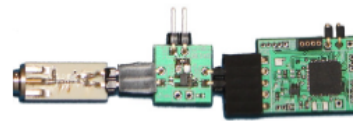


Figure 1.2: Input power density measured vs frequency [8]

as a novel system for charging battery-free camera and battery-free temperature sensor, also recharging two types of batteries. Figure(1.3) and Figure(1.4) show designs and results for the PoWiFi system.



(a) Battery Free Camera



(b) Battery Free Temperature Sensor



(c) Li-Ion Battery Charger



(d) NiMH Battery Charger

Figure 1.3: Prototype hardware demonstration of the power over WiFi (PoWiFi) [9]

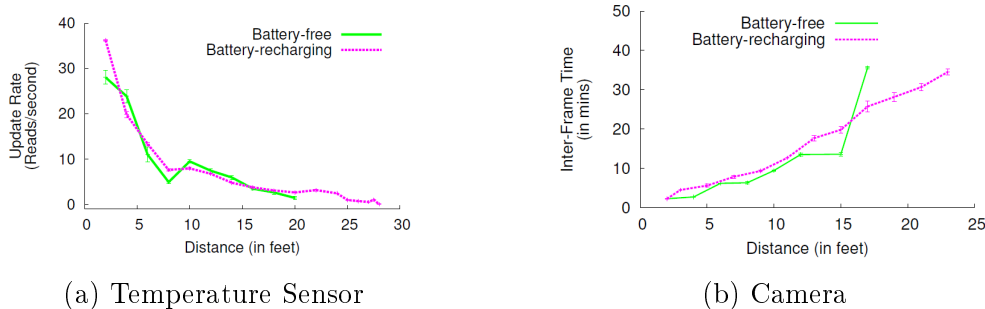


Figure 1.4: Sensor update rate [9]

### 1.3 Challenges

There are two issues facing the far-filed RF energy harvesting designers:

1. Most energy harvesters (EH) have low RF to DC conversion efficiencies owing to the low densities of the ambient RF power, ranging from  $0.1 \mu W \cdot cm^2$  on average in urban areas to some  $\mu W \cdot cm^2$  closing to WiFi access points or routers. Also, the RF-to-DC conversion efficiency rapidly decreases or at least deviates from its optimal value when a single serial diode operates with the low power which means that the rectification efficiency is directly proportional to the input power.
2. The second issue is locations of the RF sources (i.e., transmitters) or orientations of rectennas which are usually unknown or time varying. Consequently, the angle of arrival of RF signals incident on EHs are completely random.

### 1.4 Literature Review

Ambient energy harvesting is based on scavenging energy from environmental (external) sources. Since radio frequency power sources are available ubiquitously and permanently, such as Wi-Fi, mobile base station, and digital TV towers, so it is preferred over others because it can provide the power 24 hour a day. Thus,

battery replacement is avoided. Also, a constant energy transfer could be provided by the ambient RF sources over distance from away RF energy harvesters. The RF power captured is significantly limited, as observed in Table 1.2, hence this low power density limit the conversion efficiency, the factor that measures the effectiveness of the system, [10].

The first essential part is designing an efficient antenna that has the ability to capture a maximum ambient RF energy source. As in the rectifier design, several researchers have adopted effective antenna designs for the RF energy harvesting systems. Various types of antennas have been implemented in the rectenna circuits, for instance, dipole, monopole, loop, microstrip, Yagi and so on. The microstrip patch antenna is the most popular antenna type used because of its low profile, low cost, lightweight, and simple integration with other printed circuits[11].

Most antennas introduced in the literature have linear polarization, considering the RF energy emitting source is known where it is located in space. Thus, the antenna orientation and location in space are known with respect to the RF energy harvesting system designers. However, this is not the case in the real-world applications. The question here is how to overcome these two problems (i.e., known of the emitting antenna location and orientation). The answer is usually impossible. Then, what should we do? Design an antenna that is able to receive the RF signals coming from any direction and with any orientation is the best choice to overcome these two challenges. The proposed solution will be adopted in this work. The first part is to design an antenna array, while the second part is to design a circularly-polarized antenna. Adopting an antenna array is not enough to solve the problem of known a direction of the RF emitting source. The smart

feeding RF network adds more flexibility to antenna array to choose the RF signals from many directions, simultaneously. Consequently, the harvested power amount will be increased relatively, thus increasing the conversion efficiency. Furthermore, broadband or multiband antenna array configurations, with high directivity and wide spatial coverage area, are adopted in other works to increase harvested power. The authors, in [12], have reported broadband slotted antenna operating at a range of 2-3.1GHz, but only single antenna is used in the design. Whereas an antenna array consisting of 1x4 broadband microstrip quasi Yagi antennas is presented in [13]. The latter design has high gain at cost of the size occupation, but the former one offers a low footprint design at cost of the low gain antenna. Wideband fractal planer monopole antenna is proposed in [14], where the design resonates at many frequency bands. Dual polarization is adopted in [15] to deal with more ambient RF sources.

To overcome the polarization mismatch, the circular polarization (CP) is proposed to capture signals regardless of the polarization of the transmitter sources and has been reported with different techniques. The CP which is achieved in some literature is reported as in [16, 17]. The [16] introduces a square loop patch antenna with spatial feeding network, while the [17] presents the 2x2 disc patch antenna array fed with a modified sequential phase network. Another researcher has modified a shape of the patch circuit to generate a CP as in [18], in [19, 20] a square patch antenna with truncated four edges is the easiest way to implement the circular polarization. Authors, in [21], present a 2x2 truncated square patch planar array with a simplified feed network.

In terms of increasing the spatial angle coverage, an antenna array, with multi-

beam patterns, should be adopted. A lot of research has been focused on Beam Forming Networks (BFNs) to implement a multibeam antenna concept which is of great interest chosen to enable the antenna to receive a signal from several beams rather than only one beam. As the number of inputs is equal to the number of outputs, which is the same as the number of beams generated, so each output port has its own beam. The signal, arriving from a specific angle in space, enters at all the input ports, whereas only single output port will have a signal because the input signals have different phases, thereby accumulated at a specific output port. As a result, a wide view angle can be scanned. There are various techniques for BFNs, but the Butler Matrix (BM) beamforming is the simplest to implement and commonly used in the RF energy harvesting systems. The BM has been introduced differently, and the [22] has reported the BM that is constructed as a conventional schematic where the  $4 \times 4$  BM presents scanning-capability with four beams. In [23] authors present the conventional schematic of the  $4 \times 4$ -BM in addition to a miniaturized version as an attempt to reduce the overall size of the conventional schematic. A planar BM is proposed in [24] as an attempt to reduce the overall size by removing some parts from the conventional BM structure. The [25] presents a compact  $4 \times 4$  BM with a highly efficient structure and symmetrical radiation beams distributed around the broadside direction.

After antenna designing, the rectifier circuit is the next to complete the rectenna system design. A rectifier circuit is the main component in energy harvesting systems and has an essential impact on the overall performance of the system. Several types of rectifier topologies have been implemented, for instance, series [26], shunt [27], voltage doubler [12], and bridge [10]. The topology utilized is a paramount point that can affect system performance. The topology selection is dependent on

available power density, loads and how does bulky size it [6].

Input power level, operating frequency, and output load resistance are the most substantial parameters affecting the RF -DC conversion efficiency. Therefore, most previous researchers have significantly focused on optimized their designs to enhance RF-DC efficiency. Increasing the RF power harvested from space means higher conversion efficiency. Consequently, several papers reported capturing signals from several bands such as multiple-band [15, 18, 26], broadband rectifiers [16, 28], with different topologies.

To ensure the maximum power transfer from an antenna to a rectifier circuit, the matching network must exist. The rectifier circuit depends primarily on diodes in their underlying design. In other words, can say that the diodes have variable impedances with frequency, input power, and load resistance owing to their non-linear characteristics. As a result, the design performance will be sensitives for these three parameters, and reducing their impact on the overall performance is a hot research topic. There is a variety of matching circuit designs to circumvent this problem, such as RLC series resonance matching circuit and coupling technique. Recycling output harmonics and reflected power of a rectifier is adopted in some designs to increase the input power to the rectifier thereby, increasing the efficiency as in [29]. A researchers in [30, 31] have reported how to get a high-efficiency system with a variable extent of both input power and load. The authors in [30] have investigated the high impedance complex conjugate matching system. The integrated tapered matching network topology is proposed in [31]. In order to increase the range of input power as in [32–34], it is proposed to use two diodes with a different threshold voltage. The drawback of most previous

works, mentioned above, is the complexity and size of the designs, ranging from 90X90mm<sup>2</sup> to 21X12mm<sup>2</sup>.

Another approach to improve conversion efficiency is compression networks. In [35] researchers have designed an RCN (Resistance Compression Network) operating with only a single frequency, in [36] a dual-band RCN has been implemented, and an RCN working with a wide range of frequencies is reported in [28]. Figure(1.5a) explain the conventional schematic of RCN circuit.

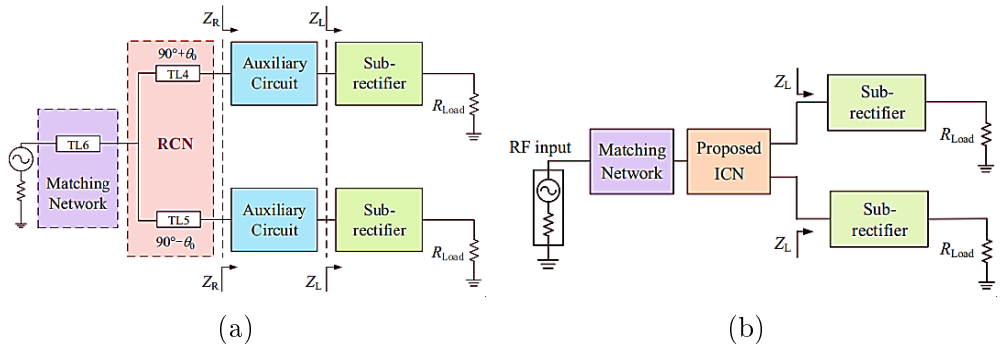


Figure 1.5: The conventional schematic for compression network [37], (a) RCN (b) ICN

All these designs, in their RCN circuits, rely on lumped elements. The lumped elements have an inherent problem which is the parasitic effects. Parasitic effects enforce them to behave differently from their main functionalities (i.e., the capacitor will have dominant inductance behaviour or vice versa), especially at high microwave frequencies. Alternatively, the transmission lines are the optimum candidate, as investigated in [38], [39]. It is a dual-branch design, so RCN increases the design complexity. In [40] a single branch RCN has proposed to reduce the input impedance variation where the design complexity is reduced as well but still using an auxiliary component to remove the imaginary part. The RCN needs only a real resistance to deal with and this is a big constraint because most nonlinear circuits have complex impedances. A procedure using the auxiliary part increases

the complexity of the design. Based on that, the compression network compresses both the real and imaginary parts at the same time being preferred to improve the efficiency of the overall performance of a circuit with as few as possible a number of the lumped components. Therefore, some researchers have reported works regarding this issue as in [41], a complex impedance compression network is introduced, which compresses the real and imaginary parts simultaneously, with dual-branch work and in [37] with single and dual-band works because of the main drawback of most previous proposed RCN and ICN circuits are the requirement for dual output branches, which increases the design complexity. In [42] author also has proposed a single branch integrated impedance compression network (IICN) to compress complex impedance but with a circuit that has a big footprint which is  $31.3 \times 25.3 \text{ mm}^2$ .

## 1.5 Contributions

1. Design and build single branch impedance compression network as a matching circuit appropriate for nonlinear rectifier circuit.
2. Optimize the matching circuit by particle swarm optimization algorithm.
3. Design and build antennas having more than one polarization in order to combat the orientation deficit.
4. Build a passive beamforming circuit.
5. Investigate four type of power combining strategies.

## 1.6 Organization of Thesis

**CHAPTER 2** presents theoretical background of energy harvesting.

**CHAPTER 3** presents antenna array design for RF energy harvesting system.

**CHAPTER 4** describes rectifier circuit design for RF energy harvesting. In addition to, Particle swarm optimization algorithm will be mentioned.

**CHAPTER 5** discuss the rectenna design with various power combining strategies.

**CHAPTER 6** carried out the conclusion and future work for this thesis.

**APPENDIX**

## CHAPTER 2

### THEORETICAL BACKGROUND

#### 2.1 RF Energy Harvesting System (RFEH)

The energy harvester collects the adequate power from RF energy sources to power the low power devices (e.g. sensors), thereby leading into batteryless devices. The main difficulty that encounters the designers and researchers is the low power density of the RF signals in space. This is why no more works existed in the previous until the emergence of the advanced semiconductor technology although the RF energy harvesting idea was existed. The sought to scavenge as much RF energy as possible from space was and still is the foremost goal for all those interested in this field.

The key component for the RFEH system is the “rectenna “. Figure(2.1) illustrates the block diagram of the rectenna which is composed of a receiving antenna and rectifier, combined in one structure. The antenna picks up the incident EM wave at a certain RF band, and the rectifier converts AC energy into DC energy. Usually, the DC power is preferred because of its compatibility with the existing electronic devices and battery functionality. The rectenna performance is usually assessed through the RF to DC conversion efficiency. To ensure the maximum power transfer from an antenna to a rectifier circuit without high reflection, the matching circuit must exist.

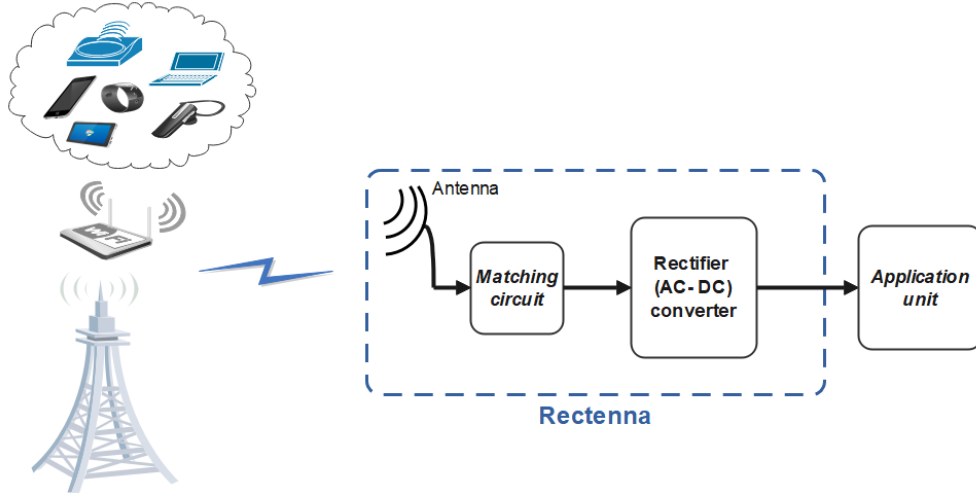


Figure 2.1: Block diagram of Rectenna model

## 2.2 Capture Power

The power captured by the antenna, located a distance away from the RF power sources, can be defined by the radiation power density multiplied by the capturing antenna area (i.e., antenna effective aperture), and the direction of capturing defined by  $(\theta, \phi)$ , by virtue of [43];

$$P_{capture}(\theta, \phi) = S_{rad}(\theta, \phi) * A_e(\theta, \phi) \quad (2.1)$$

$S_{rad}(\theta, \phi)$  is a quantity that describes the RF power associated with EM waves.  $A_e(\theta, \phi)$  is the maximum effective area by which the antenna can deliver as maximum as RF power to load. In fact, all power captured by the antenna does not deliver for load, some of the captured power is dissipated as heat, because of the losses, or scattering (re-radiated). In order to determine the dissipation and scattering power in addition to the delivered power to load, the effective area is written as:

$$P_{total\ captured}(\theta, \phi) = S_{rad}(\theta, \phi) * (A_e + A_s + A_L)(\theta, \phi) \quad (2.2)$$

$A_s$  is the scattering area, where it increases under mismatching case.  $A_L$  is the area loss. When assumed that no conduction/dielectric loss and highly matching between antenna and load exist, the effective area can be rewritten as follows:

$$P_{captur}(\theta, \phi) = \frac{\lambda^2 G(\theta, \phi)}{4\pi} = \eta_{rad} \frac{\lambda^2 D(\theta, \phi)}{4\pi} \quad (2.3)$$

$\eta_{rad}$  is the antenna radiation efficiency.  $G(\theta, \phi)$  is the gain of antenna.  $D(\theta, \phi)$  is the directivity of the antenna, which is the ratio of total power received in the given direction from the antenna to power distributed overall other directions. The increasing directivity of the antenna enables it to receive power from a larger area, thus receiving more RF power.

### 2.3 Patch Antenna

A patch antenna or also known as microstrip antennas, is one of the most types of antennas used in wireless applications because of their own various features such as low profile, simple, and inexpensive to manufacture using printed circuit technology. Moreover, it is compatible with monolithic microwave integrated circuit (MMIC), and suitable to the non-planar and planar surfaces. Patch antenna feeding can be configured in different ways, such as microstrip line feed, aperture coupled and coaxial feed line as shown in Figure(2.2c). Various forms can take in patch to meet the design requirements, such as rectangular, circular, thin strip, square, circular ring.

The patch antenna is suitable for low power application by virtue of the capability of handling low power [44]. Figure(2.2a) illustrates the structure of microstrip antenna, which composed of the two-conductor transmission line parallel to each

other and separated by a dielectric layer known as a substrate. A patch (radiated element) on the top side, while on the bottom side a thin layer metal is known as a ground plane. In this work, square patch antenna with microstrip line feed was chosen.

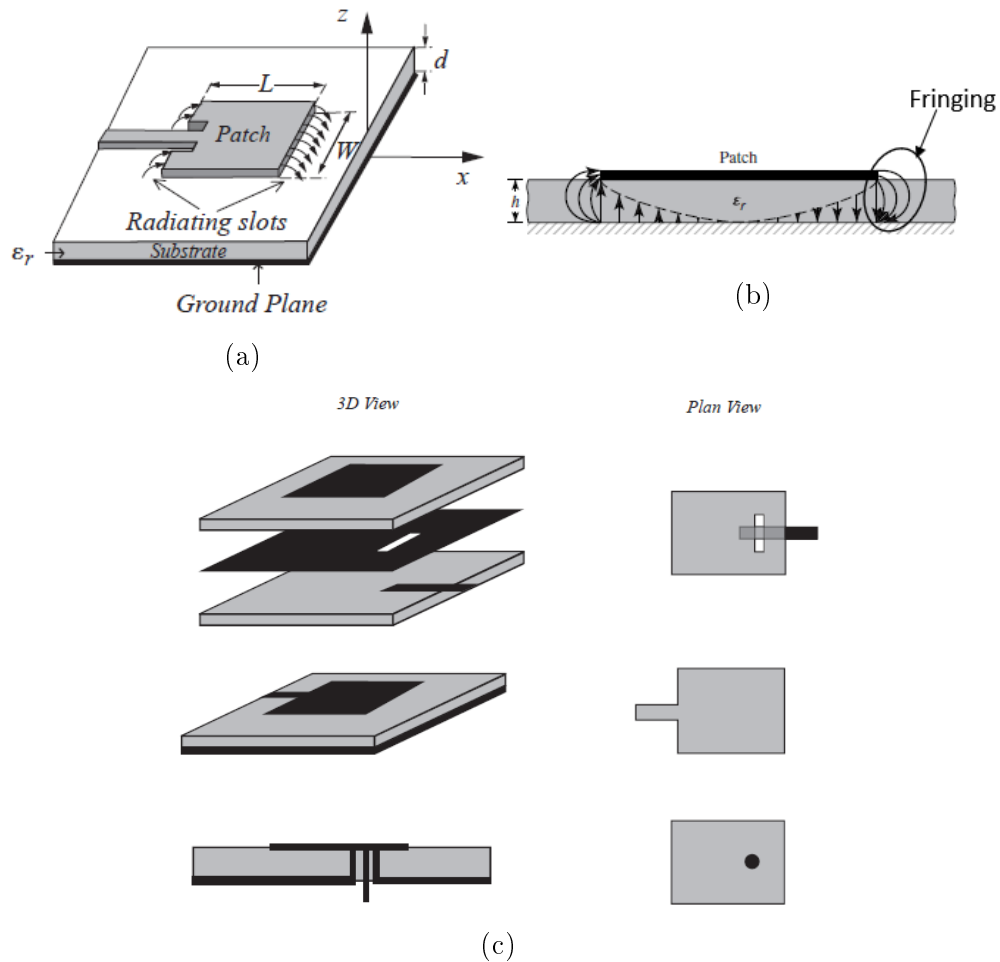


Figure 2.2: Microstrip antennas and their feeds (a) a microstrip antenna with its coordinates (b) Side view shows the effective and physical length of patch (c) three feeding configurations: coupling feed, microstrip feed and coaxial feed [44]

### 2.3.1 Analysis Square Patch Antenna

Figure(2.2a) explains some parameters that have a significant effect on controlling the properties of an antenna.  $L$ ,  $W$  represents to the length and width of a radiated element (patch), respectively. In addition,  $\epsilon_r$  represents the dielectric constant which is the expression of the ratio of the permittivity of a substrate to

the permittivity of air.  $h$  is the thickness of the substrate, and a value of this parameter must be carefully determined.

The fringing effect refers to that the fields extending from edges of the radiated element to the substrate. A fringing effect is a function of  $L$ ,  $W$ , and  $h$ . Hence fringing effects make the antenna length is larger than what the antenna seems as shown in Figure(2.2b). In addition, when  $W/h \gg 1$  and  $\epsilon_r \gg 1$ , the electric field line concentrate in the substrate. The effective dielectric constant  $\epsilon_{\text{reff}}$  introduce to take into account effects of the fringing fields and wave propagation inside the transmission line. It is a value enclosed in the range of  $1 < \epsilon_{\text{reff}} < \epsilon_r$ , obtained as in the following expression, [43]:

$$\epsilon_{\text{reff}} = \frac{\epsilon_r + 1}{2} + \frac{\epsilon_r - 1}{2} * \frac{1}{\sqrt{1 + 12h/W}} \quad (2.4)$$

The effective length  $L_{\text{eff}}$  becomes

$$\Delta L = 0.412h \frac{(\epsilon_{\text{reff}} + 0.3)(\frac{W}{h} + 0.264)}{(\epsilon_{\text{reff}} - 0.258)(\frac{W}{h} + 0.8)} \quad (2.5)$$

$$L_{\text{eff}} = L - 2\Delta L \quad (2.6)$$

$\Delta L$  is an extra length introduced by fringing effect, subtracted from the  $L$  which is the length without taking into account an effect of the fringing fields ( $L=\lambda/2$ ). Since the patch form selected is a square patch antenna. Therefore,  $W$  is equal to  $L$ , and they can be also obtained by [43]:

$$W = \frac{C}{2f\sqrt{\epsilon_r}} \quad (2.7)$$

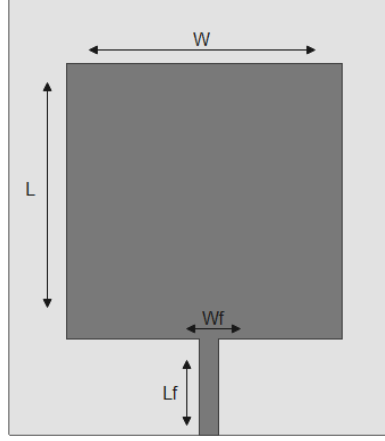


Figure 2.3: Design of square microstrip patch antenna

$$Z_o = \frac{120\pi}{\sqrt{\epsilon_r} \left( \frac{W_f}{h} + 1.393 + 0.667 * \ln\left(\frac{W_f}{h}\right) + 1.44 \right)} \quad (2.8)$$

$$L_f = \frac{C}{4f\sqrt{\epsilon_{\text{reff}}}} \quad (2.9)$$

$$Z_a = 90 \frac{\epsilon_r^2}{\epsilon_r - 1} \left( \frac{L}{W} \right) \quad (2.10)$$

$$Z_t = \sqrt{Z_o * Z_a} \quad (2.11)$$

Operating frequency expressed by  $f$  is equal to 2.4 GHz.  $C$  is the velocity of wave in free space. The input impedance of the feeding transmission line to determine the feeding line-width (transition line)  $W_f$ . The length of feeding  $L_f$  is quarter the effective wavelength.  $Z_a$  is the input impedance of radiated patch, and  $Z_t$  is the input impedance of the transition line.

### 2.3.2 Circular Polarization

Polarization is the property of an electromagnetic(EM) wave that describes the magnitude and the time-varying direction of the electric field vector. Polarization can be classified according to the the transmission ways of the electric field in space into three types linear, circular and elliptical polarized. In the linear polarization, the electric field vector moves in the same direction (i.e., one axis) throughout

the transmission, and there will be two cases which is either vertical or horizontal linear polarization.

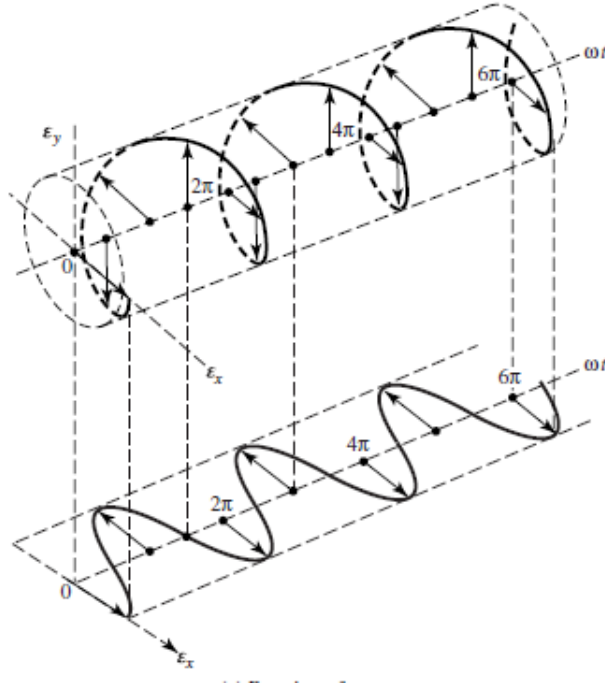


Figure 2.4: Polarization types, rotation of a plane electromagnetic wave [43]

The power received from surrounding RF power sources is very little, so in order to ensure a sufficient power reaches the into rectifier the possible higher power as should be collected to operate the harvester permanently at high and stable efficiency. Avoiding mismatch polarization between the receiver and the transmitter is the key in all communication systems to increase the power captured, where the receive and transmit antennas must be in the same orientation in a case of the linear polarization, which is adopted in the most communication systems. In the circular polarization, electric field traces are in a circle and ellipse forms which appear like a rotation with circular or elliptical motion with a direction of the wave propagation, as shown in Figure(2.4). In this work, circular and elliptical polarization is required to overcome problem of linear polarization, which is the overlapping between vertical polarized and horizontal polarized, thereby leading into higher and more stable reception signal levels without interruption.

The circular polarization waves can be obtained if the time phase difference between two orthogonal modes is  $90^\circ$ , and this can be achieved in a different way, such as using multiple feeds or by adjusting the physical dimensions of the radiating patch. The easiest way to implement typically the circular polarization antennas uses a square patch form with truncated corners with a single microstrip feeding line. Circular polarization is generated by deviating the current flow, since in the microstrip antenna the most of the flowing current is at the edges. Cutting part of some of the edges leads to a change in the polarization of the antenna in the microstrip and shifting the operating frequency.

## **2.4 Beam-Forming Network for Energy Harvesting**

Increasing the view angle area to scan a large number of the ambient RF sources is preferred in the energy harvesting systems. A multi-beam antenna is a perfect choice in order to scan a wide spatial coverage area by multi beams radiation. The adoption of the multi-beam antenna imposes dealing with beamforming network (BFN) in order to leverage from its features in accumulating RF power combination and wide radiation beam width obtained by it. As a result, the increment in the received power will be obtained.

### **2.4.1 Butler Matrix Structure**

Analog passive BFN is the simplest and easiest RF power distribution circuit to feed the antenna array elements, which is used to provide a multi-beam rectenna system design. BFN is an RF power combining network, with N input port and N output port, where N is the same number of feeds in the array also a number of generated beams. The power passing from one of the input ports is distributed with equal amplitude between the output ports, but at different phases with a

fixed phase difference angle which passively controls by BFN components. Various types of BFN has been implemented such as Rotman lens, Nolen and Blass matrix but Butler matrix configuration is the simplest and easiest to implement than the other types [45]. Figure(2.5) illustrates the architecture of a conventional N X N Butler matrix, which is composed of several hybrid branch-line couplers, crossover and phase shifters.

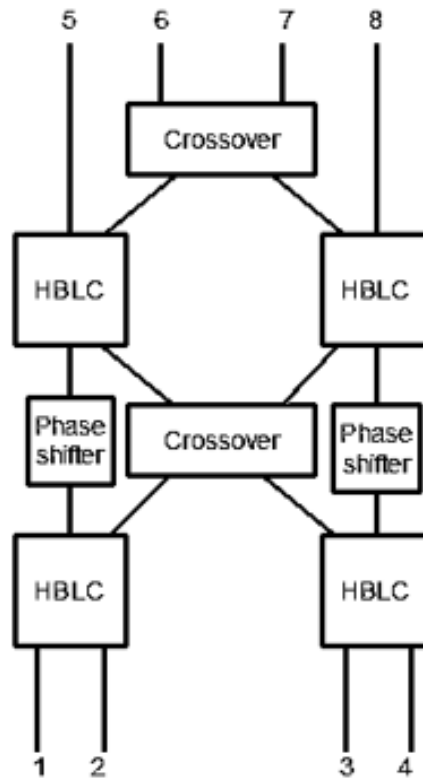


Figure 2.5: The architecture of a conventional 4 X 4 butler matrix

Hybrid branch-line couplers (HBLC), also known as  $90^\circ$  branch-line coupler, is a microwave component utilized to combining power passively. HBLC is a special case of the directional coupler circuit (called a 3dB directional coupler) that has four ports with two input ports and two output ports. The power passing into any port is separated with equal amplitude and  $90^\circ$  phase difference between output ports. The number of HBLC utilized in BFN configuration is selected according to  $((N/2) * \log_2 N)$ , [45]. Figure(2.6) shows the HBLC structure design and also

dimensions of transmission lines explain.

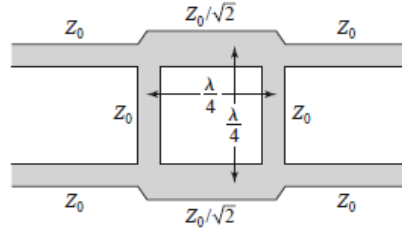


Figure 2.6: The architecture of a Hybrid branch-line coupler [46]

By virtue of [46] the scattering matrix of  $90^\circ$  HBL is given as following:

$$[S] = \frac{-1}{\sqrt{2}} \begin{bmatrix} 0 & j & 1 & 0 \\ j & 0 & 0 & 1 \\ 1 & 0 & 0 & j \\ 0 & 1 & j & 0 \end{bmatrix} \quad (2.12)$$

A crossover circuit is a cascade of two HBL. The crossover utilizes to pass the signals to the second stage without loss and with 0dB insertion loss. The scattering matrix of crossover is given as following:

$$[S] = \begin{bmatrix} 0 & 0 & j & 0 \\ 0 & 0 & 0 & j \\ j & 0 & 0 & 0 \\ 0 & j & 0 & 0 \end{bmatrix} \quad (2.13)$$

phase shifters are required to complete the butler matrix configuration. The phase shifter controls the phase difference between the output ports of the Butler matrix. The phase shifter circuit consists of two coupled transmission lines folded at one of its edges.

## 2.5 Rectifier Circuit and its Principle

The RF harvesting device is composed of an antenna which picks up the RF signals from the surrounding RF sources located everywhere. Then, the captured power will pass through the transmission lines into rectifiers, which is the second component in the RF energy harvester. In this part, the process of converting the RF signals into DC power occurs (i.e., the rectification process). Semiconductor diodes are preferred over others because of various benefits such as low cost, small form factor and the low power handling [6]. Schottky diode is typically the right choice in numerous RF harvesters for several benefits like, the operation at high frequencies, due to low junction capacity and the low turn-on voltage required to turn on the diode. These features make the Schottky diode preferred over other types of diodes in the energy harvesting systems.

A diode is an electronic component, passing an electric current in one direction and blocks it in the opposite direction. This behaviour is called rectification. The main characteristic of the diode is nonlinearity, which means the input diode impedance varies when the load resistance, operating frequency, and input power change. The nonlinear behavior due to nonlinear current-voltage characteristic is shown in Figure(2.7), I-V characteristic curve for diode, where three regions are observed as an operation principle of the diode. The first region is reverse-breakdown voltage ( $V_{br}$ ) when a low voltage less than  $V_{br}$  and conduct will be in the reverse direction. In the second region between  $V_{br}$  and  $V_f$  (forward voltage), called reverse bias, a diode is OFF through this voltage range. The last region is above  $V_f$  where, in this case, the diode is ON and called forward bias.

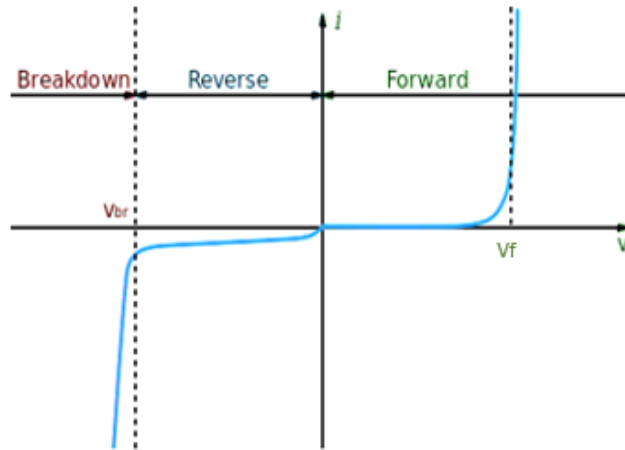


Figure 2.7: I-V (current VS voltage) characteristic curve of Schottky diode

## 2.6 Compression networks

A special case of the matching network aiming to compress the variations in input impedance thereby enhancing the overall performance. The principle of these networks is to compress the input impedance variations to small ranges, which allow for the rectifier to operate with a wide range of input power and load, although the rectifiers have nonlinear elements (i.e., diodes) in their underlying structures. It is known, diode equivalent impedances vary with power and frequency. There are two approaches for compression networks, resistance compression network (RCN) and impedance compression network (ICN). Both types are a special class of matching circuits that provide a reduction in input impedance variation at the rectifier input. Some research efforts have been done. Their works depended on dividing the load resistance into parallel branches with the same current and opposite phase. The resulting load will be a pure real impedance and it has a slow change in its value.

## 2.7 Particle Swarm Optimization Algorithm

Particle swarm optimization (PSO) is one type of meta-heuristic algorithms for optimization technique which learning from nature specifically, the principle of the survival of the fittest to solve a wide range of optimization problems where just the best and robust solution can be obtained [47]. PSO was developed by Kennedy and Eberhart in 1995 [48], and it is simple to be implemented because there is no crossover and selection. Also, there are few parameters to be modified. Meanwhile, it is efficient in solving a large number of optimization problems. In the PSO algorithm, the particles are randomly placed in the search space and then by using the fitness function they evaluate their quality in that position. Then, for a predetermined number of iterations, each particle moves to a new position providing better fitness than the previous position. With a specific velocity of the moving particle, this movement depends on the history of the particles having the current best positions with the best positions achieved by other particles in the swarm and sure with some random perturbation. Hence in subsequent iterations, the swarm achieves the optimal solution to the fitness function in the problem space, with a finite number of particles working together. Figure(2.8) illustrate the flow chart of PSO algorithm.

Various recent related work investigates by using optimization algorithms to search about the best enhancement of the harvesting system adopted. Based on the PSO algorithm in [49] authors reported a local and global optimum to adjust locations and orientations of antenna chargers to support wireless rechargeable sensor networks (WRSNs) to be sustainable. In [50] PSO algorithm was utilized to lead the swarming drone that depended on an RF power harvesting system to

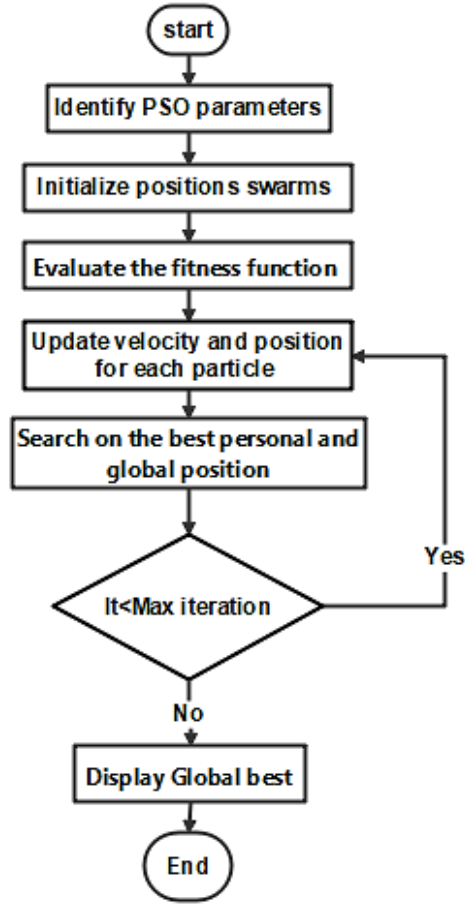


Figure 2.8: Flow chart of the PSO algorithm

recharge its batteries towards the location with the highest RF power. Moreover, the PSO algorithm has been used in another part of the RF harvester structure, as optimized power management circuits proposed in [51].

In this work, PSO is utilized to obtain the optimal dimensions of ICN components to reach as maximum as conversion efficiency of the proposed circuit. The ICN consists of only three transmission lines connected in parallel to give a maximum compression for input impedance variations. Consequently, the input impedance equation of ICN will be as a fitness function of PSO. The PSO finds the optimal possible solutions based on the movement of the particle. The search starts with initializing random swarms containing a number of particles (search

points), each single particle represents a candidate solution and encoded by a position vector with  $N$  elements where  $N$  refers to a number of decision variables. Each position vector is evaluated by the fitness function, for a finite number of iterations.

The particle swarm positions are updated by movement within the solution space and the velocity vector computed by using the velocity equation. In each iteration, comparing the best particle in the swarm (Global best position  $G_{best}$ ) for each particle in the best swarm (personal best position  $P_{best}$ ) to provide the optimal global best position particle which guides the swarms toward the optimum solution. The equation of velocity is obtained as following, [48]:

$$V_{i,t+1} = W * V_i + C1 * rand(N) * (P_{best_{i,t}} - X_{i,t}) + C2 * rand(N) * (G_{best_{i,t}} - X_{i,t}) \quad (2.14)$$

Where  $W$  is the inertia weight and it is a constant number that provides a balance between personal exploitation and global exportation. Moreover,  $W$  enhances the accuracy and the production results.  $t$  is a number of iterations,  $i$  is a number of populations.  $C1$  and  $C2$  are the personal and social acceleration coefficient. The updated position equation is obtained as following:

$$X_{i,t+1} = X_{i,t} + V_{i,t+1} \quad (2.15)$$

# CHAPTER 3

## ANTENNA ARRAY DESIGN FOR RF ENERGY HARVESTING

### 3.1 Overview

Exploiting the ambient RF signals will alleviate the need for batteries and then no need for charging, recharging, and even replacing batteries. Energy harvesting technology was introduced to provide self-powering electronic devices for IoT and WSN applications. Rectenna ( rectifier + antenna ) is a key component for the RF harvesting system technique. High gain antenna is what will be introduced in this chapter. The antenna is the transducer device that converts the electromagnetic signal to electrical, where it plays an essential role in energy harvesting technology. The selection of the main properties of an antenna (e.g. type of antenna, shape, polarization etc.) has a substantial role for leading to a higher output DC signal. A highly effective antenna with high gain and wide spatial coverage is what we seek to reach it in this chapter.

### 3.2 Single Square Patch Antenna Design and Simulation Results

The square patch antenna with microstrip feed line is chosen, a square patch form selected in order to implement the easiest circular polarization way, which is a truncated corners. Figure(3.1) illustrates the antenna design, with cutting applied at upper left and lower right corners, the dimension of cutting is obtained

by equation (3.1).

$$L_{cut} = \frac{L_{eff}}{8} \quad (3.1)$$

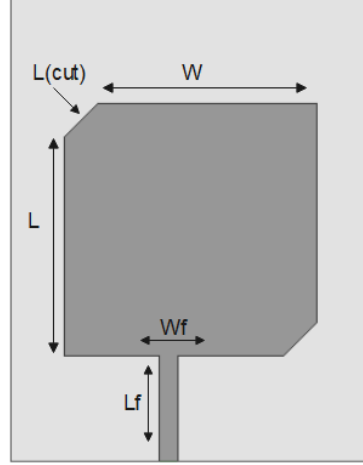


Figure 3.1: Design of square microstrip patch antenna with truncated corner

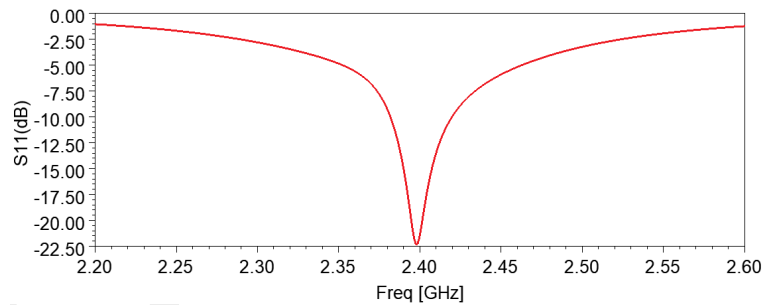
The dimensions that are determined using a mathematical model, and the optimized dimensions by the simulator, are given in the Table 3.1. HFSS software is used, and the Rogers RT/duroid 6006 laminate is selected. The substrate has 6.15 as a dielectric constant, as substrate with thickness equal to 1.7 mm.

Table 3.1: Calculation and simulation dimensions for the square patch microstrip antenna.

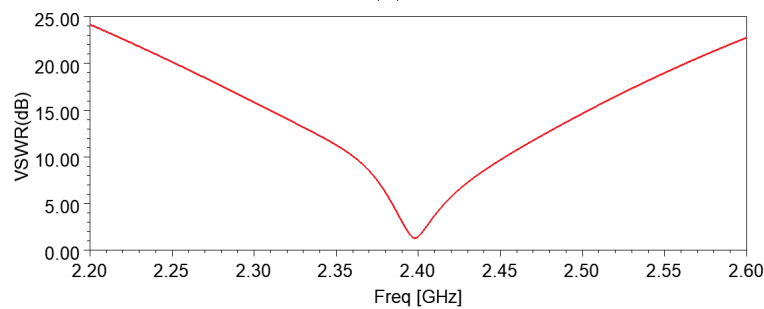
Parameters	Calculation; mm	simulation; mm
$W$	25.2	24.5
$L$	25.2	24.5
$W_f$	1.768	1.7
$L_f$	13.35	10.25
$L_{cut}$	3.15	3.2

Return loss (reflection coefficient) and VSWR are plotted in Figure(3.2). As can be seen, the antenna works well at desired frequency. Axial ratio (AR) which

evaluates the effectiveness of circular polarization and its value must be less than 3 dB, is given in Figure(3.3).



(a)



(b)

Figure 3.2: Simulated results for a single element square patch antenna(a) The simulated S11 (b) VSWR and its almost equal to zero at 2.4GHz

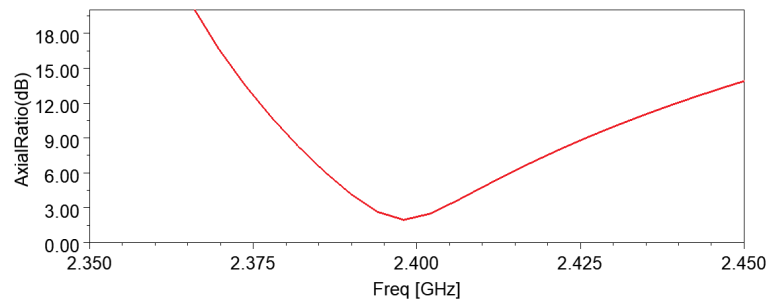
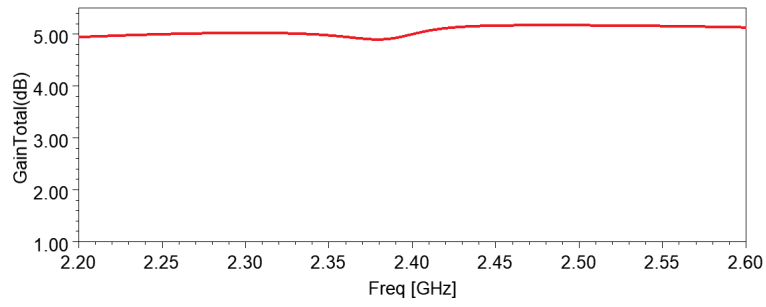


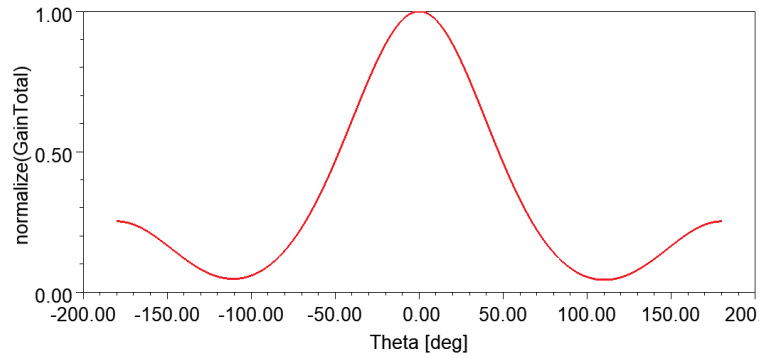
Figure 3.3: simulated axial ratio

Gain of 5dB has been accomplished as observed in Figure(3.4). The radiation efficiency of single element for square patch antenna designed illustrated at Figure(3.5), which it is close to 85% at the resonance frequency.

A Left hand circular polarization (LHCP) is radiated by the antenna at Z direction as shown in Figure(3.6). Figure(3.7) shows the radiation pattern in 3D



(a)



(b)

Figure 3.4: Simulated gain for a single element square patch antenna (a) Gain achieved for single element square patch antenna (b) The normalized total gain as function of theta angle

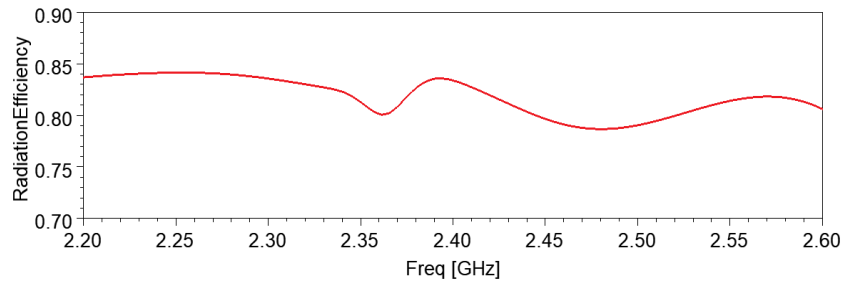


Figure 3.5: Radiation efficiency for single element

and 2D for E and H plane. The current distribution and E field in Figure(3.8) demonstrate successfully an occurrence of the circular polarization.

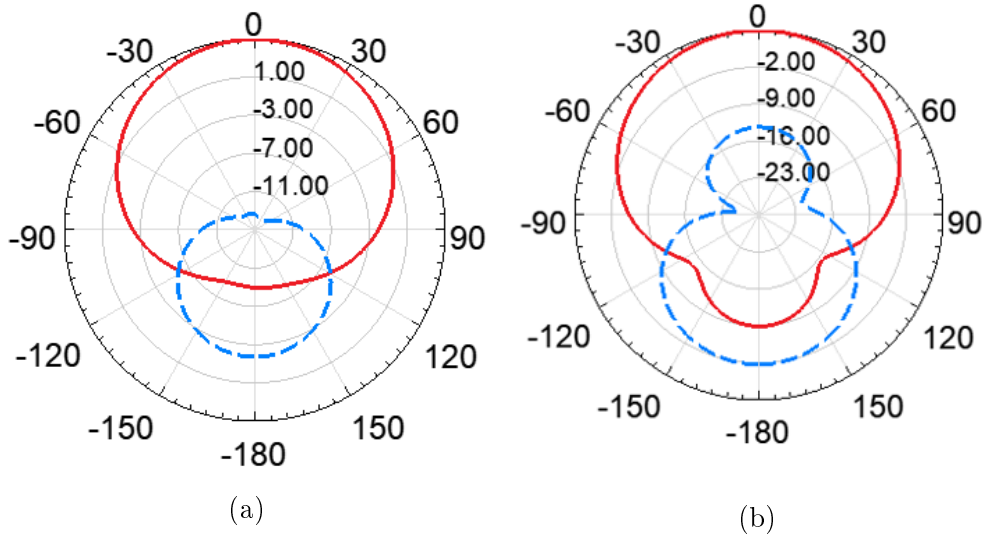


Figure 3.6: The gain of radiation pattern (red line LHCP , blue line RHCP)(a) yz plane (b) xz plane

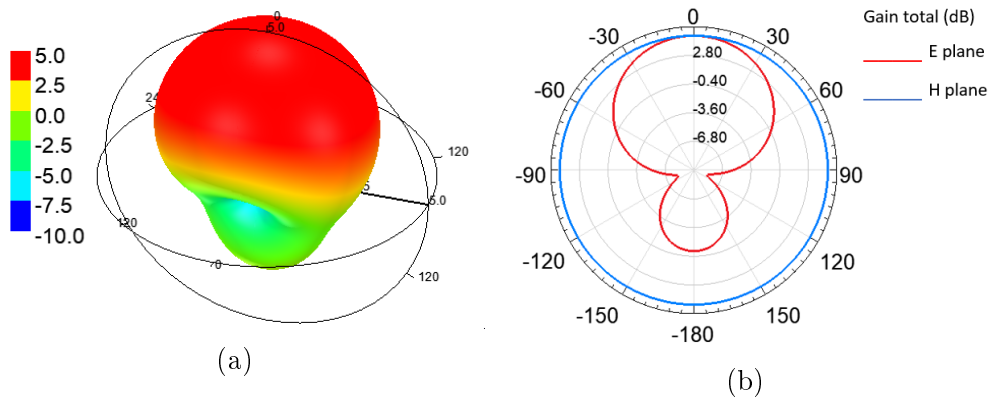


Figure 3.7: The simulated radiation pattern for antenna, radiate at Z direction (a) 3D (b) 2D for two plane

### 3.3 Linear Array Patch Antenna Design and Simulation Results

To increase the gain of the square patch antenna and make the radiation pattern more direct to meet the demands of long-distance RF sources, multi-element is what it need. A multi-element is also known as an array, where multi patch elements are arranged in line and planer form. The radiated field from each element of the array combines constructively in the desired direction and destructively in the other undesired directions. Thus, the pattern of the radiated field generated by an array is high directivity . There are various parameters that can be used to

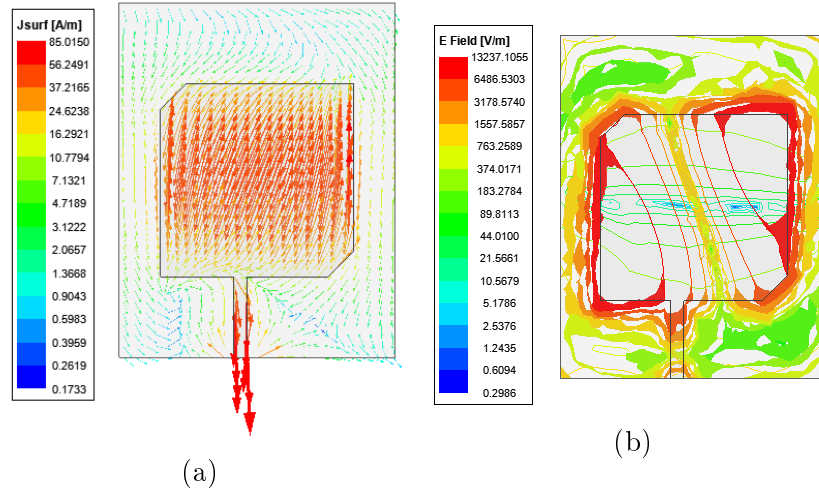


Figure 3.8: Simulated animation results for a single element square patch antenna (a) Current distribution (b) The magnitude of E field radiation

control the overall radiation pattern for a square microstrip antenna such as the distance between the elements, the radiation pattern of the individual element, amplitude excitation and phase excitation of the individual elements. The total fields of the array are computed by multiplication the electrical field of a single element by the array factor (AF) [52]. As shown in Figure(3.9), antenna elements of the linear array is placed along one axis and separated by the  $d$  distance, excited with  $\beta$  (phase difference) and the same amplitude.

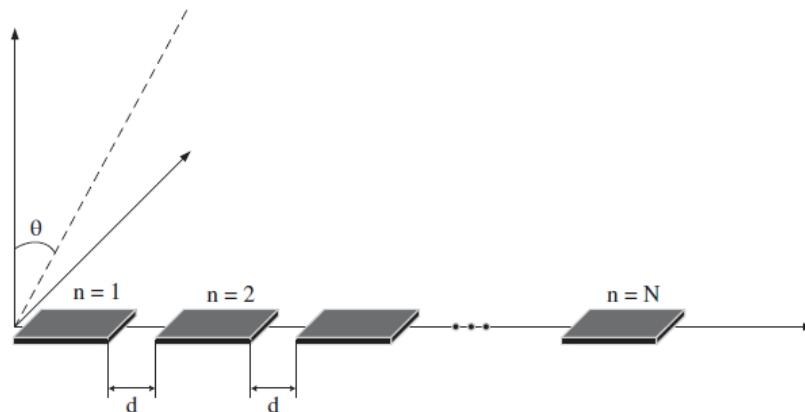


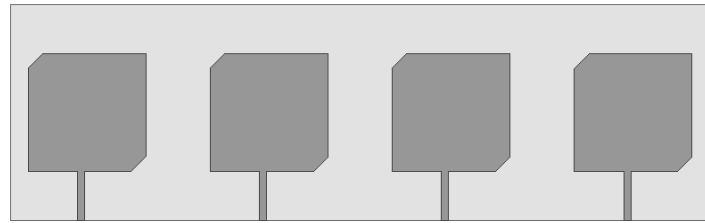
Figure 3.9: A linear patch antenna configuration [52]

Array factor can be determined by;

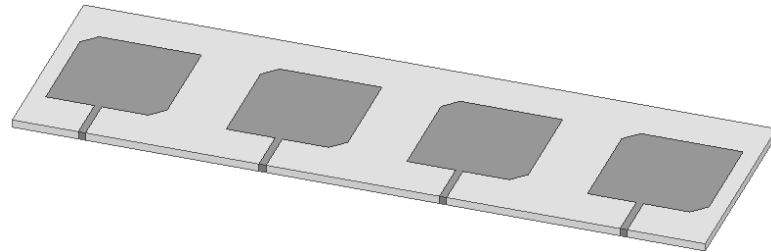
$$AF = \sum_{n=1}^N \exp j(n-1)\psi \quad (3.2)$$

$$\psi = kdcos(\theta) + \beta$$

Where  $k$  is the propagation number ( $k = \frac{2\pi}{\lambda}$ ),  $n$  is an array element number and  $\theta$  represents to the scan angle of the array. The  $d$  has a significant role, and it should be larger enough to avoid the mutual coupling between the elements, also should not be very large to avoid the grating lobe. Figure(3.10) shows the identical square microstrip linear antenna array designed.



(a) Top view



(b) Trimetric view

Figure 3.10: A linear patch antenna configuration

Using four identical antenna elements, each with its own feed, with a separation distance between elements that were selected by measuring the distance from the center of an element to the center of the adjacent element, it is optimized at 37.9 mm ( $\lambda/3.3$ ). This distance is sufficient to obtain a high matching for all output ports. So that Figure(3.11) illustrate the reflection coefficient in dB at operating frequency which is close to the -20 dB for all ports. Also, the voltage of the re-

flected signals (VSWR) is close to zero, in addition, mutual coupling between the elements was obtained with a value of less than -10 dB, as shown in Figure(3.12).

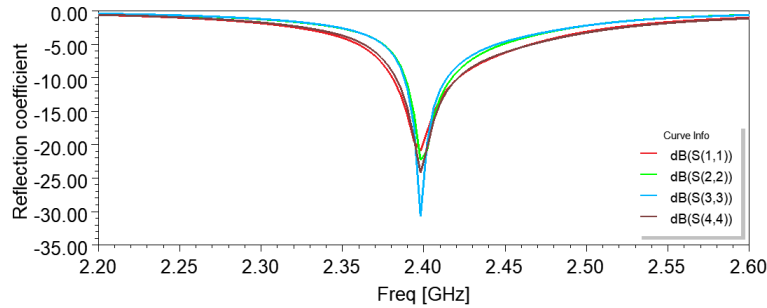
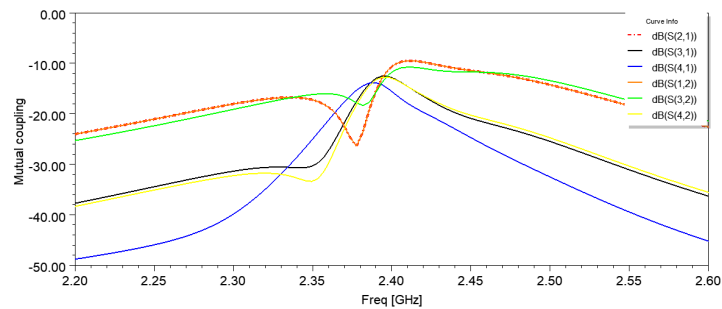
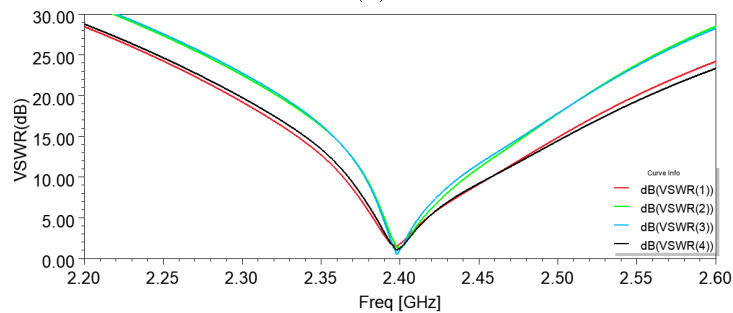


Figure 3.11: The simulated S11 for the linear patch antenna



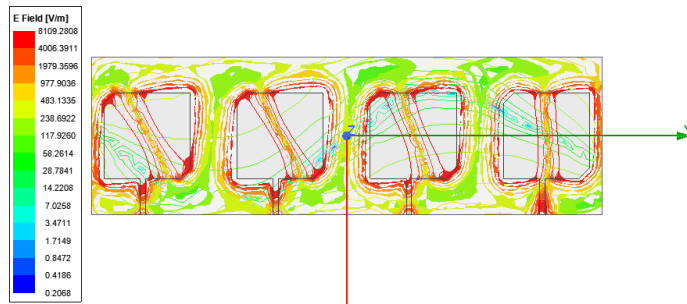
(a)



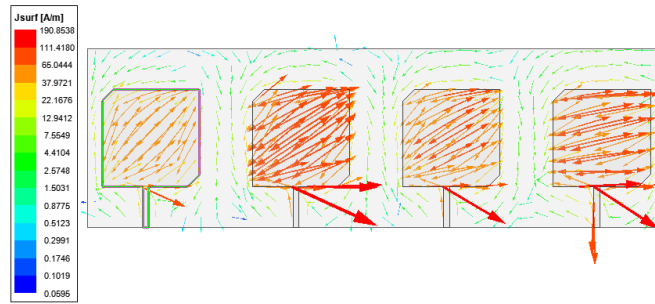
(b)

Figure 3.12: Simulated results for square patch antenna array (a) Mutual coupling between array elements (b) VSWR and its almost equal to zero at 2.4GHz

Typical circular polarization has been carried out for linear array, where all elements the array are circularly-polarized. As illustrated in Figure(3.13) the E field and current distribution animation is introduced to proof concepts of the circular polarization. Two degenerate modes generated along symmetrical sides of the square with 90 degree phase shift. This will be very useful to capture the



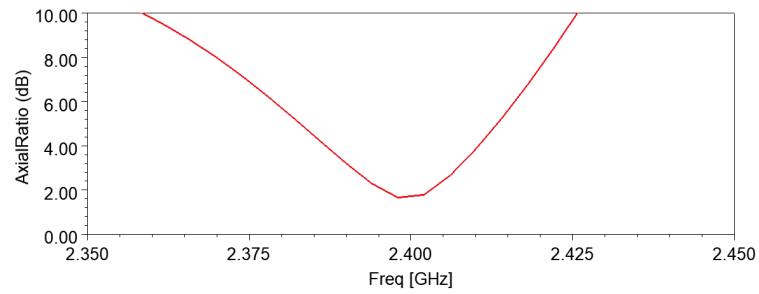
(a)



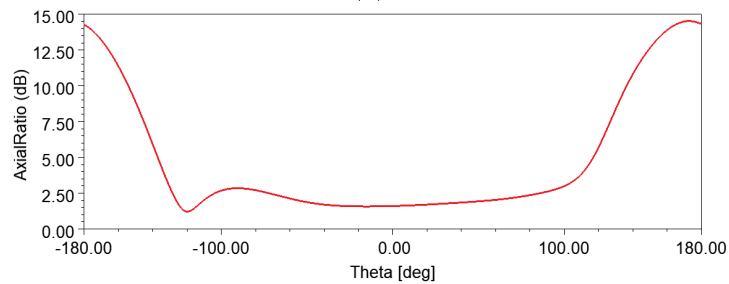
(b)

Figure 3.13: Simulated animation results for square patch antenna array (a) Current distribution (b) The magnitude of E field radiation, for square patch array antenna

energy from space at any orientation. Figure(3.14b) shows the axial ratio versus



(a)



(b)

Figure 3.14: Simulated axial ratio

the frequency at the broadside direction (i.e.,  $\theta = \phi = 0$ ), while Figure(3.14a) shows

the axial ratio versus  $\theta$  with fixed frequency equal to 2.4 GHz and  $\phi = 0$ . As can be observed, the value of axial ratio is less than 3 dB. In Figure(3.15), the 2D radiation pattern of the array depicts the gain in LHCP (co-polarization component) and RHCP (cross-polarization component) at xz and yz planes, respectively.

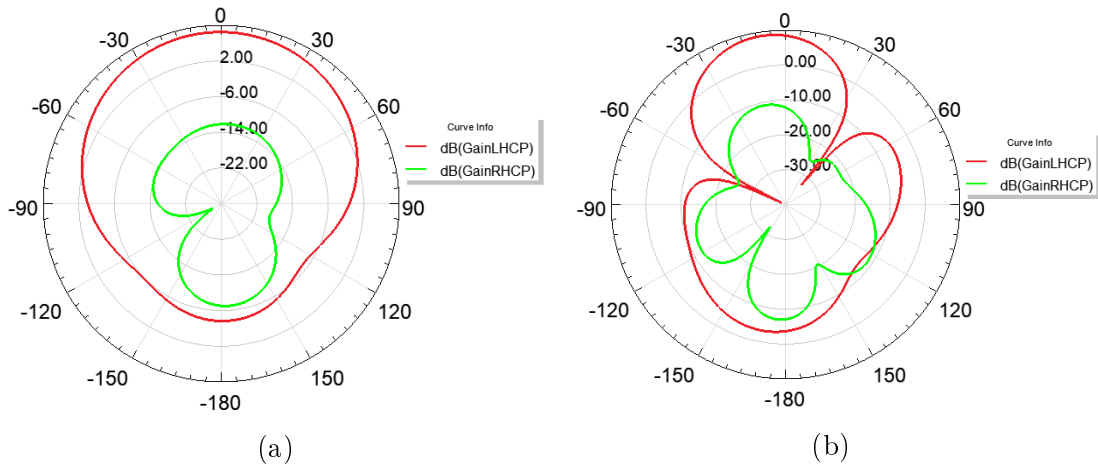
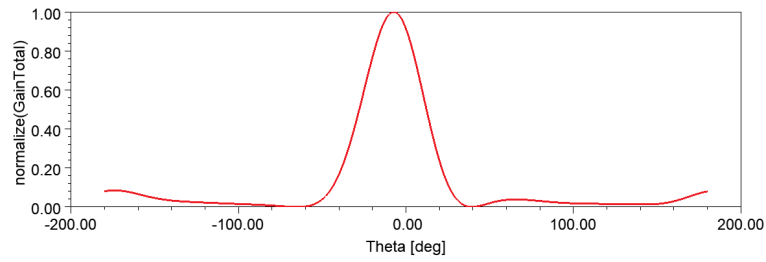


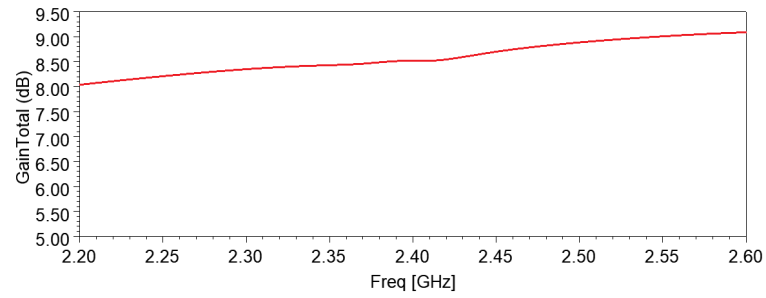
Figure 3.15: The gain of radiation pattern for antenna array (red line LHCP , green line RHCP)(a) xz plane (b) yz plane

The purpose of designing multiple elements of the individual square patch antenna is to obtain a higher gain compared to a gain achieved in the individual antenna, enabling the proposed energy harvesting system to pick up signals from long distances. Figure(3.16) shows the achieved total gain of the antenna array.

Figure(3.17)shows the radiation pattern in 3D and 2D for E and H plane. The efficiency obtained from the individual patch antenna at the operating frequency was 85%, while in the array design, the efficiency increased by 10% and became 95% as shown in the Figure(3.18).

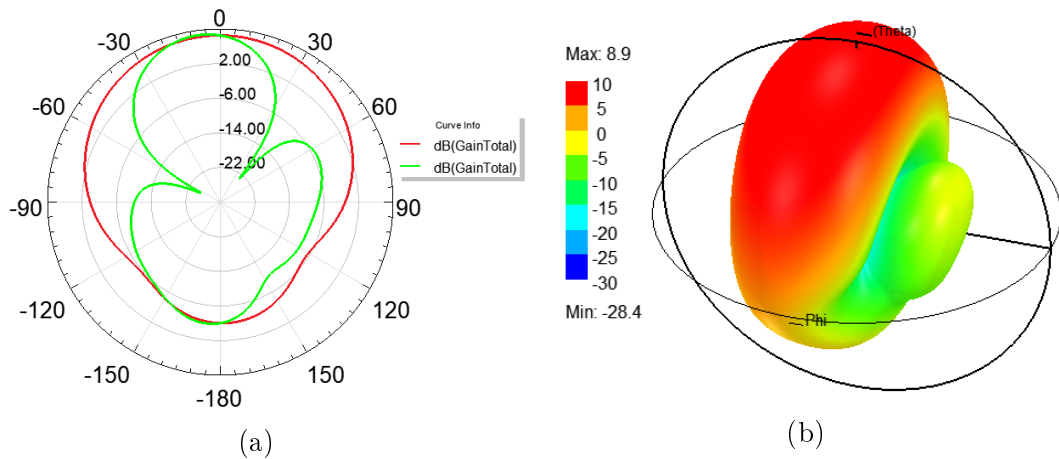


(a)



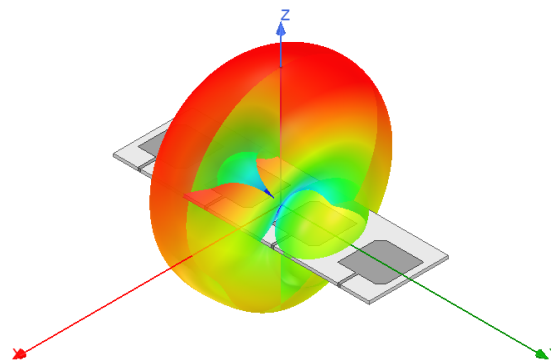
(b)

Figure 3.16: Simulated gain for square patch antenna array (a) The normalized total gain as function of theta angle (b) Gain total achieved for square patch antenna array VS frequency



(a)

(b)



(c)

Figure 3.17: The simulated radiation pattern for antenna, radiate at Z direction (a) 3D (b) 2D for two plane (c) Radiation pattern figured on the array structure

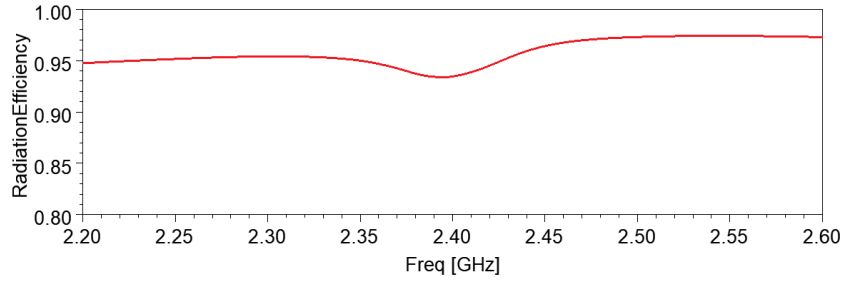


Figure 3.18: Radiation efficiency for single element

### 3.4 Simulation and Results for 4X4 Butler Matrix Design

The Butler matrix is simulated by using Keysight ADS software, at centre 2.4 GHz as an operating frequency and Rogers RT Duroid 6006 as substrate with 6.15 relative permittivity and thickness 1.7 mm. Also, it is matched to  $50 \Omega$ . Figure(3.19) shows the structure of the Butler matrix based on the conventional geometry of the Butler matrix which is shown in Figure(2.5).size configuration, it is unsuitable to integrating with the square patch antenna array designed in the previous section. The Butler matrix designed is a bulky In an attempt to reduce

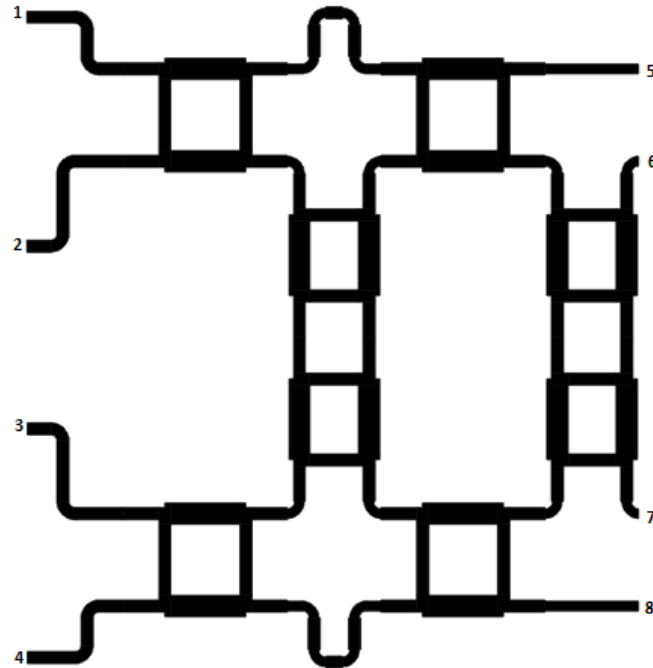


Figure 3.19: The butler matrix designed as a conventional geometry of butler matrix

the size of the Butler matrix, it is re-designed and optimized to obtain the simplest design, although small dimensions which have been realized. Figure(3.20) illustrates the improved copy after reducing one of the crossovers. Where the new Butler matrix consists of 4 hybrid branch line coupler, 2 phase shifters and one crossover, in addition to the feeding lines utilized to connect the antenna with the Butler matrix.

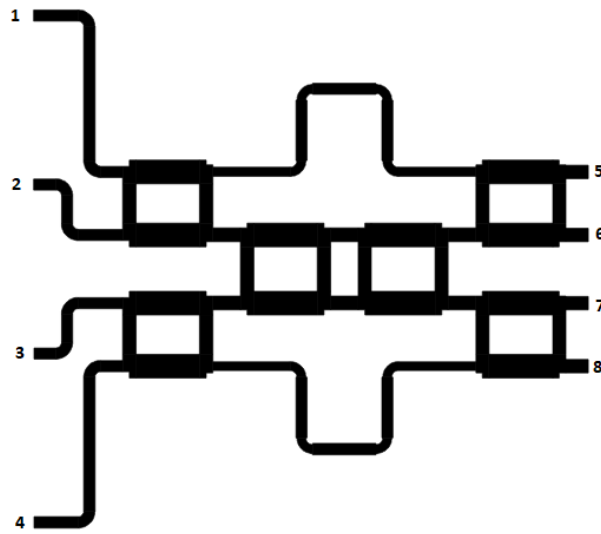


Figure 3.20: The optimized butler matrix designed

The Butler matrix design begins with the hybrid branch line coupler. The shape in the Figure(2.6) is used as a reference for the hybrid branch line coupler design. Parallel transmission lines are connected vertically once and horizontally in another, as shown in Figure(3.21) with impedance characteristics ( $Z_o$ ) equal to  $50\Omega$ . In order to get a 3dB branch line coupler that provides equal division of the magnitude amount between the two output ends and with a phase difference of  $90^\circ$ . Four feed lines per port in the hybrid branch line coupler dimensions are  $Z_1$  and  $\theta_1$ ,  $Z_1=Z_o$  and  $\theta_1= 45^\circ$ , as shown in Figure(3.21). The parallel transmission line, which is connected in horizontal with  $Z_2$  and  $\theta_2$ ,  $Z_2= Z_o/\sqrt{2}$  and  $\theta_2= 90^\circ$ .

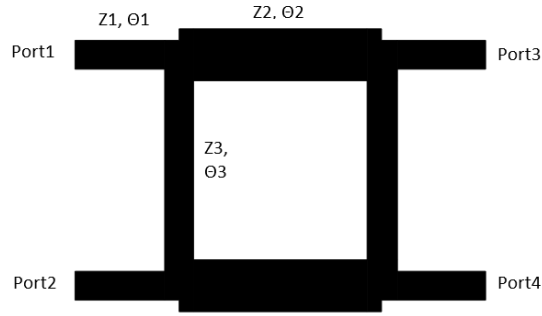
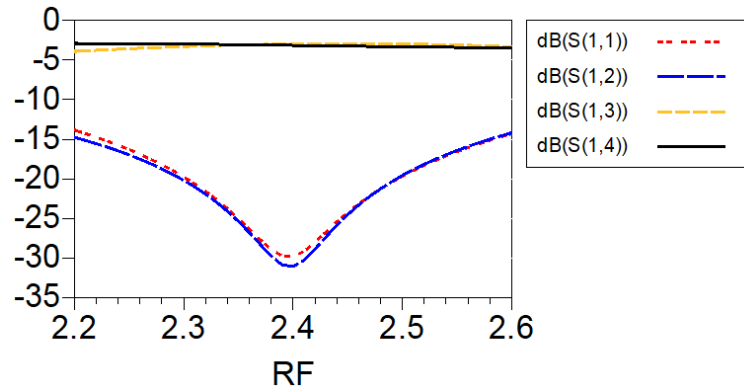
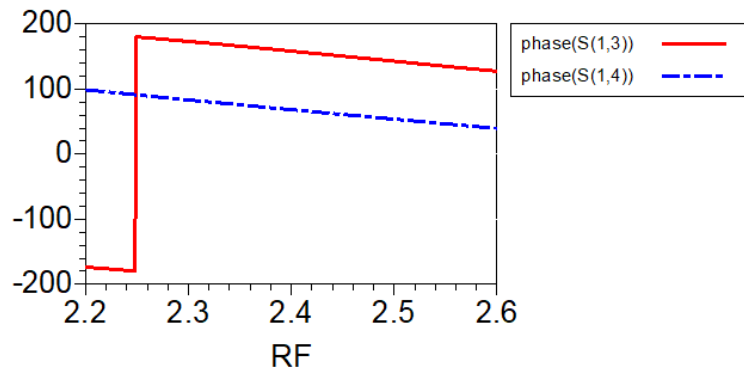


Figure 3.21: The Hybrid branch-line coupler designed

Thereafter the parallel transmission line, which is connected in vertical with  $Z_3$  and  $\theta_3$ ,  $Z_3=Z_o$  and  $\theta_3= 90^\circ$ . Figure(3.22) explains the HBLC designed results, which demonstrate a  $90^\circ$  phase difference between output ports and  $-5\text{dB}$  insertion loss that means maximum transfer from input to output ports, furthermore almost  $-30\text{dB}$  isolation loss at operating frequency.



(a)



(b)

Figure 3.22: Simulated results for the hybrid branch-line coupler designed (a) The insertion loss and isolation loss (b) The output phases

Crossover is the second component required for the Butler matrix design, the crossover can be obtained from merging two HBLC to pass the signal to the second stage as shown in Figure(3.23). Crossover has demonstrated successful per-

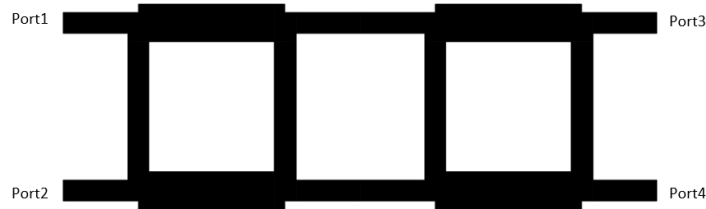
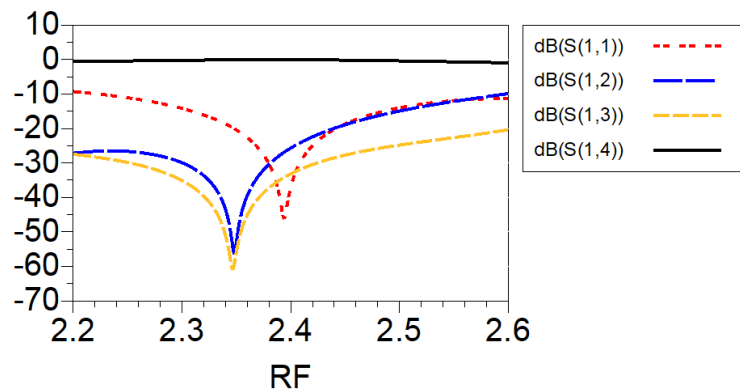
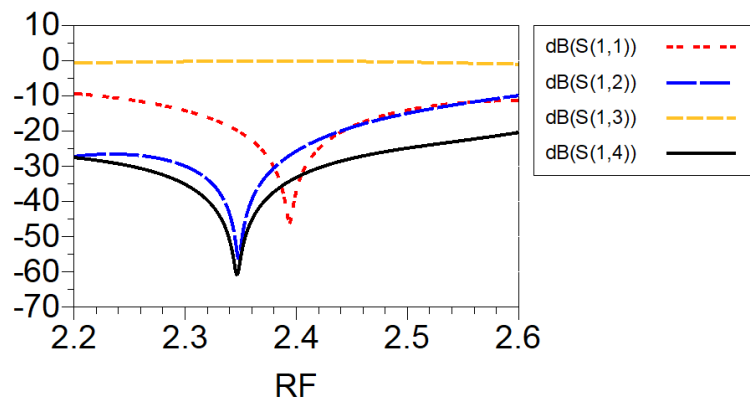


Figure 3.23: The crossover designed

formance as in Figure(3.24). When exciting port1 the 0dB insertion loss from port1 to port4 and less than -20dB isolation loss for all other ports. In the second case, When exciting port2 the 0dB insertion loss from port2 to port3 and less than



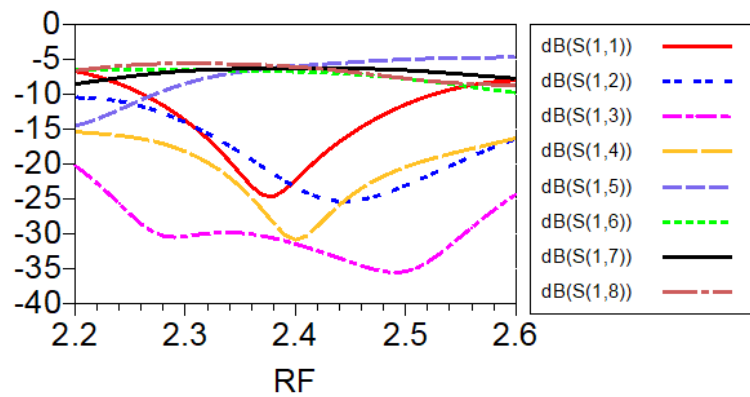
(a)



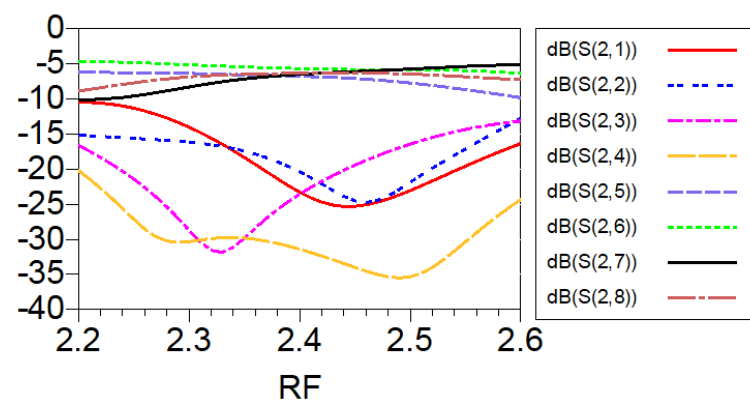
(b)

Figure 3.24: The insertion loss and isolation loss for crossover designed when excite (a) port 1 (b) port 2

-20dB isolation loss for all other ports. Also two phase shifter designed. After integrating the components of the Butler matrix shown in a Figure(3.20), where it consists of 8 ports, 4 of which are dedicated to the input of the RF power captured by the square patch antenna array, the other 4 ports on the opposite side are mapped to the outputs of the Butler matrix network, then they are connected to four rectifiers. Each rectifier will receive an RF power from a phase that differs from adjacent output ports. The magnitude of the power received from the rectifiers is 3 times more than the received signal, because of the accumulation process that occurs within the Butler matrix network. The magnitude in dB of isolation loss illustrated in Figure(3.25) is less than -20dB for all ports and that interpret there is no return loss also no mutual coupling between input and output ports.



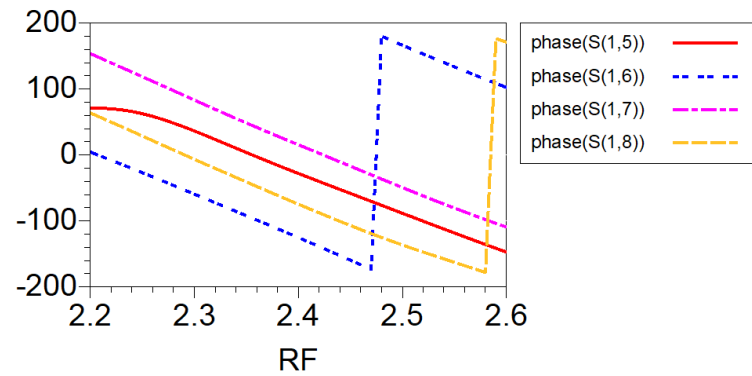
(a)



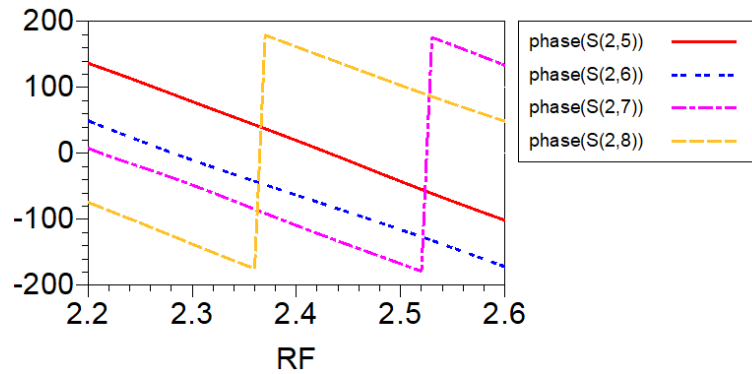
(b)

Figure 3.25: The insertion loss and isolation loss for a butler matrix designed (a) when excite ports one and four (b) when excite ports two and three

One of the significant features of the Butler matrix network is symmetric, where port1 is symmetrical with port4 and port2 is symmetrical with port3, so the results for all symmetrical ports are identical. The phase difference between output ports with various exciting input ports shown in Figure(3.26) when exiting port 1 and port 4 the phase difference is around  $45^\circ$  but this does not stand to obtain the same phase difference for port 2 and port3, although they still give the purpose to its design in this work.



(a)



(b)

Figure 3.26: The output phases for butler matrix designed (a) when excite ports one and four (b) when excite ports two and three

The progressive phase or the excitation angle is range from  $-180^\circ$  to  $180^\circ$  and for this range for each port has own angle by which the port is excited. The ph is a symbol for the progressive phase. Figure(3.27a) illustrates the RF power received in watts from the output ports as a function of the Theta angle.

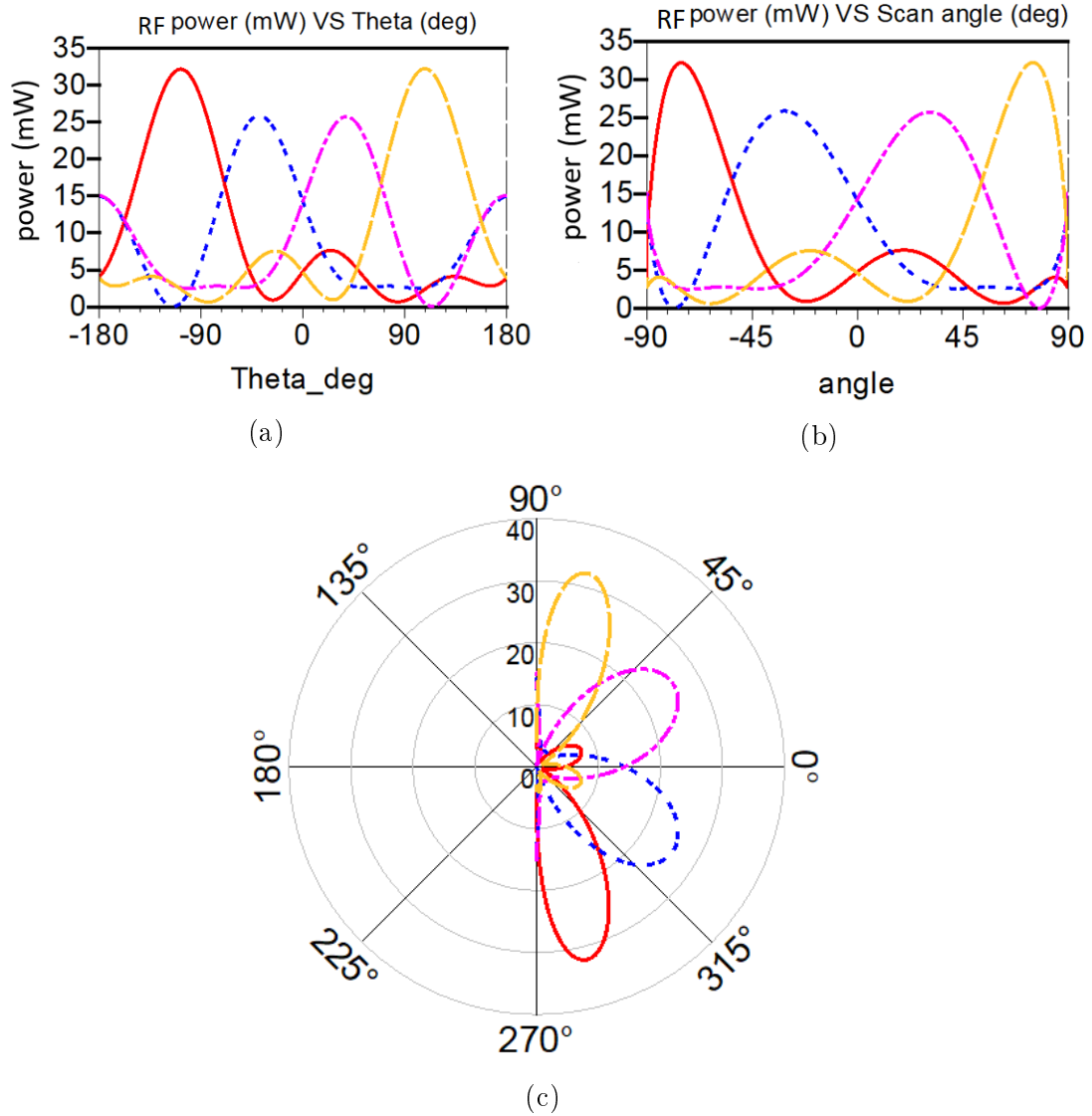


Figure 3.27: Output power simulated for port1(Red, solid line), port2(Blue, dash line), port3 (Pink, dot dash line), port4 (Yellow, long dash line) (a) The output power in mW as function to the excitation angle for butler matrix network (b) The output power in mW as function to the scan angle for design (c) polar plot for the radiation pattern VS output power in mW

In order to determine the beam scan angle (angle) for each output port by following equation:

$$angle = \sin^{-1}\left(\frac{ph\lambda}{2\pi d}\right) \quad (3.3)$$

Where d represents the distance between output ports. Figure(3.27b) shows the RF power received in watts from the output ports as a function of the beam

scan angle (angle), the angle range extends from  $-90^\circ$  to  $90^\circ$ . The 2D radiation pattern of output power to angle is present in Figure(3.27c). Table 3.2 shows the progressive phase difference for each port when the single input port is excited every time.

Table 3.2: The progressive phase difference and scan beam angle for output ports.

Port no.	Progressive phase	scan beam angle
5	$-108^\circ$	$-82^\circ$
6	$-40^\circ$	$-21.5^\circ$
7	$40^\circ$	$21.5^\circ$
8	$108^\circ$	$82^\circ$

The simulation results implemented in ADS software is plotted in Figure(3.28) with a clear explanation for BFN principle work. The signal injected in any input port will be distributed through the Butler network and arrive into all output ports. As observed, there is no mutual coupling and the designed circuit has high isolation.

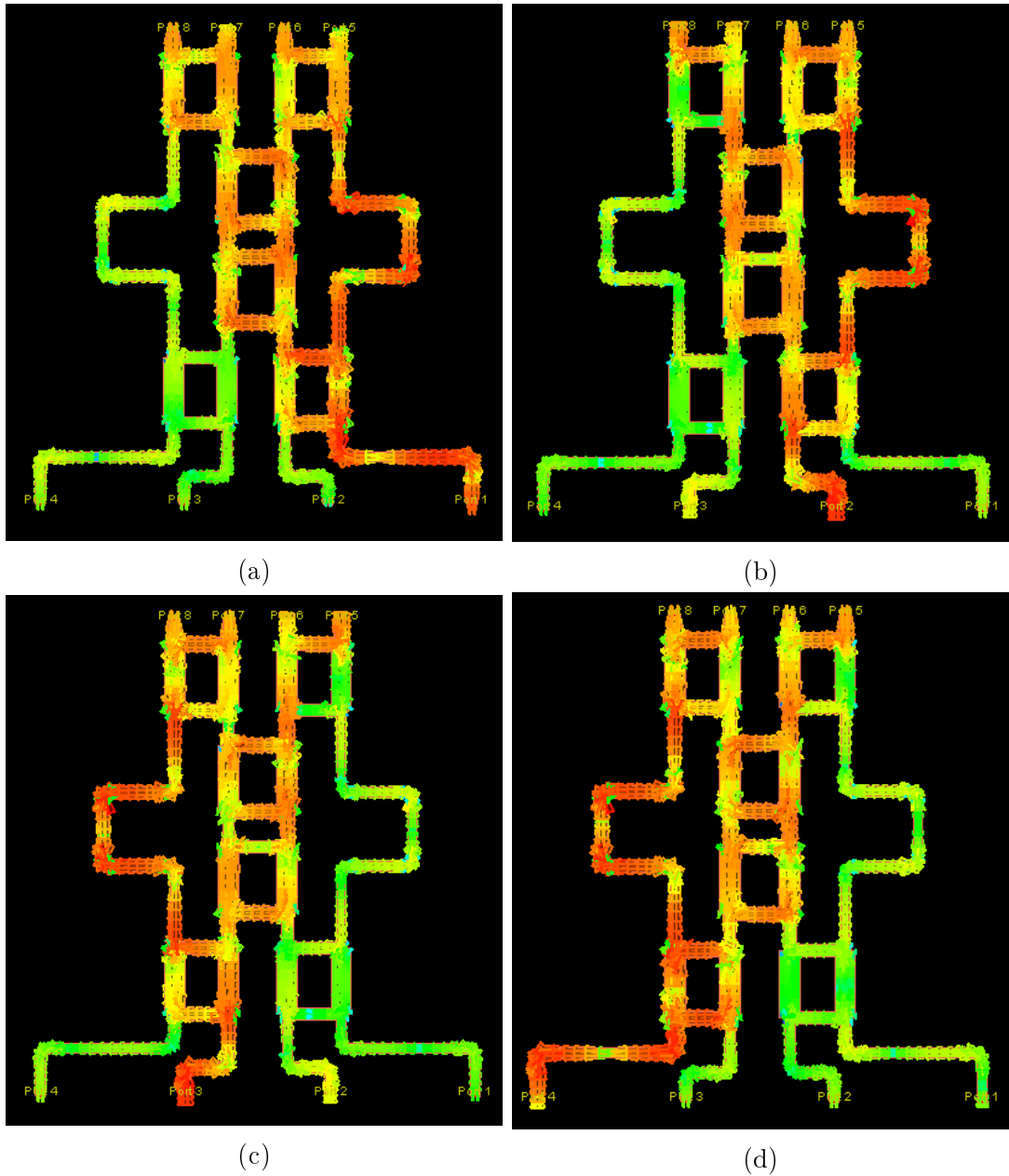
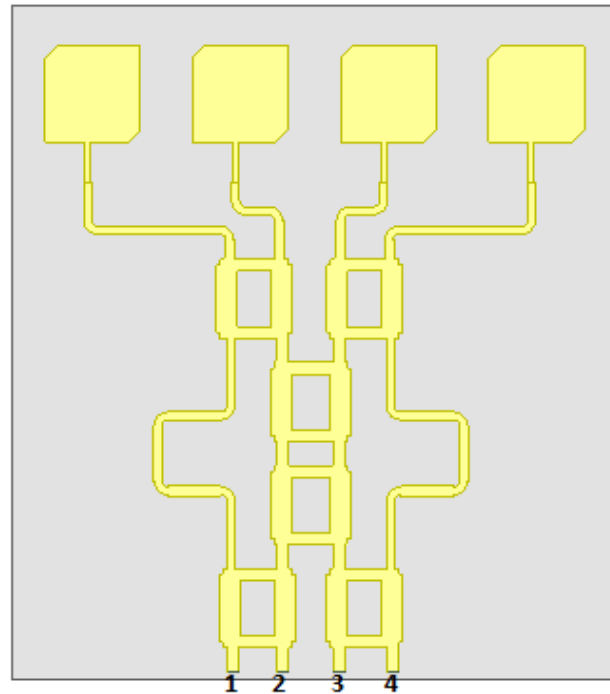


Figure 3.28: The simulation result for a butler matrix configuration designed in various case for excitation (a) excite the input port one (b) excite the input port two (c) excite the input port three (d) excite the input port four

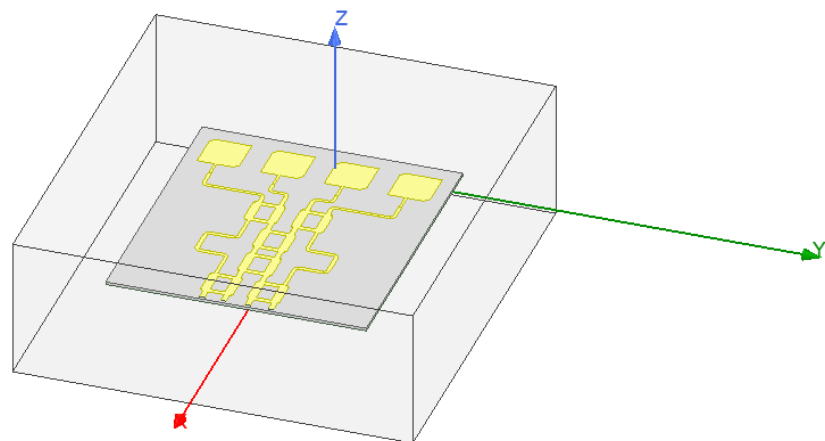
### 3.5 Multi-Beams Antenna Simulation and Results

In order to perform a multi beams antenna array, the antenna array is incorporated with a beamforming network as is shown in the Figure(3.29). An Ansoft HFSS simulator was utilized, and the Rogers RT Duroid 6006 substrate for all configuration with 6.15 relative permittivity and thickness 1.7 mm is adopted. The

operating frequency is 2.4 GHz as illustrated in the Figure(3.30a), with relatively high matching. The mutual coupling among all the output ports is less than -10dB as shown in Figure(3.30b).



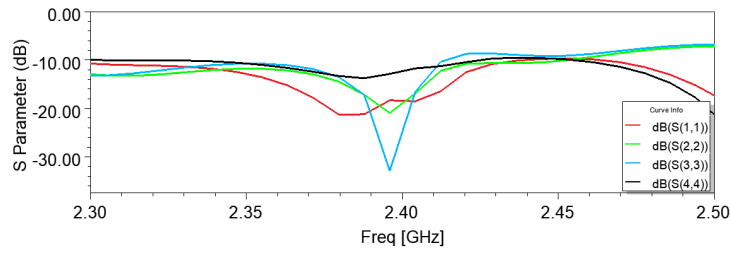
(a)



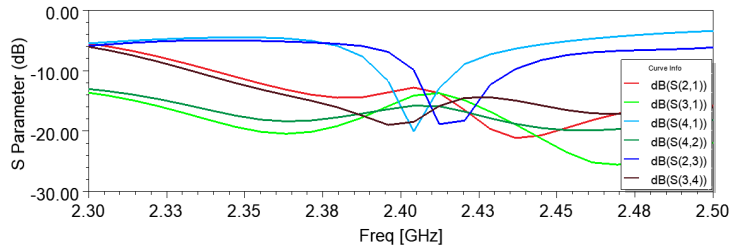
(b)

Figure 3.29: Multi-beams antenna designed (a) A configuration for BFN compacted with a square patch antenna array. (b) 3D view with radiation box

For each input port, the simulated 3D radiation pattern is displayed in Figure(3.31). The radiation patterns of the entire design (i.e., integrating the BFN and antenna array to each other), when each input port is excited at 2.4 GHz, are

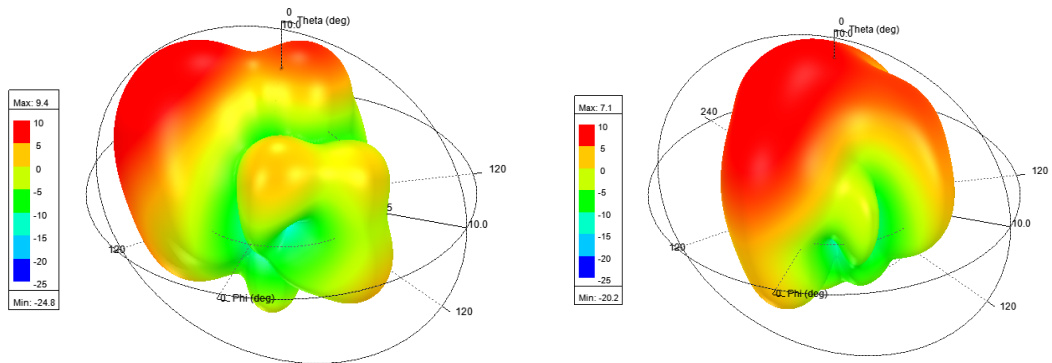


(a)



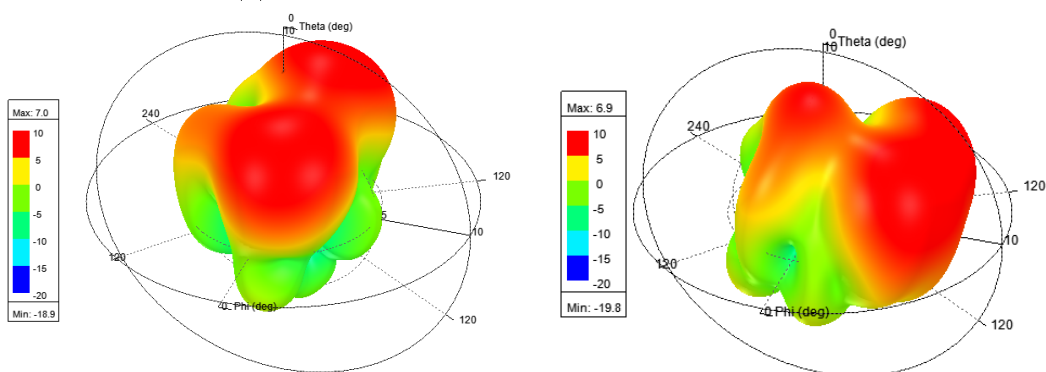
(b)

Figure 3.30: Simulated results for a multi-beams antenna (a) A reflection coefficient for compact design (b) A mutual coupling or reflection coefficient between adjacent ports



(a)

(b)



(c)

(d)

Figure 3.31: The 3D gain pattern simulated at 2.4GHz correspond to (a) Port1 (b) Port2 (c) Port3 (d) Port4.

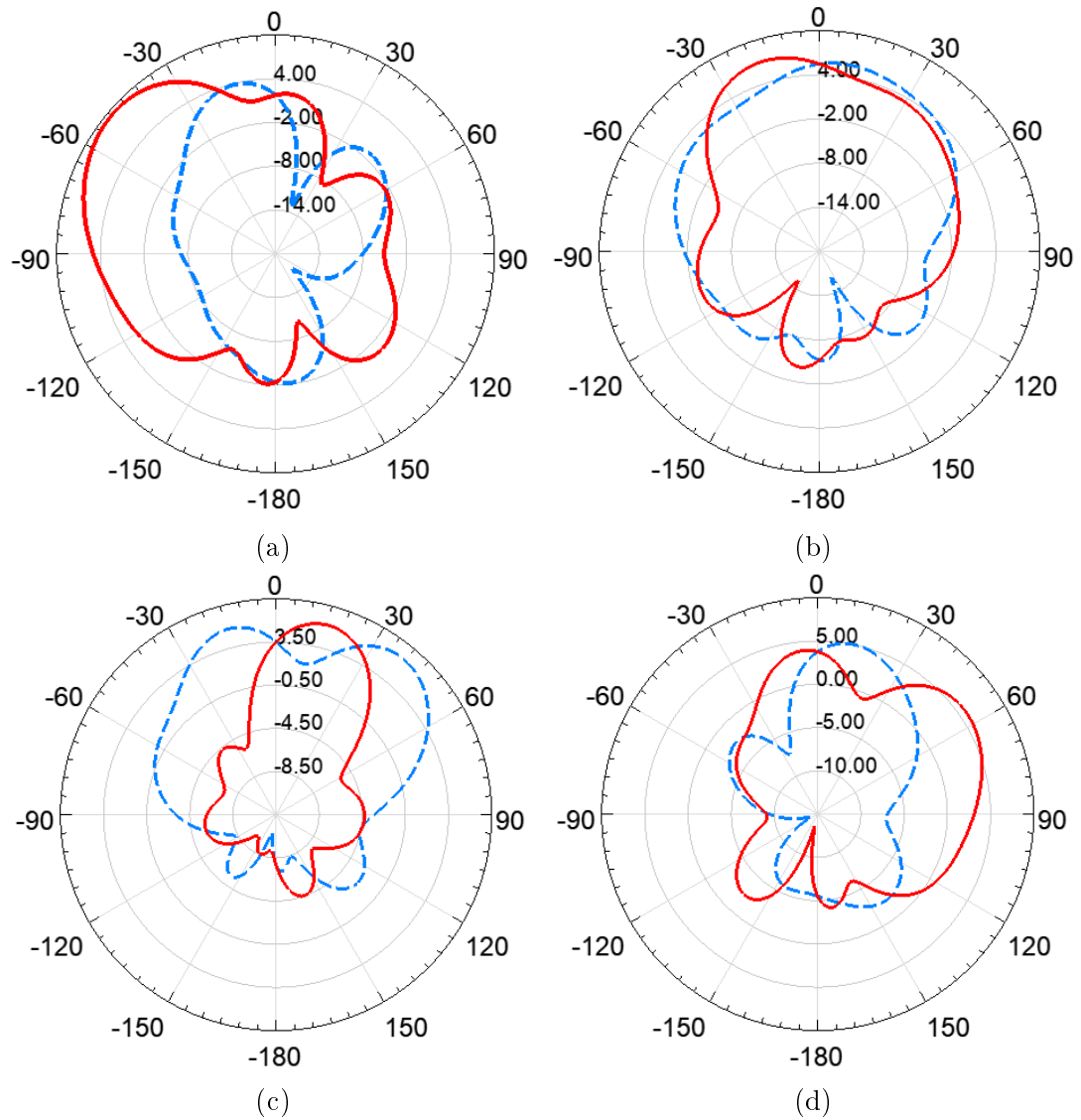


Figure 3.32: The simulated radiation pattern for incorporating design (BFN and antenna) at two plane, solid line for yz plane and dash line for xz plane. Results correspond to (a) Port1 (b) Port2 (c) Port3 (d) Port4.

illustrated in Figure(3.32). Radiation plots are carried out in xz and yz planes.

The plots demonstrates that the design can have a wide beam width and can cover a wide scan that will be useful for the energy harvesting systems to capture the RF signals from almost all directions. As shown in the Figure(3.33), the direction of the radiation propagation is able toward  $90^\circ$  plane, and in this plane, the lobes look quite different. The input ports were excited sequentially. As can be seen, the main direction is  $-50^\circ$ ,  $-16.5^\circ$ ,  $15.5^\circ$ ,  $56^\circ$  when excite port1, port2, port3 and

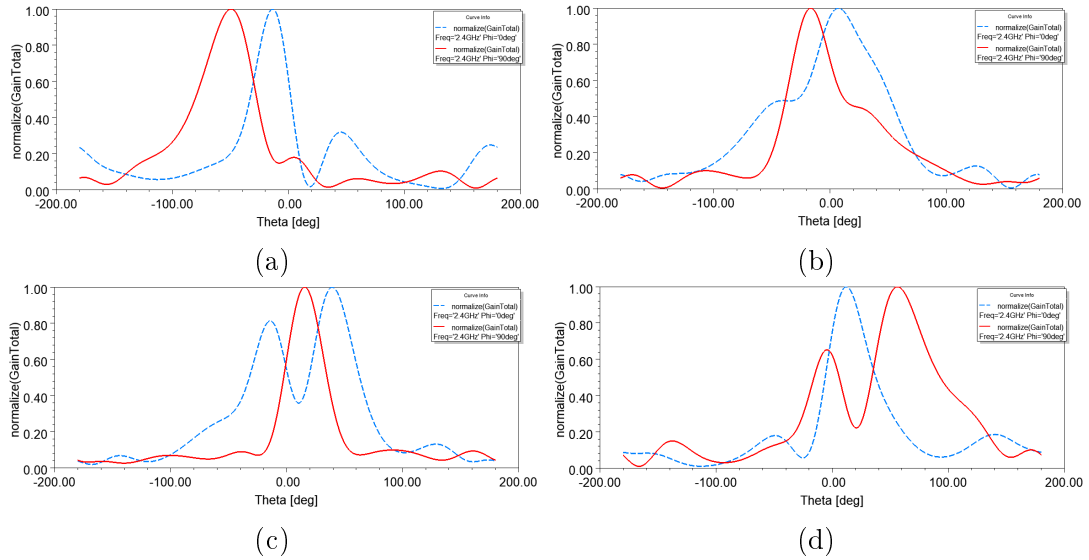


Figure 3.33: The simulated radiation pattern for incorporating design (BFN and antenna) cuts in main lobe at perpendicular plane correspond to (a) Port1 (b) Port2 (c) Port3 (d) Port4

port4, respectively.

Directivity for ports 1, 2, 3 and 4 is 6.8, 7.1, 8.3, 10.3 dB, respectively. Figure(3.34) illustrates the gain versus the scan angle (theta) when antenna elements of the array are fed directly or are fed by using the Butler matrix (BFN). There is very obvious discrepancy between the two curves overlaid on the same plot of Figure(3.34), because the BFN has inherent phase errors introduced by the internal structure.

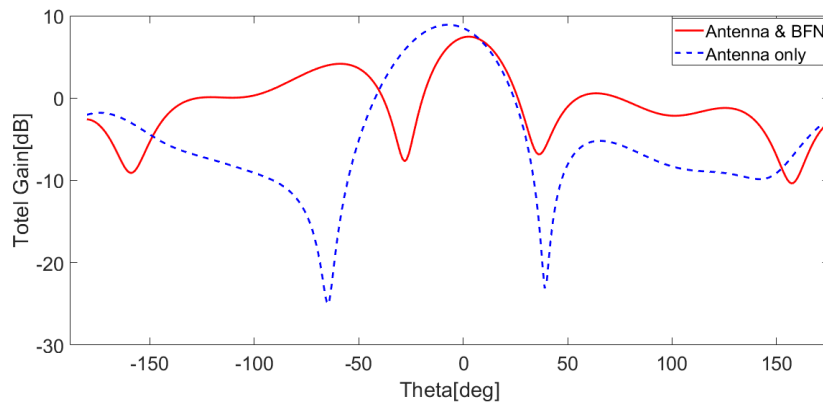


Figure 3.34: The simulated total gain in dB as function of theta for two case BFN and antenna design and only antenna array design

The comparison between the antenna present in this work and the related work is given in Table 3.3.

Table 3.3: The Comparison of the proposed antenna array single beam and some related designs

Ref.(year)	Freq.[GHz]	Gain(dB)	Polarization	Microstrip Type
[12] (2018)	2-3.1	2.73	LP	Single slot
[13] (2013)	1.8-2.1	9.9-13.3	LP	1X4 Yagi
[14] (2020)	0.91-2.55	5-8.3	LP	2X2 fractal
[15] (2019)	1.8-2.5	11	dual polarize	2X2 square
[16] (2020)	1.7-2.9	4.5	CP	single square loop
[17] (2015)	5.75	8.25	CP	2X2 disc
[18] (2016)	0.55-2.5	3-5.5	dual CP	single annular ring
[20] (2019)	multi-band	10.56	CP	4X2 square
[21] (2019)	10.4	9.8	CP	2X2 square
<b>Our work</b>	<b>2.4</b>	<b>9</b>	<b>CP</b>	<b>1X4 square</b>

## CHAPTER 4

### RECTIFIER CIRCUIT FOR RF ENERGY HARVESTING

#### 4.1 Introduction

In this chapter, describes rectifier circuit design for RF energy harvesting. In the begin, rectifier and matching circuits, discussion their selection, topology and mathematical model and simulation results. In addition to, Particle swarm optimization algorithm will be mentioned.

#### 4.2 Rectifier Selection

In order to design rectification structure (RF to DC signal) with high efficiency in RF energy harvesting systems. Several topologies of rectifiers had been checked with different types of Schottky diodes as a step to choose the better entire configuration in order to obtain the highest output DC power. The right diode element used with an appropriate topology, followed by the DC pass filter to prevent the DC propagation back into the rectifier, operate as a combination. The DC pass filter also operates to remove the fundamental frequency and harmonics signals produced by the nonlinear behavior of the diode to propagate forward into the output. The one reason that in the circuit mentioned above cannot harvest the large power is the difference in impedances of the input rectifier and the RF source. This causes the impedance mismatching. So, the matching circuit will be used to ensure the maximum power transfer from an antenna to a rectifier circuit.

As an operating frequency, 2.4 GHz is considered because of the widespread use of 2.4 GHz applications, less attenuation in free space. Moreover, it is free-licensed to use. In this thesis, the load resistance is varied under a range (0.4-1.4) K $\Omega$ , which provides the possibility to test the proposed work under different loads (i.e., different real-life applications).

#### 4.2.1 Diode Selection

The input power range considered in this thesis is from -5 dBm to 20 dBm (0.316 mw to 100 mw), thereby guaranteeing sufficient forward voltage above 0.3 V, to ensure a current to flows in the forward direction. The silicon P-N (Positive-Negative) diode has a forward voltage of 0.6 to 0.7 V, while the Schottky diode has a forward voltage of 0.15–0.45 V. Schottky diode is a lower forward voltage that allows higher switching speeds, the low energy can be harvested and better system efficiency can be obtained.

Schottky diode consists of a metal conductor layer, and the typical metal used is platinum, where the semiconductor layer (P or N) with a low barrier junction between two layers is realized. Figure(4.1) shows the equivalent circuit model of the Schottky diode, which is composed of  $R_s$  (series resistance) that represents the parasitic series resistance.  $R_s$  is a sum of loss due to semiconductor resistance, contact and jacket component loss, all lost as heat.  $R_j$  and  $C_j$  denotes resistance junction and capacitance junction, respectively.  $R_j$  and  $C_j$  are time-varying with applied voltage of a diode. There are different types of Schottky diode, a difference between them by the values of  $R_s$ ,  $R_j$  and  $C_j$  consequently, changing some features of diode e.g. frequency range, input power range and forward voltage (threshold voltage).

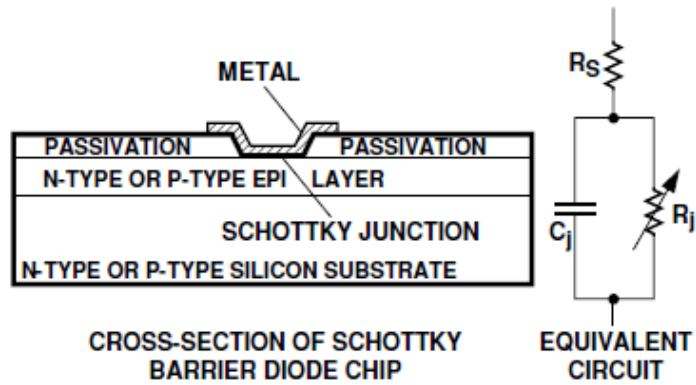


Figure 4.1: Schottky diode chip with the equivalent circuit at high frequency

In purpose of presenting the diode characteristics that are suitable for the desired application, the SPICE (Simulation Program with Integrated Circuits Emphasis) model is used to simulate commercial diode into the simulation circuit environment. The SPICE model is more appropriate than the vendor model to observe diode characteristics, while the other is typically similar to practical cases in the measurement. Schematic in Figure(4.2) is a construction of SPICE model diode with parasitic elements, and its performance analysis is monitored using the Advanced Design System (ADS) software from Keysight Inc. by the aid of HB (Harmonic Balance) solver, the parameter sweeps, AC power source and power meters for input and output. The diode is connected in series to capacitance and load, which are connected in parallel to each other to act as a DC pass filter. The simulation circuit is built in the absence of the matching.

Four types of the schottky diode from the HSMS-28XX (Hewlett-Packard Surface Mount Schottky) series are selected to choose one of them that is a compatible with our given application, as in Table4.1. The built-in ADS library for high-frequency diodes consist of 164 diodes from 7 manufacturers for the nonlinear

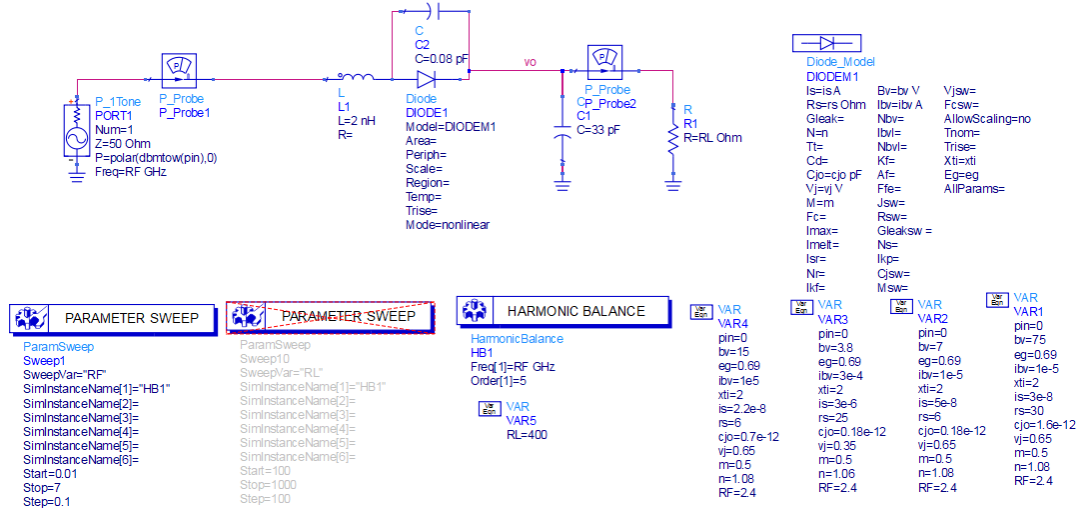


Figure 4.2: Schematic of the simulation diode in SPICE model at ADS software diode models , all these diodes differ between them by the small changes in main parameters of the diode (g.e., junction voltage  $V_j$ , saturation current  $I_s$ , diode quality factor  $n$ , breakdown voltage  $b_v$  etc.) as shows in Table4.1.

Table 4.1: A parameters of Schottky diode HSMS-28XX

Parameters	HSMS-280X	HSMS-282X	HSMS-285X	HSMS-286X
Frequency(GHz)	RF	RF	below 1.5	0.915-5.8
$R_s$ ( $\Omega$ )	30	6	25	5
$C_j$ (PF)	1.6	0.7	0.18	0.18
$V_j$ (V)	0.65	0.65	0.35	0.65
$V_f$ (mV)	0.41	0.34	0.15-0.125	0.25-0.35
n	1.08	1.08	1.06	1.08
$I_s$ (A)	3e-8	2.2e-8	3e-6	5e-8
$b_v$ (V)	75	15	3.8	7

The circuit examines by applying variable load, input power and frequency as shown in Figure(4.3). Figures(4.3c, 4.3a) shows the efficiency versus the input power and in Figures(4.3d, 4.3b) the output power versus a wide range of the input power. As can be seen, HSMS-285x has higher efficiency and higher output power at low input power below 5dBm. HSMS-280x has higher efficiency and higher output power at high input power above 25dBm. HSMS-282x and HSMS-286x both have high efficiency and high output power at a moderate range between

5 dBm to 25 dBm. Relatively a HSMS-282x requires higher input power than HSMS-286x, and it therefore has higher efficiency because the forward voltage is 0.34 V while 0.25-0.35 V is for HSMS-286x. Since the input voltage range adopted in this thesis starts at 0.316 V, the HSMS-286X is the best choice. The HSMS-286X diode has a high efficiency at an adopted range of the input power and load at the operating frequency, as seen in Figure(4.3).

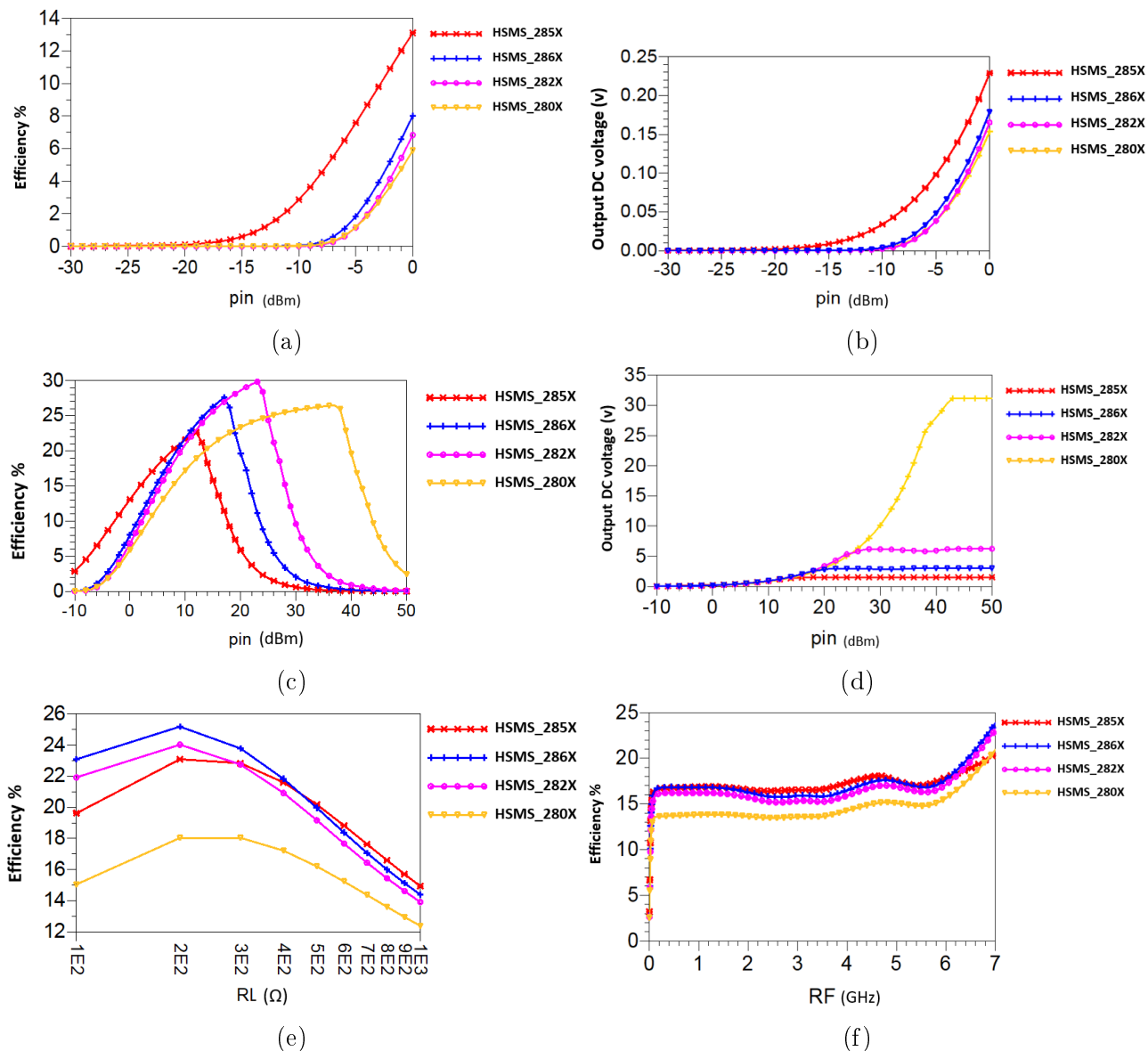


Figure 4.3: The simulation results show some types of diodes in terms of (a) comparison efficiency VS low transmitted power (b) Output voltage VS low transmitted power (c) comparison efficiency VS high transmitted power (d) Output voltage VS high transmitted power (e) comparison efficiency VS variable load resistance (f) comparison efficiency VS frequency

### 4.2.2 Diode Topology Selection

It is paramount to implement a diode circuit within the appropriate topology to obtain a sufficient output DC voltage compatible with the harvested power. There are multiple ways to implement RF energy harvesting rectifier circuits, and Figure(4.4) illustrates the most common topologies used in the previous works. The half-wave rectifier topology uses one diode connected in series and followed by a DC pass filter (shunt capacitor). A parallel single diode also used in single shunt rectifier topology, and a quarter-wave transformer utilizing between the diode and dc pass filter in order to reflect back the harmonic signals.

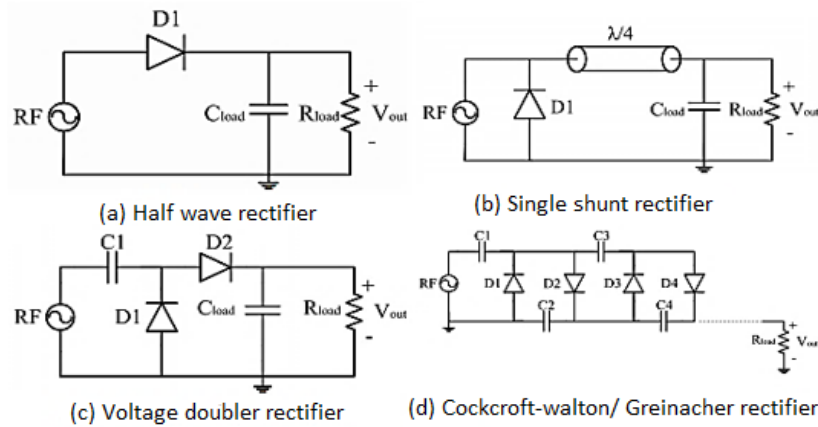


Figure 4.4: Various RF energy harvesting rectifier topologies

The voltage doubler is a combination of two topologies, shunt, and series. Hence, a double DC output power will be produced compared to the topologies with single diodes. Greinacher rectifier topology is a combination of two-voltage doubler topology that is means the power higher than a single voltage doubler but, at the expense of increasing complexity and losses for overall circuit. Consequently, a voltage doubler is a more appropriate topology to implement the rectifier circuit.

Three methods of topology are simulated in ADS software, voltage doubler, half-wave and shunt single. Figure(4.5) and Figure(4.6) clarify the comparison of the output DC voltage results from these circuits. As observed in the results, voltage doubler has a maximum output power, so the voltage doubler topology is adopted in this work.

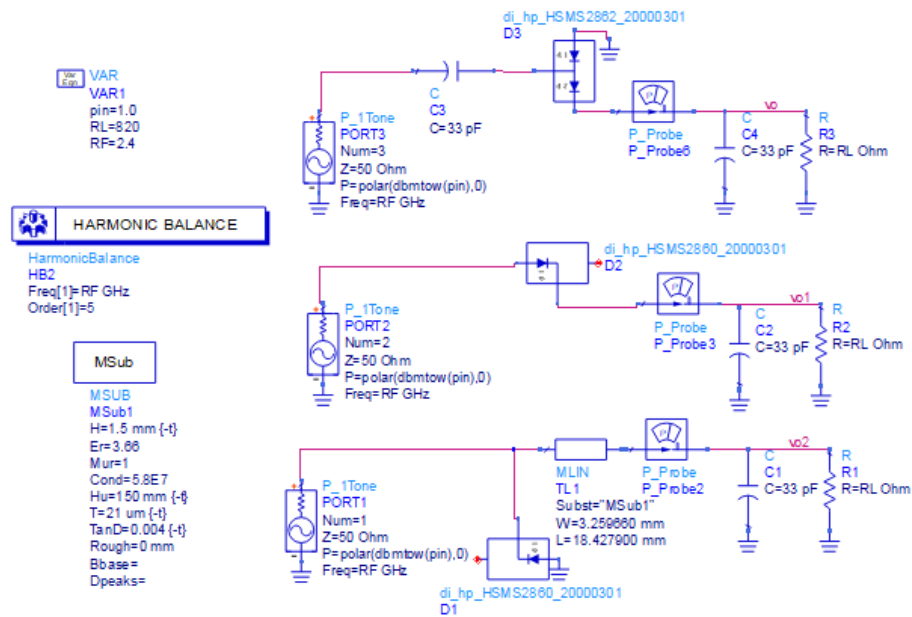


Figure 4.5: Schematic of the three methods of topologies by using HSMS-286X diode

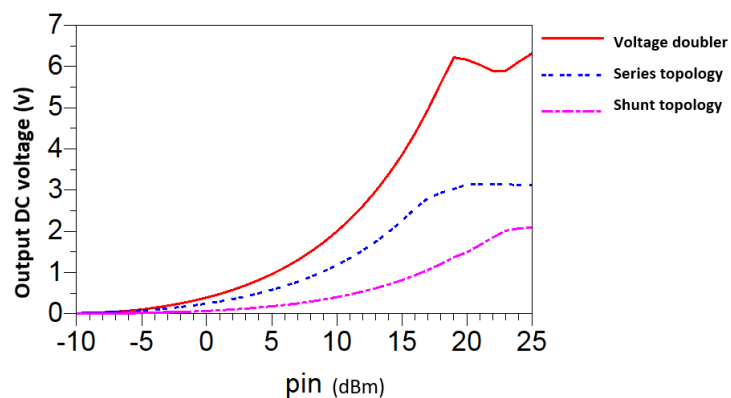


Figure 4.6: The comparison between output DC voltage for three methods of topologies by using HSMS-286X diode

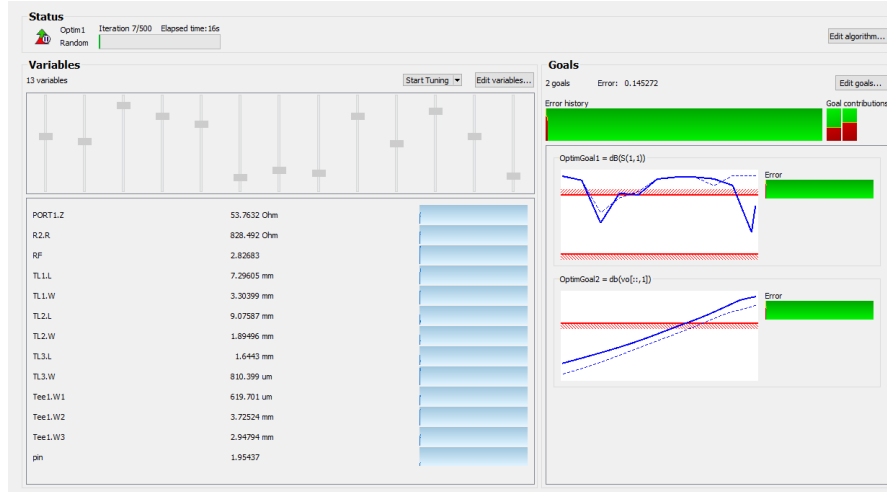


Figure 4.7: The optimization tool in ADS software

### 4.2.3 Mathematical Model for the Voltage Doubler Diode

As shown in Figure(4.8a) the block diagram of the typical voltage doubler rectifier, Schottky HSMS2862 is used. Figure(4.8b) shows the equivalent circuit of voltage doubler. Based on the assumptions presented in [53] for expression, the rectifying efficiency and the effective impedance of dual voltage are derived as follows.

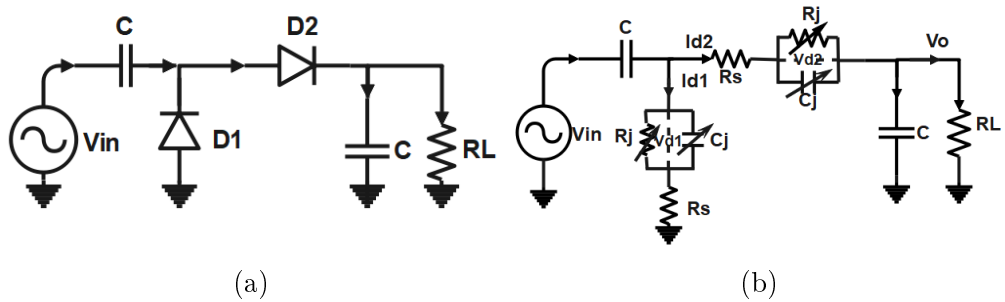


Figure 4.8: Rectifier equivalent circuit (a) voltage doubler rectifier (b) equivalent circuit of the voltage doubler.

$$V_1 = V_{dc1} + V_{in} \cos(\omega t) \quad (4.1)$$

$$V_2 = -V_{dc2} + V_{in} \cos(\omega t) \quad (4.2)$$

$V_1$  and  $V_2$  in equations (4.1) and (4.2) are RF waveform for diode1 and diode2,

respectively. For both diodes, the RF signal consists of DC output voltage ( $V_{dc}$ ) for each diode and fundamental frequency component ( $V_{in}COS(\omega t)$ ). As noted in equations (4.1),(4.2) the fundamental component signals are equal for both diodes because of the parallel connection between them.

$$V_{dc1} = -V_{dc2} = V_{dc}/2 \quad (4.3)$$

$V_{dc}$  is output DC voltage for voltage doubler circuit. The output voltage from each diode can be expressed as a following:

$$V_{d1} = \begin{cases} V_{d1dc1} + V_{d11}COS(\omega t - \Phi_1) & \text{D1 OFF} \\ V_f & \text{D1 ON} \end{cases} \quad (4.4)$$

$$V_{d2} = \begin{cases} V_{d2dc2} + V_{d21}COS(\omega t - \Phi_2) & \text{D2 OFF} \\ V_f & \text{D2 ON} \end{cases} \quad (4.5)$$

The phase delay between RF signal  $V_1$  and the DC signal  $V_{d1}$  can be represented by  $\Phi_1$ . Also,  $\Phi_2$  represents phase delay between  $V_2$  and  $V_{d2}$ . In equations (4.4) and (4.5), the terms  $V_{d11}, V_{d21}$  denote to the fundamental frequency component of junction voltage for diode1 and diode2. The value of  $V_{d1}$  has two probability according to a threshold voltage of diode model,  $V_f$  if input signal greater than threshold voltage and equal to the other value if it is lower than threshold voltage.  $V_f$  is a forward voltage drop of the diode. According to Appendix(A) in [54], since the junction capacitance of Schottky HSMS2862 diode is small ( $C_j = 0.18pF$ ), so, phase delay negligible because it will be very small, so that ( $\omega t = \theta$ ). The input impedance of the diode circuit can be defined as:

$$Z_D = \frac{V_{in}}{I_{in}} \quad (4.6)$$

The fundamental component of input current  $I_{in}$  can be calculated by applying Kirchhoff's current law as shown in Figure(4.8b).

$$I_{in} = I_{d1} + I_{d2} \quad (4.7)$$

$I_{d1}$ ,  $I_{d2}$  are complex values with real and imaginary parts of fundamental component that can be expressed as following:

$$I_{in} = I_{d1r} + I_{d2r} - j(I_{d1i} + I_{d2i}) \quad (4.8)$$

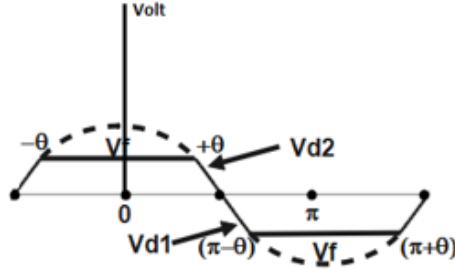


Figure 4.9: Time domain waveform of output voltage across diodes

Fourier series is used to analyze the fundamental frequency component current by taking full period as shown in Figure(4.9), where is given a time domain cosine waveform of output voltage across diodes. Thereby, the current across the diodes can written as following, [53]:

$$I_{d1r} = \frac{1}{\pi R_s} \left[ \int_{-(\pi-\theta)}^{\pi-\theta} (V_{in} - V_{d1}) \cos(\theta) d\theta + \int_{\pi-\theta}^{\pi+\theta} (V_{in} + V_f) \cos(\theta) d\theta \right] \quad (4.9)$$

$$I_{d1i} = \frac{1}{\pi R_s} \left[ \int_{-(\pi-\theta)}^{\pi-\theta} (V_{in} - V_{d1}) \sin(\theta) d\theta + \int_{\pi-\theta}^{\pi+\theta} (V_{in} + V_f) \sin(\theta) d\theta \right] \quad (4.10)$$

When the diode1 is ON to rectify signal ( $V_1$ ), the equation for the current flowing through series resistance ( $R_s$ ) is given below, where it is calculated by using Kirchoff's voltages law as following:

$$R_s \frac{dC_j V_{d1}}{dt} = V_{in} - V_{d1} \quad (4.11)$$

$$I_{d2r} = \frac{1}{\pi R_s} \left[ \int_{\theta}^{2\pi-\theta} (V_{in} - V_{d2}) \cos(\theta) d\theta + \int_{-\theta}^{\theta} (V_{in} - V_f) \cos(\theta) d\theta \right] \quad (4.12)$$

$$I_{d2i} = \frac{1}{\pi R_s} \left[ \int_{\theta}^{2\pi-\theta} (V_{in} - V_{d2}) \sin(\theta) d\theta + \int_{-\theta}^{\theta} (V_{in} - V_f) \sin(\theta) d\theta \right] \quad (4.13)$$

When the diode2 is ON to rectify signal ( $V_2$ ), the equation for the current flowing through series resistance ( $R_s$ ) becomes, calculated by using Kirchoff's voltages law as well.

$$R_s \frac{dC_j V_{d2}}{dt} = V_{in} - V_{d2} \quad (4.14)$$

By substituting equations (4.1), (4.2) into (4.11), (4.14), respectively, then they will be as

$$V_{in} - V_{d1} = V_{in} - V_{d2} = -R_s C_j w \sin(\omega t) \quad (4.15)$$

From (4.6)-(4.15), the input impedance of rectifier before diode breakdown can be derived as in equation(4.16), and the details explained in APPENDIX-A.

$$Z_D = \frac{\pi R_s}{(2\theta - 1) \sin(2\theta) + j(R_s C_j w)(2\pi - 2\theta + \sin(2\theta))} \quad (4.16)$$

The ratio of output DC power ( $P_o$ ) to input RF power ( $P_{in}$ ) in addition to power loss ( $P_l$ ) on the diode during one full period and after breakdown, determines a

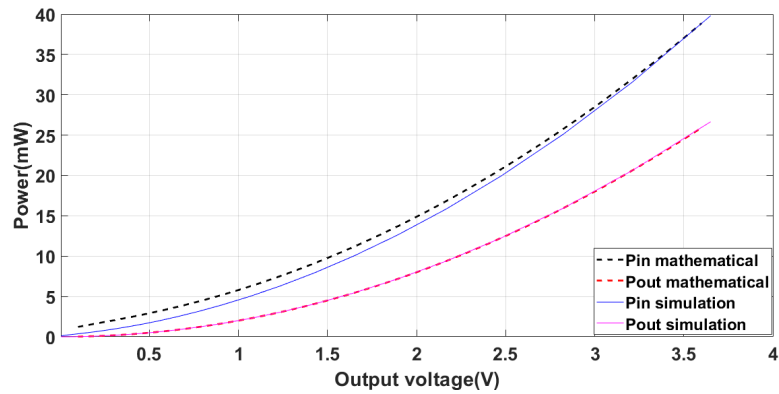
conversion efficiency value, efficiency derived as  $\eta$

$$\eta = \frac{P_o}{P_{in} + P_l} \quad (4.17)$$

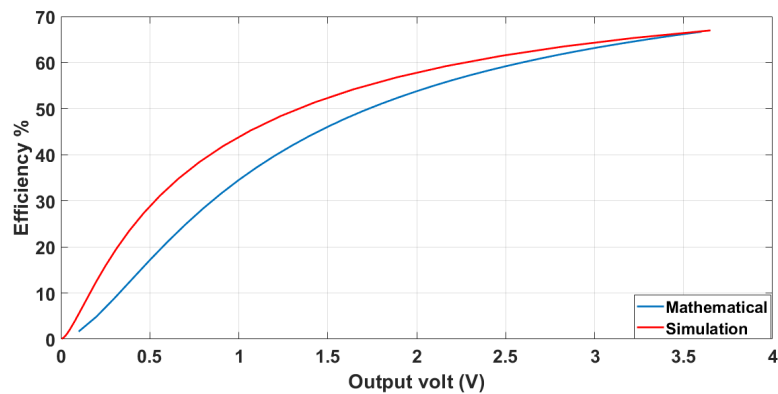
Power losses are assumed to be between all losses generated inside both diodes owing to threshold and reverse voltage, series resistance, junction capacitance. The output DC power is expressed as

$$P_o = \frac{V_{dc}^2}{R_L} \quad (4.18)$$

A comparison between simulation and calculation results of voltage doubler rectifier are clarify in Figure(4.10), where schottky diode HSMS-2862 is used at



(a)



(b)

Figure 4.10: Comparison between simulation and calculation results of voltage doubler rectifier as a function of (a) Output voltage with power (b) Efficiency with output voltage

simulation case. Figure(4.10a) illustrates the input and output power in (mW) with respect to the output voltage in volt. Figure(4.10b) illustrates the efficiency (%) with respect to the output voltage in volt.

### 4.3 Matching Circuit

The AC power is converted into DC power by the rectifier circuit. To ensure the maximum power transfer from an antenna to a rectifier circuit, the matching network must exist. The rectifier circuit depends primarily on diodes in their underlying design. The diodes have variable impedances with frequency, input power, and load resistance owing to their nonlinear characteristics. A special case of the matching network aiming to compress the variations in input impedance thereby enhancing the overall performance, is utilized. The compression network technique acts to reduce the impedance variation to maintain a good matching over wide ranges of frequencies, input powers, and load resistances.

#### 4.3.1 Single Branch Impedance Compression Network

A single-branch complex impedance compression network is simulated to demonstrate the compression in the input impedance variations of the microwave rectifier. By using only three transmission lines in the proposed design, the results show that compression of the input impedance has been noticeably obtained when the load and input power vary over wide ranges. Figure(4.11) shows the schematic of the single branch ICN. It consists of three main parts, open-ended stub with an impedance characteristics  $Z_{o1}$  and electrical length  $\theta_1$ , short-ended stub with an impedance characteristics  $Z_{o2}$  and electrical length  $\theta_2$ , and a transmission line with an impedance characteristics  $Z_{o3}$  and electrical length  $\theta_3$ . They are connected in parallel.  $Z_D$  represents the variable load, but in the real-life application this vari-

able load is active microwave circuit such as power amplifier, low noise amplifier, mixer, rectifier, etc. All these circuits contain nonlinear electronic elements such as transistors and diodes where their internal impedances vary with RF power, frequency and loads.  $Z_{in}$  denotes the compressed impedance.

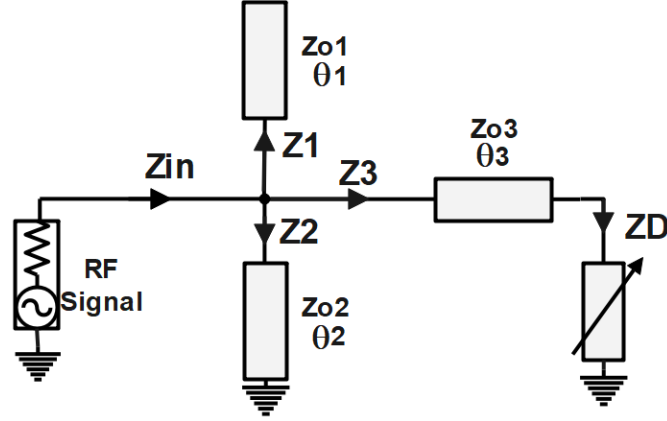


Figure 4.11: Schematic of single branch impedance compression network (ICN) proposed for RF energy harvesting system

After capturing the RF signals from space, they will travel through the ICN to reach the  $Z_D$ .  $Z_3$  acts to compress the  $Z_D$  but it has a high mismatch.  $Z_1$  and  $Z_2$  maintain the compression and match the input impedance. Figure(4.12) displays different impedances on the Smith chart. As can be seen, the input impedance is compressed and matched. The ICN circuit designed in this work can perform both compression and matching by the same circuit. Thus, it is a very compact and simple design as well. The circuit is designed and simulated using the ADS to come up with the final values for the proposed circuit. The  $Z_{o1}$ ,  $Z_{o2}$ , and  $Z_{o3}$  are  $20.2\Omega$ ,  $51.3\Omega$ , and  $9.85\Omega$ , respectively, while  $\theta_1$ ,  $\theta_2$ , and  $\theta_3$  are  $6.45^\circ$ ,  $13.75^\circ$ , and  $28.78^\circ$ , respectively.

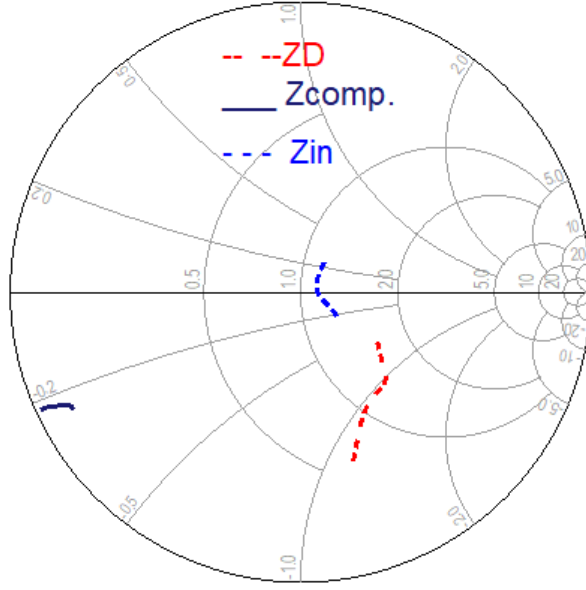


Figure 4.12: Simulated impedances of the ICN at three reference planes as a function of the wide input range, on the Smith chart

#### 4.3.2 Mathematical Model for the Single Branch Impedance Compression Network

By virtue of [46], the mathematical model of the ICN can be derived as in the following. The input impedance of the open-ended stub is:

$$Z_1 = jZ_{o1}\cot(\theta_1) \quad (4.19)$$

To obtain the compression, electrical lengths of stubs should obey the role  $\theta_1 = 90^\circ - \theta_2$ , accordingly:

$$Z_1 = jZ_{o1}\tan(\theta_2) \quad (4.20)$$

$$Z_2 = -jZ_{o2}\tan(\theta_2) \quad (4.21)$$

$Z_3$  is given as [46]:

$$Z_3 = Z_{o3} \frac{Z_D + jZ_{o3}\tan(\theta_3)}{Z_{o3} + jZ_D\tan(\theta_3)} \quad (4.22)$$

where  $Z_D$  is assumed to be complex.

$$Z_D = R - j * X \quad (4.23)$$

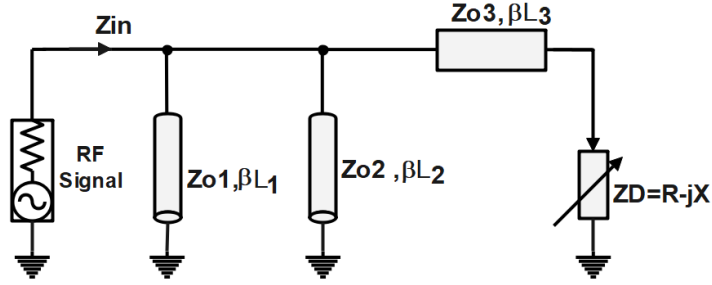


Figure 4.13: Equivalent circuit design for signal branch impedance compression network

$Z_D$  is the rectifier impedance. The rectifier circuit consists of a voltage doubler diode with variable resistance load. From Figure(4.13), which shows the equivalent circuit of the single branch ICN circuit designed, the connection between stubs can be written as following:

$$Z_{in} = Z_1 || Z_2 || Z_3 \quad (4.24)$$

The input impedance variations range decreases when variations of the input power and load are the main goal to design compression network. By substituting the equations (4.20), (4.21), and (4.22) into (4.24), and the details explained in APPENDIX-B, it leads to:

$$Z_{in} = \frac{Z_D + jZ_{o3}\tan(\beta L_3)}{\left(1 - \frac{Z_{o3}(Z_{o1}+Z_{o2})\tan(\beta L_3)}{Z_{o1}Z_{o2}\tan(\beta L_2)}\right) + jZ_D\left(\frac{\tan(\beta L_3)}{Z_{o3}} + \frac{(Z_{o1}+Z_{o2})}{Z_{o1}Z_{o2}\tan(\beta L_2)}\right)} \quad (4.25)$$

Where as shown in Figure(4.13) the  $\beta L_1$ ,  $\beta L_2$  and  $\beta L_3$  represents to the electrical lengths  $\theta_1$ ,  $\theta_2$  and  $\theta_3$ , respectively.

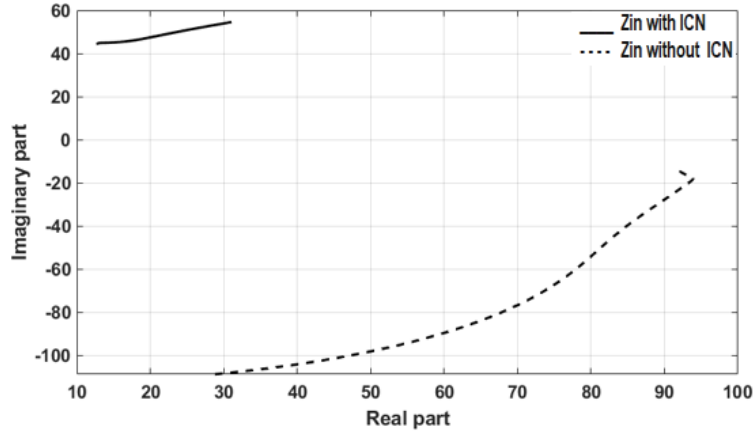


Figure 4.14: The variation range of input impedance of diode impedance comparing with mathematical compressed impedance results after utilized of single branch ICN proposed

As shown in Figure(4.14), the real part of  $Z_D$  is assumed to vary from 30  $\Omega$  to 94  $\Omega$ , while its imaginary part varies from -100  $\Omega$  to -20  $\Omega$ . These variations are wide. After adding the ICN, the real part varies from 14  $\Omega$  to 30  $\Omega$  and the imaginary part varies from 45  $\Omega$  to 57  $\Omega$ .

#### 4.4 Implementation of the Single Branch Rectifier Based on ICN

Single branch rectifier based on impedance compression network at 2.4 GHz is designed and optimized using keysight ADS software from Agilent technologies. Taking into account, the nonlinear characteristics of rectifier diode, Large Signal Scattering Parameter (LSSP) and Harmonic Balance (HB) employed for the evaluation of the reflection coefficient, input impedance and conversion efficiency under input power from -5 dBm to 20 dBm and load resistance from 400  $\Omega$  to 1400  $\Omega$ . The Roger-RO3010, with a thickness of 0.15 mm, is selected. Figure(4.15) shows the overall rectifier circuit designed in this thesis based on single branch ICN.

As shown in Figure(4.16) the TL1, TL6, TL10, TL11, TL13, TL14 are the transmission lines that have no noticeable effect on the circuit. Also, TL5, TL9,

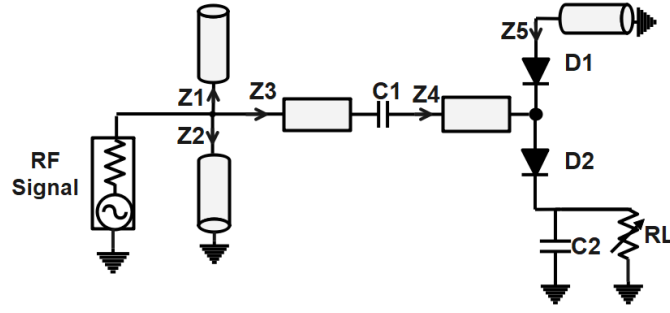


Figure 4.15: The whole proposed rectifier circuit based on the ICN

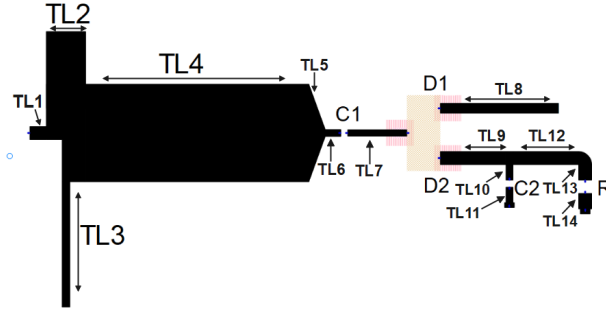


Figure 4.16: Configuration of the single branch rectifier based on (ICN)

Table 4.2: Dimensions of the proposed rectifier, unit:mm

TL	W	L
TL1	0.2	0.25
TL2	0.6	0.8
TL3	0.12	1.9
TL4	1.48	3.4
TL5( Taper)		0.25
TL6, TL10, TL11	0.11	0.24
TL7	0.1	0.9
TL8	0.15	1.8
TL9, TL12	0.2	1
TL13, TL14	0.2	0.24

TL12 are transmission lines but have a little tuning effect on the overall performance of the design, while TL7 and TL8 have a big effect on overall performance. Table4.2 illustrates dimensions of the 2.4 GHz single branch rectifier based on ICN for schematic simulation

#### 4.4.1 Rectifier Design

As shown in the Figure(4.8b), the equivalent diode circuit is composed of three elements,  $R_s$ ,  $C_j$  and  $R_j$ . The rectification performance depends on all elements of the equivalent circuit of the diode mentioned above when frequency or junction capacitance increases, the  $R_j$  will be shorted out and RF energy diverted to  $R_s$  where it is converted into heat thereby reducing the output voltage [55]. The single-stage full-wave rectifier (voltage doubler rectifier topology) is used. According to the schematic shown in Figure(4.15), the rectifier design consists of HSMS2862 Schottky diode, two Murata (where Murata is an electronic component library in ADS) capacitors of 33pF and a variable resistance load. The DC pass filter where placed after D1 is composed of capacitor C1 in parallel with the DC output load. The filtering capacitor will pass only the DC signal and suppress of the fundamental signal and its harmonics. The transmission line TL7 with a characteristic impedance  $Z_4$  achieve a good match between dc block capacitor and diodes.

#### 4.4.2 The Proposed ICN Design

The configuration of the proposed design with true microstrip transmission lines is shown in Figure(4.16). TL2, TL3 and TL4 represent the entire ICN circuit. TL4 is employed to compress the variations of input impedance as small as possible. TL2 and TL3 are optimized to match the compressed impedance with diode impedance. When the input power is varied from -5dBm to 20dBm according to simulation results, the input impedance of the rectifier varies from  $(12.852-j*53.395) \Omega$  to  $(78.537-j*31.437) \Omega$ . Inserting the ICN circuit into the rectifier circuit will produce compressed input impedance varies from  $(65.19-j*53.395) \Omega$  to  $(46.668+j*24.575) \Omega$ , as shown in Figure(4.17a).

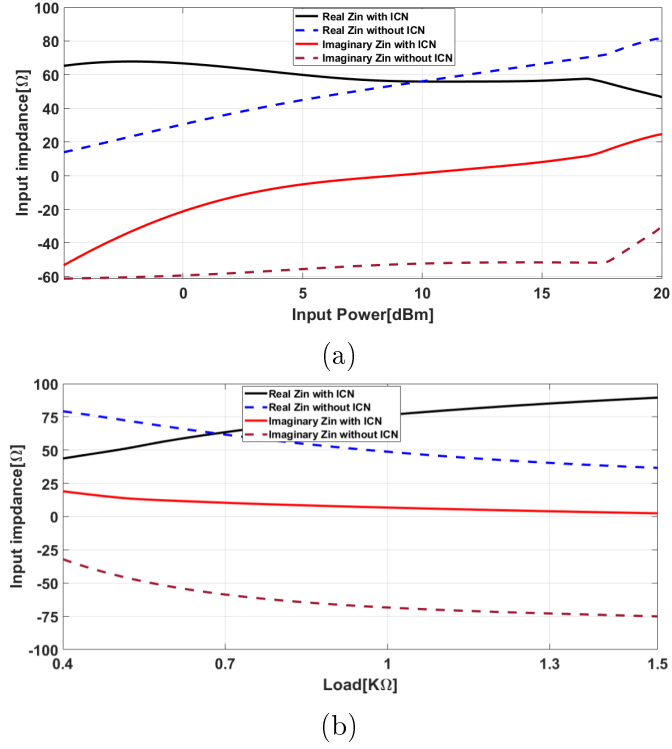


Figure 4.17: Input impedance variations with and without ICN as a function of (a) Input power (b) Load

Also, the proposed circuit is designed under an output load ranging from 400  $\Omega$  to 1400  $\Omega$  and the input impedance of the rectifier without ICN circuit varies from  $(79.224-j*32.029) \Omega$  to  $(36.68-j*75.029) \Omega$ . By using the proposed ICN circuit has got compressed input impedance ranging from  $(43.714+j*19.066) \Omega$  to  $(89.499+j*2.498) \Omega$  as shown in Figure(4.17b). The proposed ICN improve the RF-DC conversion efficiency as shown in Figure(4.18) because it improves the impedance matching at an operating frequency under wide input power range and with the variable output load resistance.

As can be seen in Figure(4.19), the ICN has a significant ability to compress the input impedance variation. The impedance variations confine inside a small region of impedances. This is a clear evident that ICN proposed design is able to

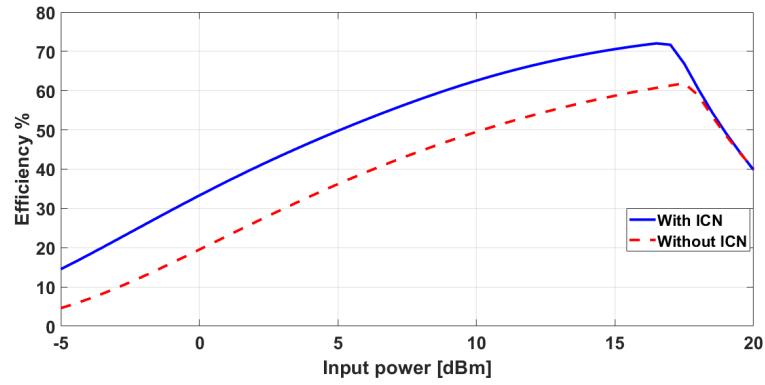


Figure 4.18: Comparison of the rectifier efficiency with and without using the proposed ICN

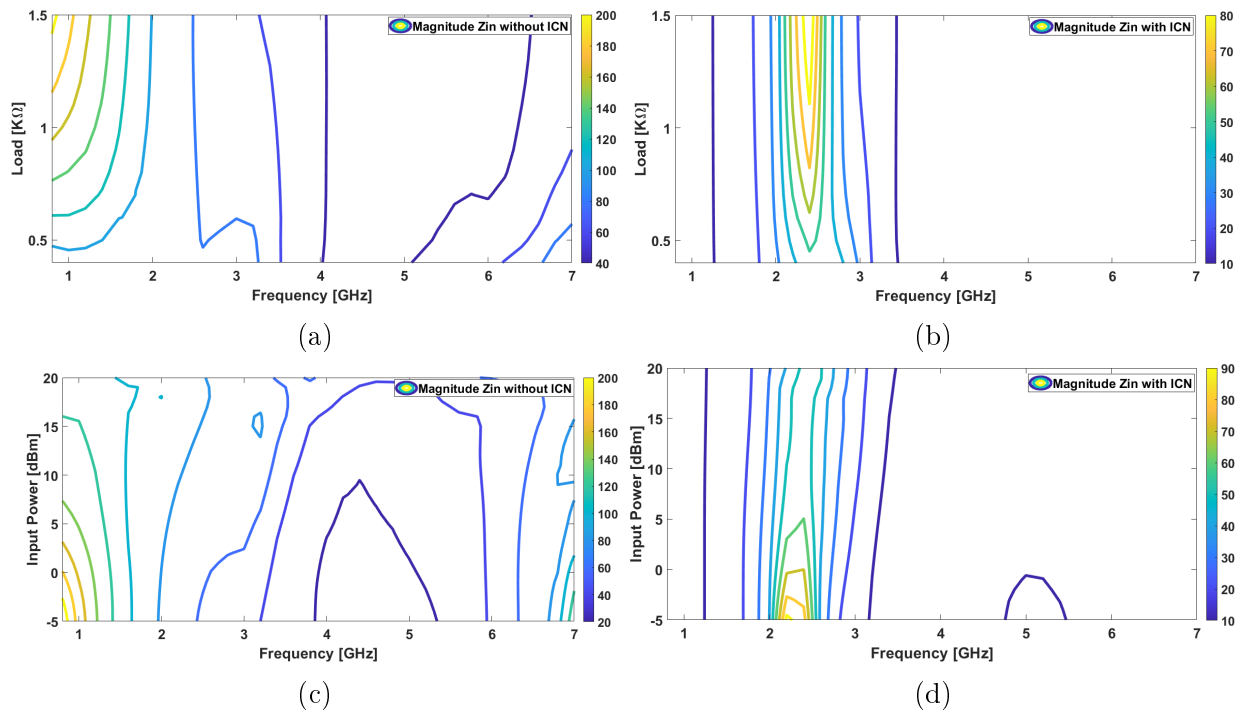


Figure 4.19: Input impedance as a function of load and frequency for the proposed rectifier circuit (a) without ICN (b) with ICN. Input impedance as a function of input power and frequency for the proposed rectifier circuit (c) without ICN (d) with ICN

compress the large variation in impedances to small variations. To have fair comparison, someone can see the difference in the values range as indicated in color map for each plot in Figure(4.19). The color bar shows the magnitude of input impedance before compression at Figure(4.19a) and Figure(4.19c) range from 20 to 200  $\Omega$ , while at Figure(4.19b) and Figure(4.19d) the color bar shows the magnitude of input impedance after compression range from 10 to 90  $\Omega$ .

These figures are plotted for the input impedance with and without the ICN in proposed design. The reflection coefficient (i.e., the scattering parameter S11) evaluates the reflected power from the rectifier circuit to the antenna, which is an essential parameter to evaluate the performance of the matching impedance network. Figure(4.20) illustrates the simulated S11 of the single branch rectifier based on ICN. Figure(4.20a) illustrates the S11 as a function of the input power and load. The color bar shows the return loss in dB, range from below -10 dB to -26 dB. As can be observed, the rectifier is well matched for wider ranges of the input power and load. The reflection coefficient S11 extends from -14 dB to -26 dB over wider ranges of the input power and load which are (-2 to 19) dBm and (400 to 1400)  $\Omega$ , respectively. The operating central frequency is 2.4 GHz.

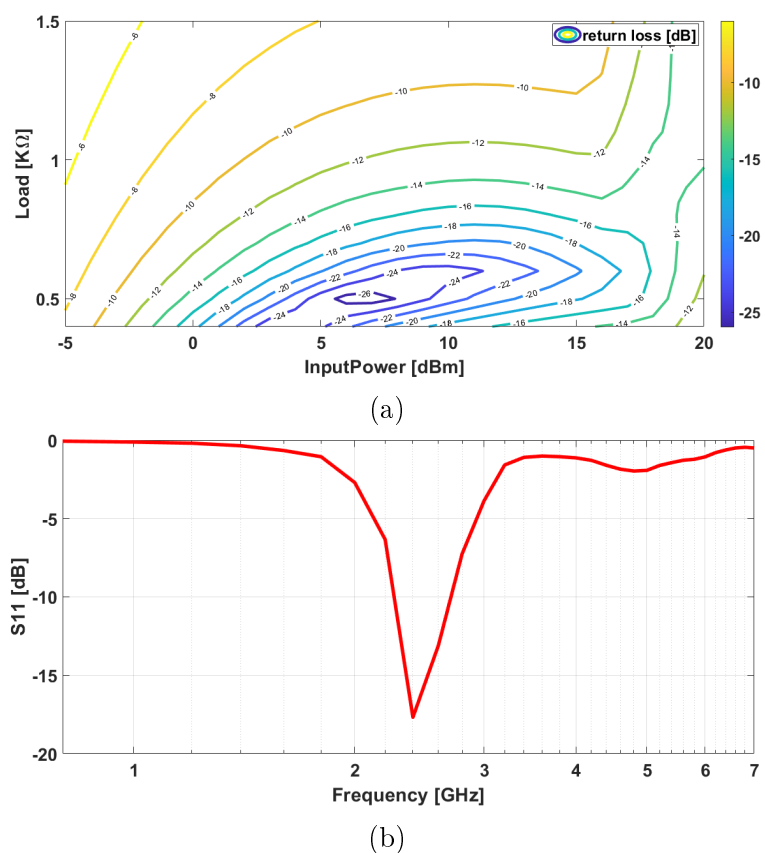


Figure 4.20: The simulated S11 for rectifier circuit with (a) vs. the load and input power (b) vs. the frequency.

Figure(4.21) shows the output voltage versus the input power and load, the color bar shows the output DC voltage (V) ranges from 0 to above 5.5 V, where 5.5 V is the maximum output DC voltage can be obtained.

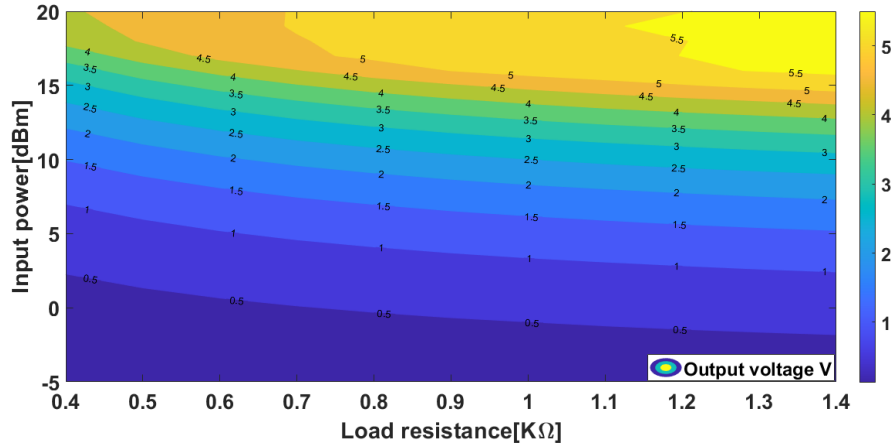
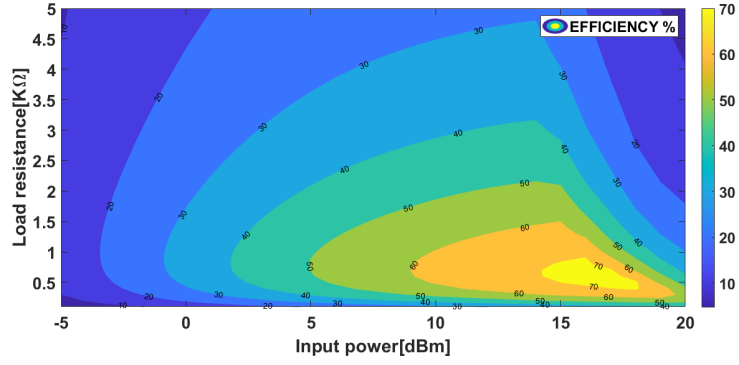
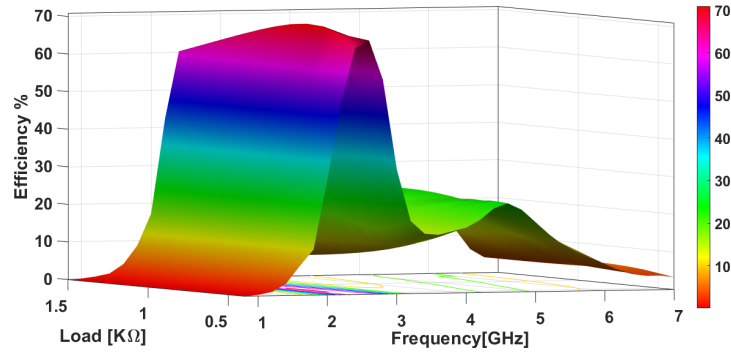


Figure 4.21: The simulated output DC voltage versus the variable input power and load

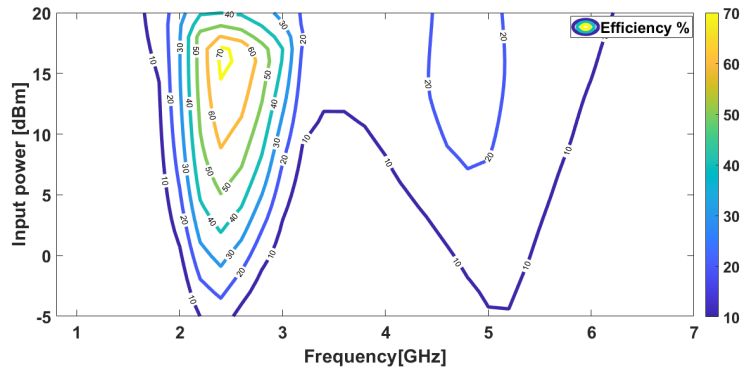
As a function of frequency, load, and input power, the Figure(4.22) reports the simulated RF-DC conversion efficiency. As observed in Figure(4.22a) the efficiency under variable load and input power. A maximum efficiency 73.4% can be obtained is at 17 dBm and  $600\Omega$ , and from 5 to 19 dBm the efficiency remains above 50%. Figure(4.22b) illustrates the efficiency as a function of variable load and frequency, and the maximum frequency is realized at operating frequency 2.4 GHz. Finally, Figure(4.22c) shows the efficiency versus the input power and frequency. From all the simulated results demonstrated above, the color bar shows the RF-DC conversion efficiency ranges from 0 to above 70 %, it can deduce that proposed rectifier design based on the ICN can sense and operate almost at a moderate input power.



(a)



(b)



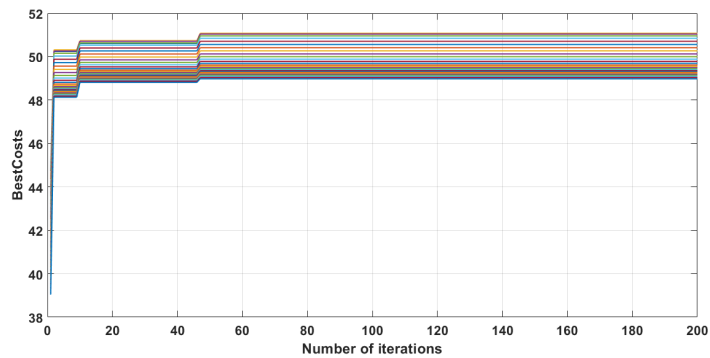
(c)

Figure 4.22: RF-DC conversion efficiency (a) vs. the input power and load (b) vs. the frequency and load (c) vs. the input power and frequency

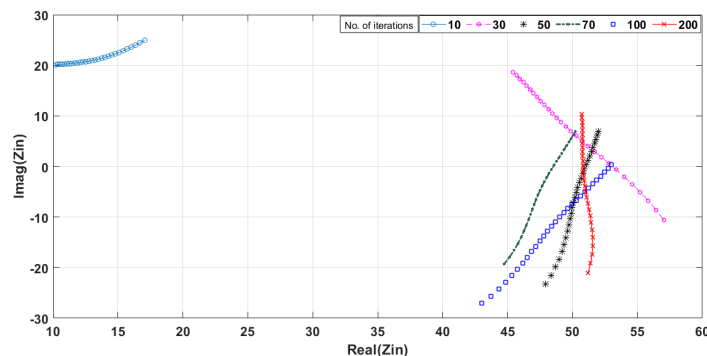
#### 4.5 Implementation and Results for ICN Optimized by the Particle Swarm Optimization Algorithm

A formula of the input impedance  $Z_{in}$  given in equation (4.25), is governed by five parameters namely  $(Z_{o1}, Z_{o2}, \theta_2, Z_{o3}, \theta_3)$  where  $Z_{in}$  represents the best fitness function in PSO algorithm procedure to come up with the optimum dimensions for the whole design with the ICN. The constraint of the algorithm utilized

in this work is to make the input impedance  $50+i0\Omega$  for a wide range of input power. Figure(4.23a) shows the best personal position (BestCost) convergence of the PSO algorithm. Results are good enough to produce a significantly narrow input impedance variations range despite a wide input power range. Figure(4.23b) depicts the input impedance variations for different number of iterations. As can be seen, as a number of iteration is increased, the desired results are obtained.



(a)



(b)

Figure 4.23: PSO algorithm impelmentation results (a) the best fitness value of the real part of input impedance for a number of iterations (b) real and imaginary parts of the input impedance for a number of iterations

To show the usefulness of the ICN, efficiency is the most important rectification metric parameter. In addition, the reflection coefficient  $S_{11}$  is illustrated because this parameter determines how much power transfers from the RF signal source (i.e., an antenna) to the rectifier.

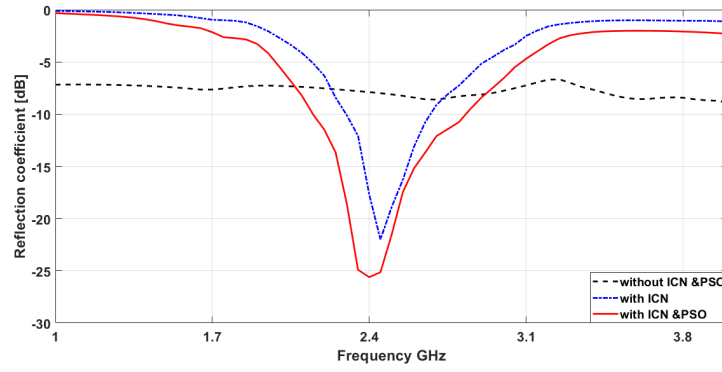
Table 4.3 introduces the PSO parameters. Figure(4.24a) illustrates how matching is improved by having lower reflection coefficients, especially when employing the PSO.

Table 4.3: PSO parameters

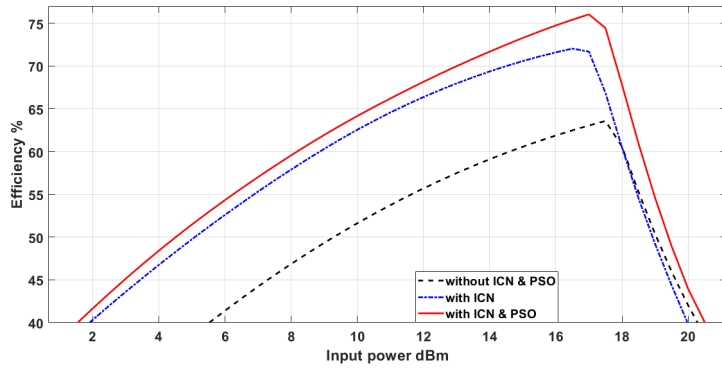
Parameters	Range
Inertia weight	1
C1 , C2	2
N	5
Swarm No.(i)	50
Iterations No.(t)	200

The PSO with ICN case has the best matching about -25 dB. Moreover, Figure(4.24b) shows that the efficiency is improved by almost 10% when using the circuit with only ICN and 15% with the ICN and PSO. The efficiency remains above 50% for the input power range of (4.5-19.5) dBm and a load range of (0.4-1)K $\Omega$ . As expected, the PSO algorithm has achieved the goals, being matching enhancement and RF-to-DC conversion efficiency. By virtue of the PSO, this has been done only in few minutes, whereas the ICN without optimization take hours or days depending on the designers experience and how to deal with the software. This is the key point how the optimization techniques accelerate the design process and reduce the time.

Figure(4.25) shows a rectifier with ICN after applying the PSO. The final physical size will be (8.86x4.3x0.15) mm<sup>3</sup>. The whole size of the circuit is slightly increased compared to the circuit without optimization, but this increment does not have a big effect on the overall reduction form.



(a)



(b)

Figure 4.24: Enhanced results by using PSO algorithm (a) Simulated return loss before and after optimization also, without ICN. (b) Simulated conversion efficiency of the rectifier with and without ICN in addition to PSO efficiency

The Matlab code adopted in this thesis is given in the APPENDIX-C.

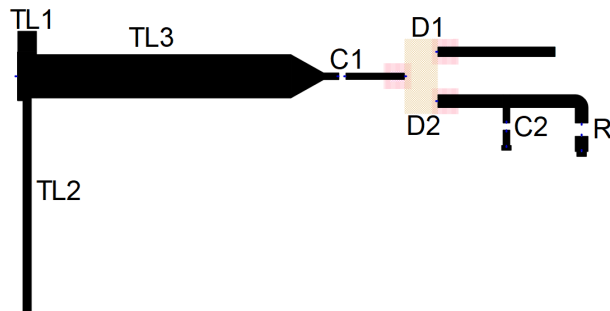


Figure 4.25: Configuration of rectifier based on single branch (ICN) optimized by using PSO

Table 4.4 gives a comparison between the rectifier present in this work and the previous related work.

Table 4.4: The Comparison of the proposed rectifier and some related designs

Ref.(year)	Freq.[GHz]	O/P volt(V)	Load( $\Omega$ )	Size(mm <sup>2</sup> )	Max Eff.(%)
[34] (2020)	0.9	3.1	1000-5000	45.4x7.8	60
[31] (2017)	2.45	1.9	800-2800	41x21	57
[29] (2018)	2.45	-	820 ,1200	-	63
[32] (2019)	2.41	12 , 3.9	430 , 1500	55x38	72.8
[33] (2020)	5.8	2.7	220	21x12	70.2
[42] (2019)	2.45	-	360	31.3x25.3	73.6
[54] (2016)	0.915	-	1000-3000	-	84.8
[37] (2017)	2.45	-	80-200	-	79.2
<b>Our work</b>	<b>2.4</b>	<b>5.5</b>	<b>400-1400</b>	<b>8.65x4.2</b>	<b>73.4</b>
<b>With PSO</b>	<b>2.4</b>	<b>6</b>	<b>400-1400</b>	<b>8.86x4.3</b>	<b>76</b>

# CHAPTER 5

## RECTENNA ARRAY DESIGN FOR RF ENERGY HARVESTING

### 5.1 Overview

In this chapter, both of the antenna arrays with BFNs and rectifiers will be integrated together to have the whole RF energy harvesting system. As shown earlier, the output of the antenna array has several outputs. Each single output can be integrated with a rectifier. Thus, first, the DC power combining technique is introduced since this will enable us to accumulate the power as much as possible. Some combining techniques impose to make each single output port from the BFN has its own rectifier. In other words, several DC sources will be available.

After that, all DC power that has resulted from all outputs rectifier branches will adding these DC sources in somehow will enforce the system to provide the highest power. As demonstrated in the previous chapter, each port in the BFN has different beam of the radiation pattern that covers different direction in space. This means that the incoming RF signals from different direction excite different rectifiers integrated with the different ports of the BFN. The whole energy system can harvest the power from a wide range of the spatial angles. Figure(5.1a) shows a schematic of the RF power combining technique. Conventional antenna arrays cannot cover most spatial directions simultaneously, and then the DC power level will decrease as the main scan angle is deviated from the intended directions. How-

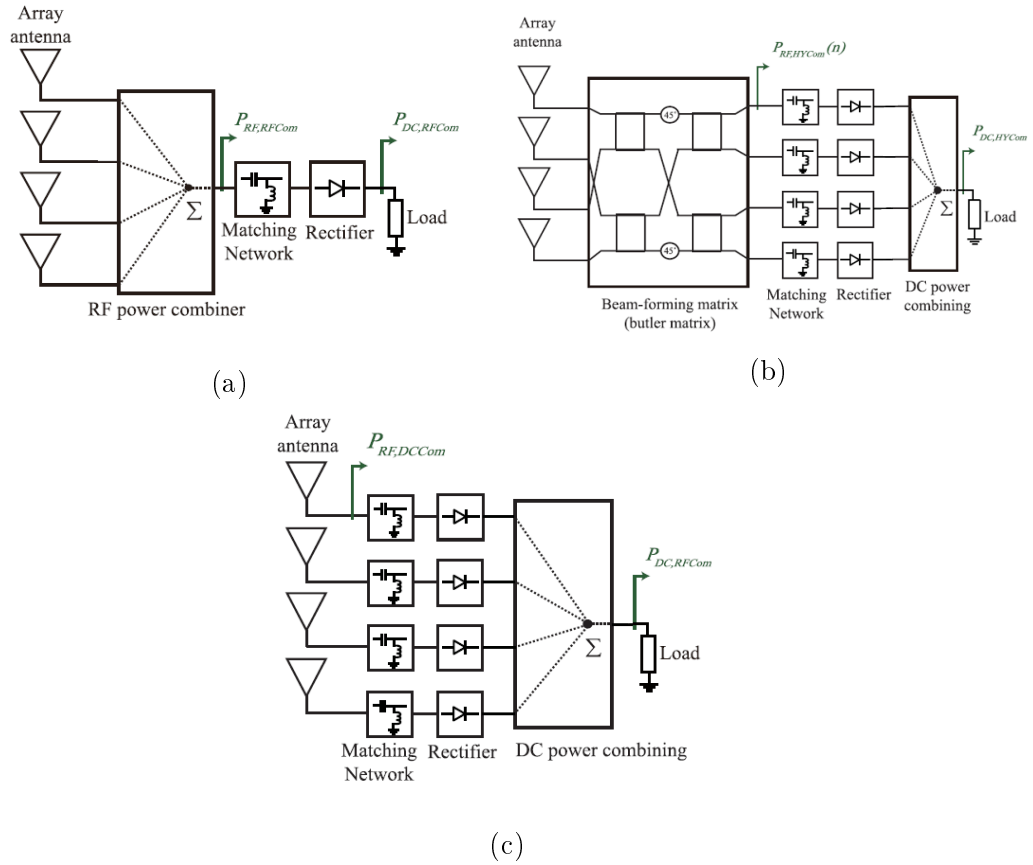


Figure 5.1: The combination power methods (a) RF power combining method (b) The hybrid power combining system using Butler matrix network (c) DC power combining method, [56]

ever, our BFN makes our antenna array has several beams directed to different directions at the same time. As indicated in the previous chapter, a multi-beam antenna is required. Figure(5.1b) illustrates BFN and DC combining approach to provide wide view angle to scan.

The BFN is utilized as an RF combining method, which exhibits an effective employment to enable a multi beams antenna array to be introduced, and therefore an output DC power with a broad incident angle will be guaranteed. This circuit has advantages over the one introduced in Figure(5.1a) because the former can capture the RF signals from different directions with the same efficiency, whereas the latter it works well with only one direction. In the proposed BFN, the rectenna

can harvest the RF signals through four beams and each beam is associated with a specific direction, thereby having four RF output signals with different phase between them, signals pass over Butler matrix network and directly pass to rectifier circuits to convert the RF signals to DC signals. Figure(5.1c) shows the DC power combining technique where each out port of the single antenna element is integrated with a rectifier. Then, output ports of rectifiers are added in somehow (i.e., either in series or in parallel).

## 5.2 DC Power Combining System

The DC power combining technique is the first rectenna design scenario that will be investigated. The 1x4 antenna array that was designed in the previous chapter is used. Figure(5.2) depicts the DC combining strategy adopted here. Four RF-DC rectifiers based on a single branch complex impedance compression network are arranged in parallel to the 1x4 multi-feed antenna array.

After that, the RF signals pass through rectifiers and then are converted to DC signals. At this point, four output loads have been presented. Figure(5.3a) illustrates the DC output voltage for all loads as a function of the theta. Figure(5.3c) and Figure(5.3d), compare the contrast among the outputs. The maximum voltage has obtained from the first output which is 5V at 20dBm RF harvested power, and 52.5% is maximum RF-DC efficiency at 16dBm RF harvested power. For the second output, the output DC voltage is 3.6V at 20dBm RF harvested power, and 35.7% is maximum RF-DC efficiency at 3dBm RF harvested power. A 3.6V at 20dBm RF harvested power, 35.7% is maximum RF-DC efficiency at 3dBm RF harvested power and a 5V at 20dBm RF harvested power, 57% is maximum RF-DC efficiency at 18dBm RF harvested power, for both outputs three and four, respectively. To obtain the single load for rectenna design by a DC power com-

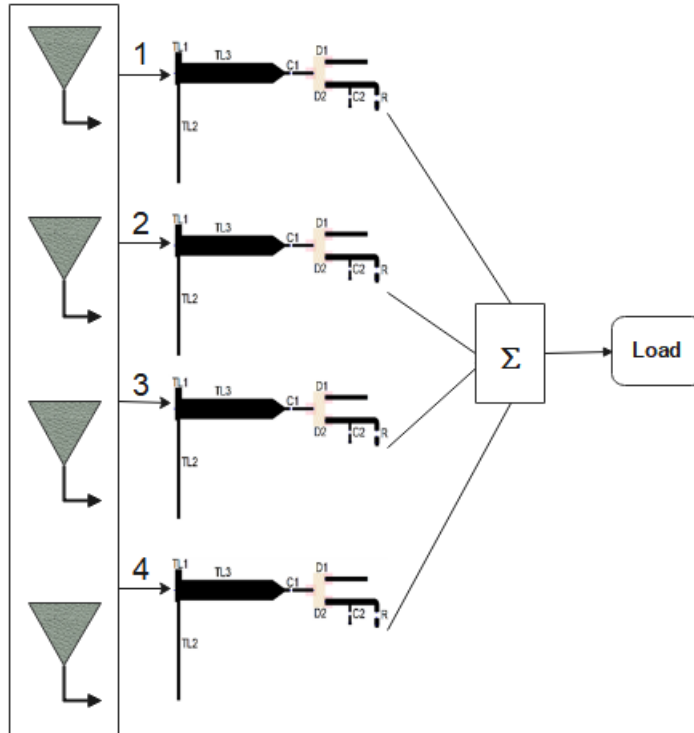


Figure 5.2: The schematic of the rectenna design employing the DC power combining technique

binning system the parallel accumulation for all outputs is what is adopted, as demonstrated in Figure(5.2). Figure(5.3b) introduces the output as a function of theta. From Figure(5.3c) and Figure(5.3d), a 6V at 20dBm RF harvested power, one can deduce that the proposed DC combining technique operates with a wide range of the input RF power and with efficiency above of 40% from -3 to 17 dBm and maximum RF-DC efficiency is 53%.

### 5.3 RF Power Combining System

The RF power combining strategy is implemented by using an RF power combiner circuit to accumulate every two RF branches and pass it through three combiners to produce one RF power port. The same 1x4 antenna array is connected to two Wilkinson power combiners, and their resulting terminals are combined to a third Wilkinson power combiner to obtain a single RF power line. Figure(5.4)

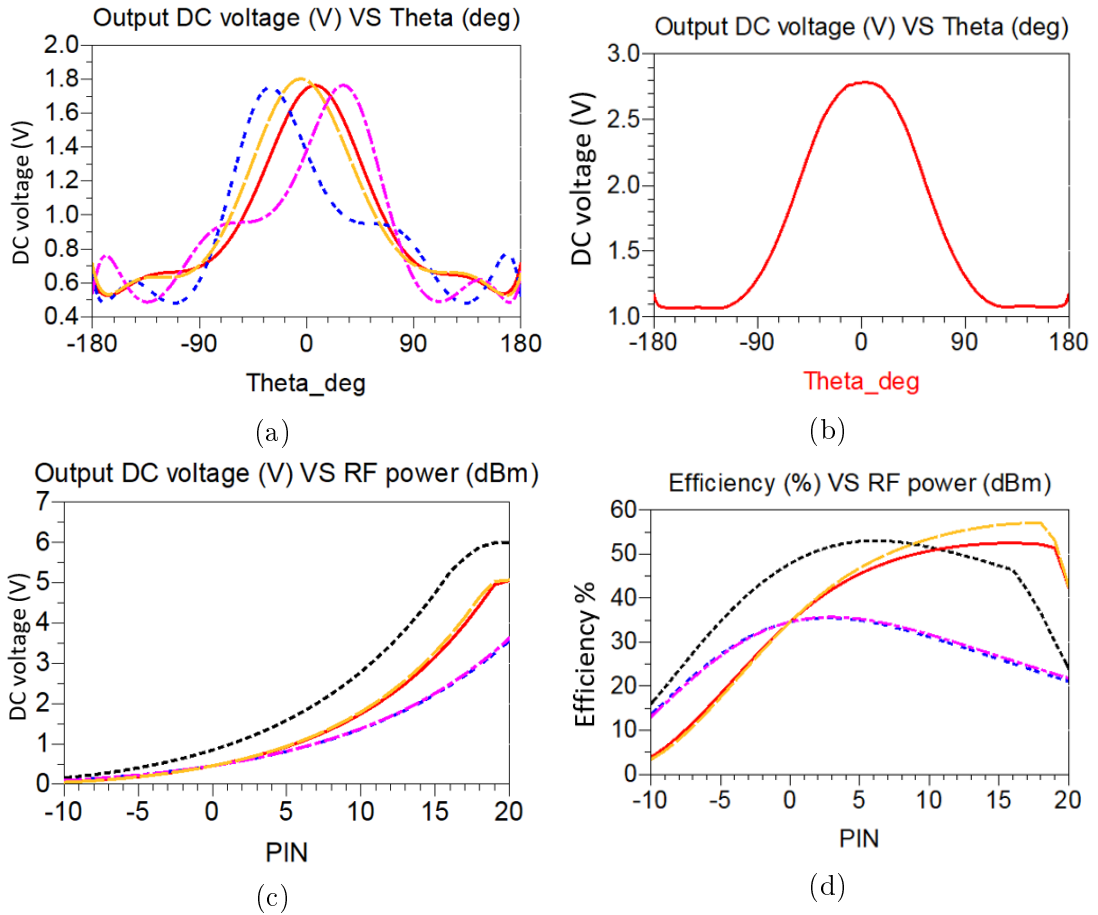


Figure 5.3: The simulated results (output1(Red, solid line), output2(Blue, dot dot line), output3 (Pink, dot dash line), output4 (Yellow, long dash line), the single output(black, dot line) ) (a) output DC voltage (V) related to Theta (deg) angle for all outputs for multi-output DC combining design (b) output DC voltage (V) related to Theta (deg) angle for a single output for DC combining design (c) DC voltage (V) to the RF power harvested (dBm) (d) the rectification efficiency to the RF power harvested (dBm)

illustrates the RF combining strategy. Wilkinson power combiner is simulated with high matching at the operating frequency with 0dB insertion loss.

A single line that has been generated from an RF combining system is connected directly to only one RF-DC rectifier. Figure(5.5a) presents the output as a function of theta. From Figure(5.5b) and Figure(5.5c), a 5V at 20dBm RF harvested power, the system has efficiency above of 50% from -15 to 11.5 dBm and maximum RF-DC efficiency is 66%.

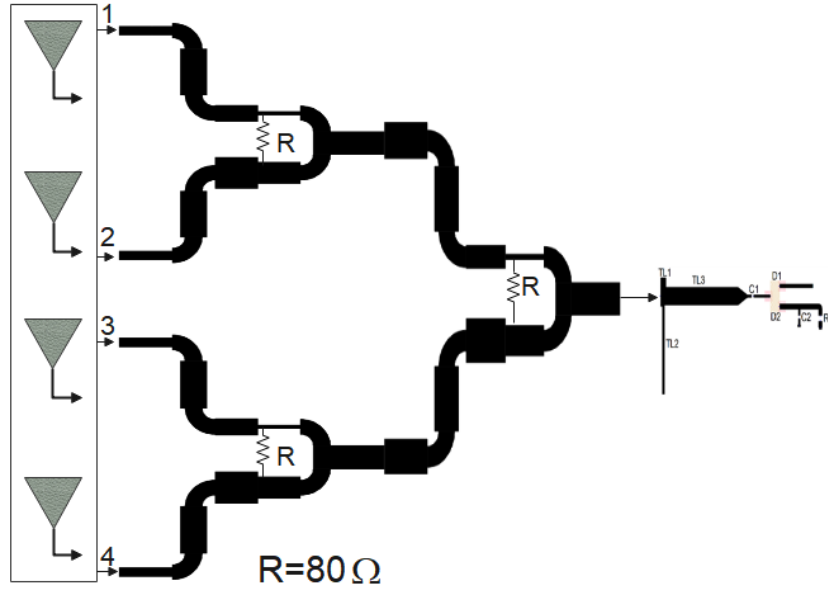


Figure 5.4: The schematic of the rectenna design employing the RF power combining technique

#### 5.4 Hybrid Power Combining System

To take benefit of the characteristic features of both RF and DC combining systems. The signals will be combined in front of the rectifier and behind the rectifier circuit. The arrangement of hybrid combining strategy is as follows; the same 1x4 antenna array which is with four feed lines, each two lines are added by the Wilkinson power combiner in order to produce two outputs. Then, these two RF power outputs are connected directly to a couple of RF-DC rectifier circuits.

At this point, an RF combining was attained. The DC combining is made by adding the two DC ports in parallel form. Figure(5.6) illustrates the adopted hybrid combining approach. Figure(5.7a) presents the output as a function of theta. From Figure(5.7b) and Figure(5.7c), a 5.5 V at from (16-20) dBm RF harvested power, the system has efficiency above of 60% from -10 to 15 dBm and maximum RF-DC efficiency is 81.3%.

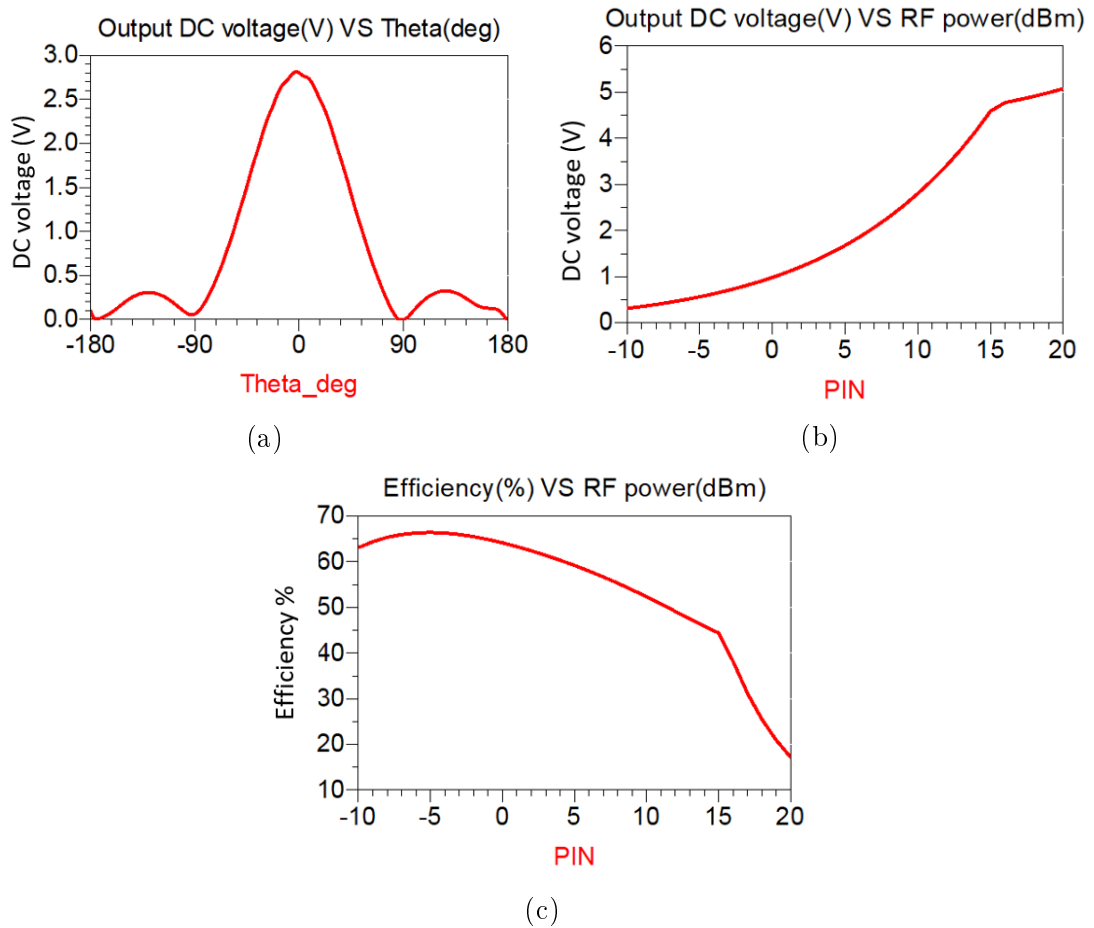


Figure 5.5: The simulated results for the RF power combining system (a) output DC voltage (V) related to Theta (deg) angle for RF combining design (b) DC voltage (V) to the RF power harvested (dBm) (c) the rectification efficiency to the RF power harvested (dBm)

## 5.5 BFN/DC Power Combining System

There are two ways to investigate the BFN/DC power combining system :

### 5.5.1 Simulation for the Multi-Beam/Multi-Output rectenna

As indicated in chapter two, a rectifier circuit design has been fully investigated. A rectifier circuit composed of two diodes as a voltage doubler in addition to a single branch impedance compression network is employed as a matching network. A 2.4GHz rectifier design has demonstrated a high-efficiency approximately 76% after optimizing the ICN dimension using the PSO algorithm, in addition to the

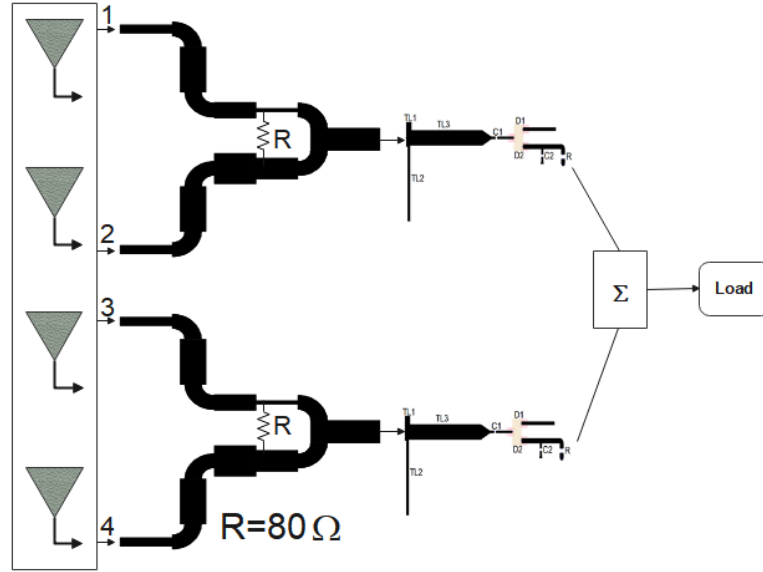


Figure 5.6: The schematic geometry for rectenna design by the Hybrid power combining

wide RF input power range of (-5 to 20)dBm. Furthermore, the rectifier circuit performance was simulated with a variable load resistance within a range 400 to 1400  $\Omega$ . A rectifier circuit is shown in Figure(4.25).

To implement a multi-beams structure with four of the rectifiers are utilized and connected to the output ports 1, 2, 3 and 4, as shown in Figure(5.1b). In order to present a rectenna which is able to harvest the RF signals from 4 beams with different scan angles (  $56^\circ$ ,  $15.5^\circ$ ,  $-16.5^\circ$ ,  $-50^\circ$ ), it only can be achieved with multi-beam feeding network. Furthermore, a circular polarization has been adopted to overcome the mismatching case in polarization problem and to harvest from several different directions of ambient RF sources. Hence, utilizing the Butler matrix will be the useful circuit, as an RF combiner, and increases the RF power at rectifiers because of the accumulation of the RF signals received by all four input ports and distributed it over the output ports with a constant phase difference. The Figure(5.8a) shows the output DC power in watt as a function of antenna scan angle, the value of power varies between 0.023 watts at the first and fourth ports,

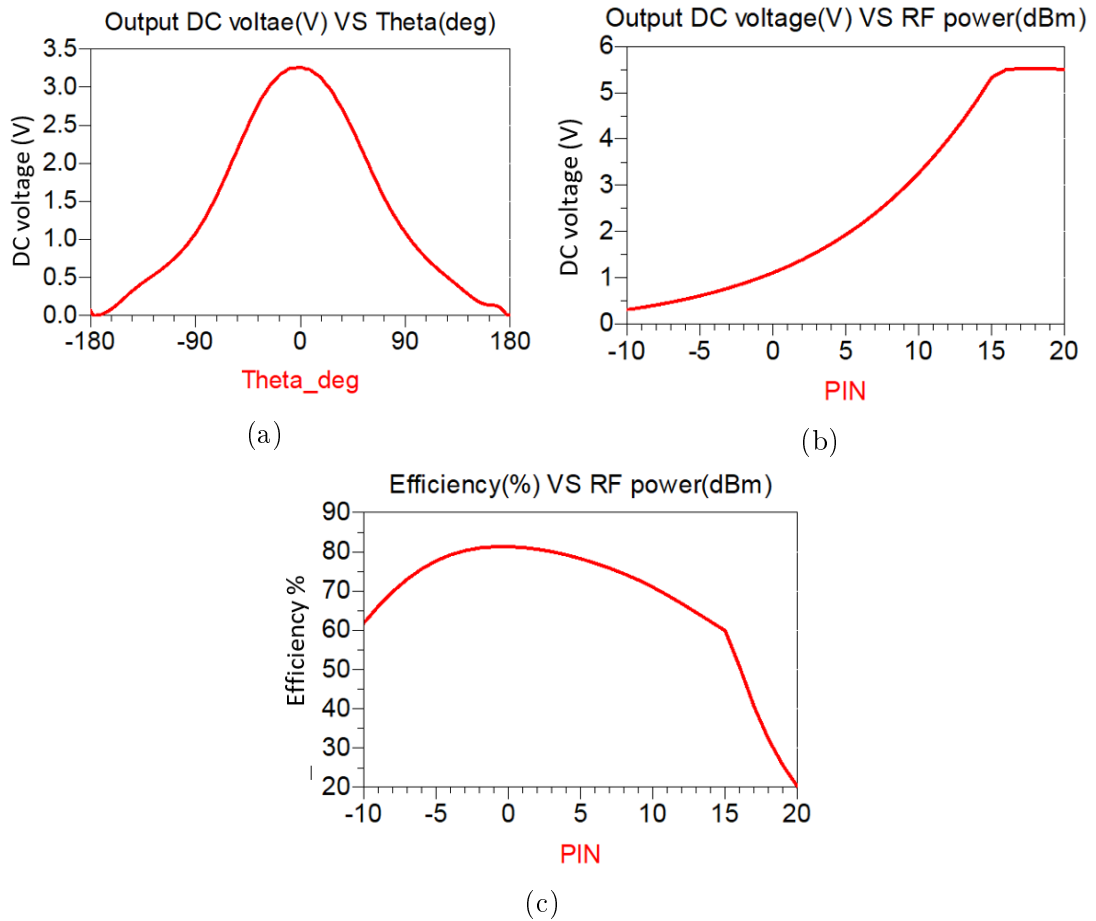


Figure 5.7: The simulated results for the hybrid power combining system(a) output DC voltage (V) related to Theta (deg) angle for Hybrid combining design (b) DC voltage (V) to the RF power harvested (dBm) (c) the rectification efficiency to the RF power harvested (dBm)

to 0.019 watts at the second and third ports.

Figure(5.8b) illustrates the magnitude of the DC voltage signals as a function of the antenna scan angles, to observe the DC signals produced by rectennas, as they will be generated through four beams at angles of  $(-48.4^\circ, -16.5^\circ, 16^\circ, 47.9^\circ)$ , the magnitude can reach to 3.74V at first rectifier, 3.38V at second, 3.37V at third, 3.75V at last rectifier. These results occur when the RF power harvesting is equal to 10dBm from all antenna elements, and the load resistance is fixed at  $600\Omega$ .

The rectification efficiency related to the antenna scan angle is presented in

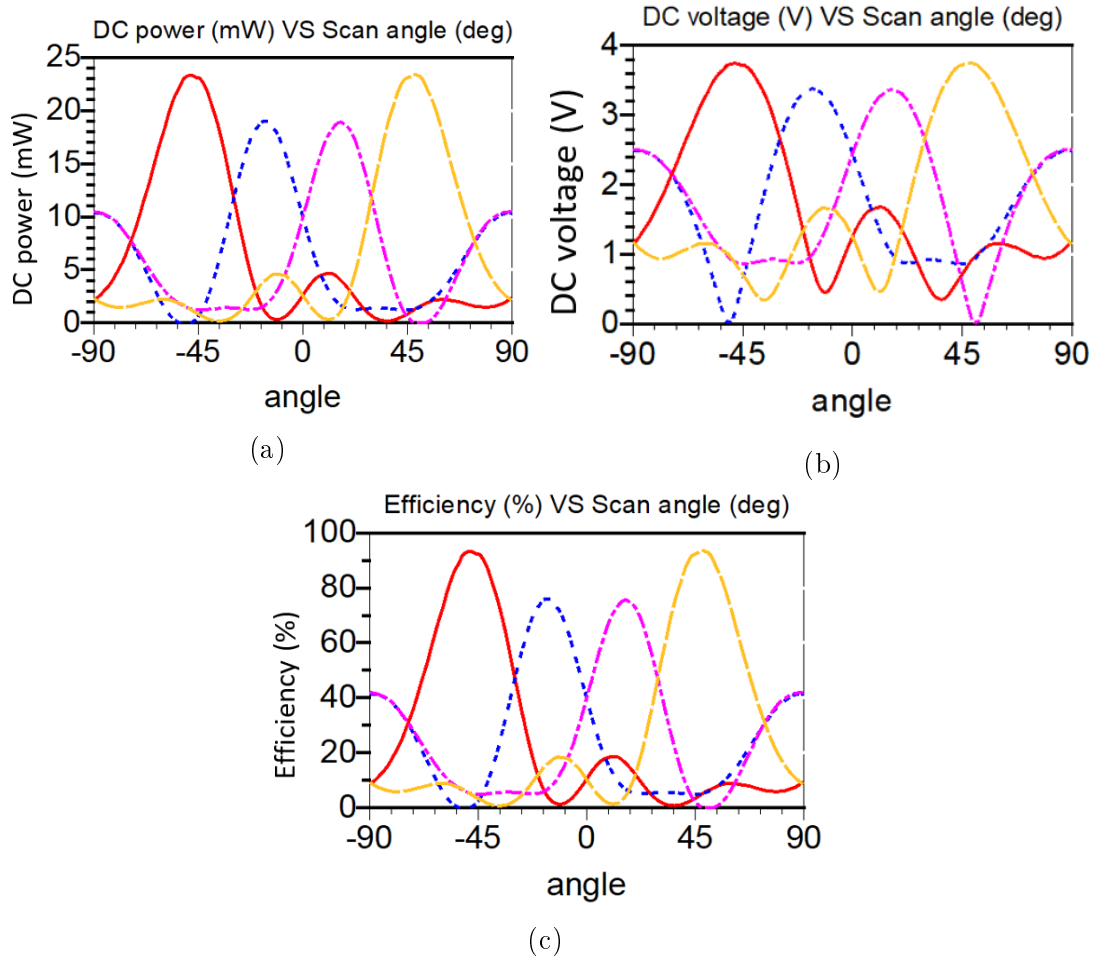


Figure 5.8: The simulated results (port1(Red, solid line), port2(Blue, dash line), port3 (Pink, dot dash line), port4 (Yellow, long dash line)) related to antenna scan angle with: (a) output DC power (W) (b) output DC voltage (V) (c) rectification efficiency

Figure(5.8c). The efficiencies for ports 1, 2, 3 and 4 are 93.4%, 76%, 75.6%, 93.6%, respectively. The output voltage for the DC signal (V) as a function of RF power (dBm) clarified in Figure(5.9a). As observed, the maximum DC signal for the rectenna reaches to a 5V at the maximum RF input power over ports of 2 and 3, and 4.5 over ports of 1 and 4. The DC power versus the RF input power in Figure(5.9b) shows that one can observe that the maximum DC power for the rectenna reaches to 43 mW at the maximum RF input power over ports of 2 and 3, and 34 mW over ports of 1 and 4. Figure(5.10) illustrates the rectification efficiency as function to RF input power and theta angle in a form of the 3D simulation.

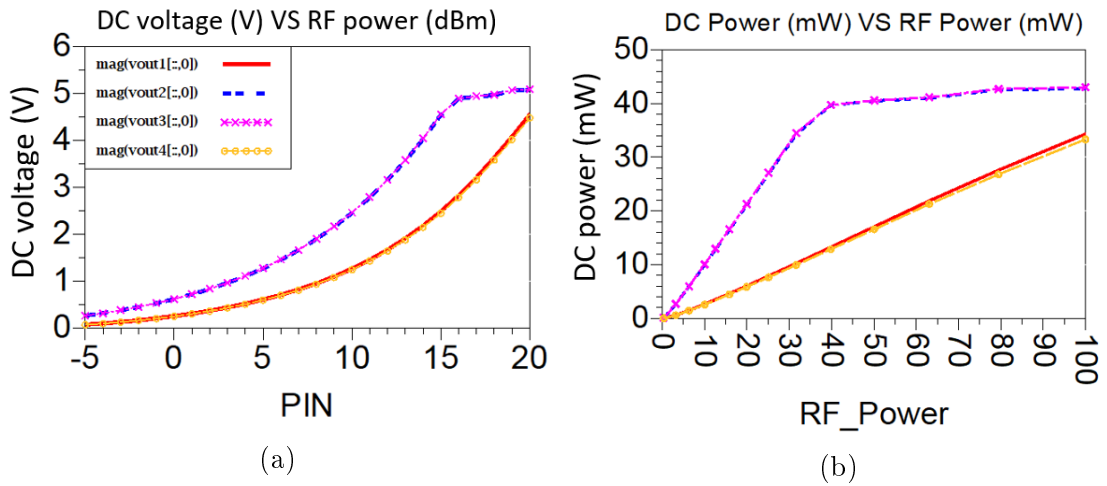


Figure 5.9: The simulated results (port1(Red, solid line), port2(Blue, dash line), port3 (Pink, solid line with star symbol), port4 (Yellow, solid line with circle symbol)) for: (a) The simulated magnitude of DC signals (V) for rectenna output ports VS RF power (dBm) (b) the relationship between the DC power to the RF power (mW)

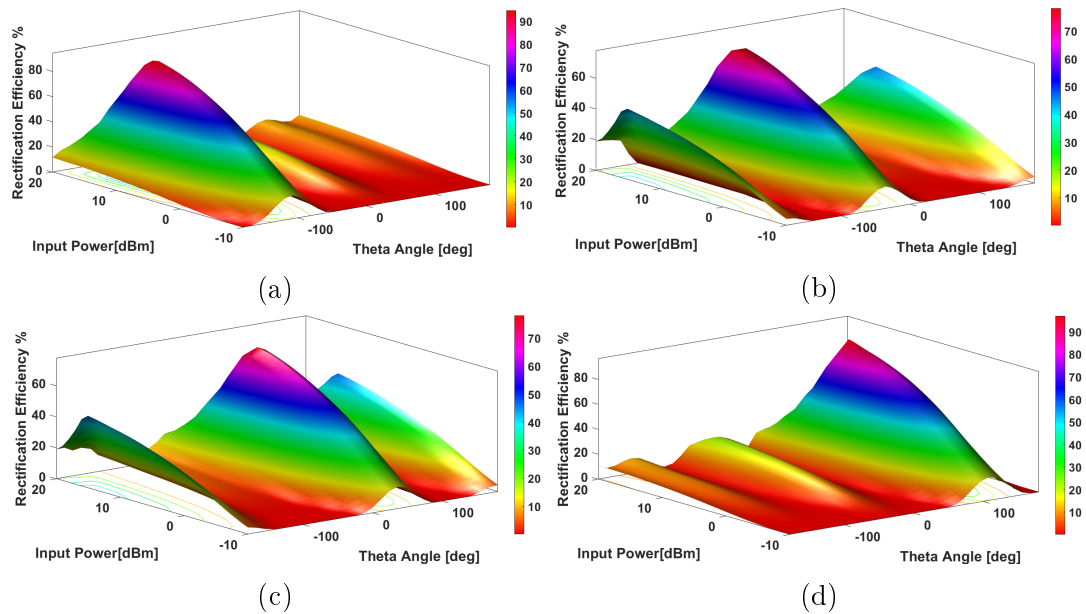


Figure 5.10: The 3D simulation results for BFN and DC combining compact when excite (a) port1 (b) port2 (c) port3 (d) port4

### 5.5.2 Simulation for the Multi-Beam DC Combining System

A single branch rectenna is the easiest and simplest than a multi-branch one. The DC combining will be implemented to complete the rectenna designed above

to be a rectenna system with a compact BFN DC combining system geometry as shown in Figure(5.11). The DC power generated from each single rectifier will be accumulated at single port to provide a sufficient power to power sensors or to recharge batteries. A parallel DC combining approach is what will be used with the BFN.

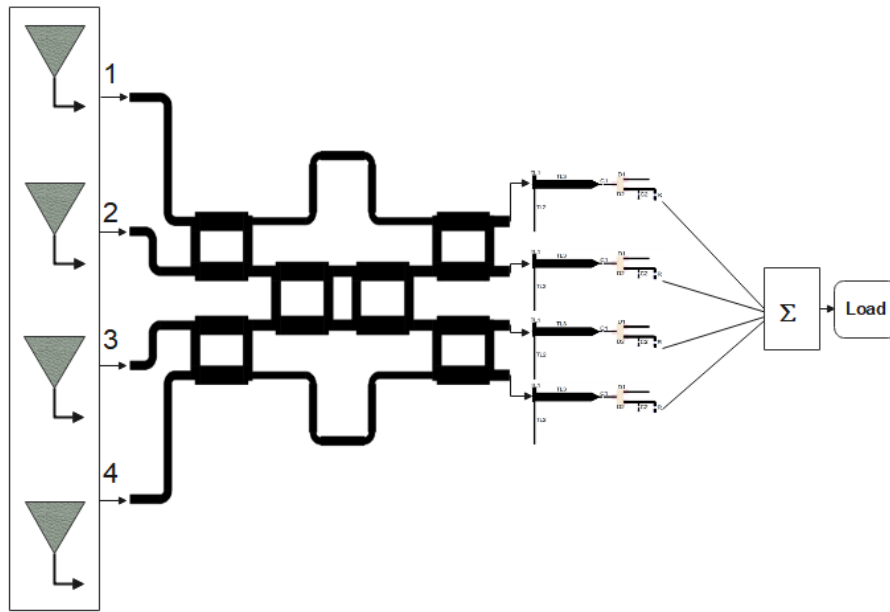


Figure 5.11: The schematic geometry for rectenna design by the BFN and DC combining

In this work, the parallel connection is more appropriate and easier than the series connection. A passively accumulating DC for voltage, Figure(5.12a) illustrates the output voltage for the single branch to the RF power in dBm. The maximum voltage that can be reached to 6.6V when RF also is a maximum. Figure(5.12b) present the relationship between DC power to RF power, 72.3 mW is a maximum power. A 83.7% at 13 dBm is a maximum RF-DC efficiency obtained as shows in Figure(5.12c) and from 1.5 to 16 dBm has efficiency above 60%.

The rectification efficiency as a function of scanning angle is illustrated in

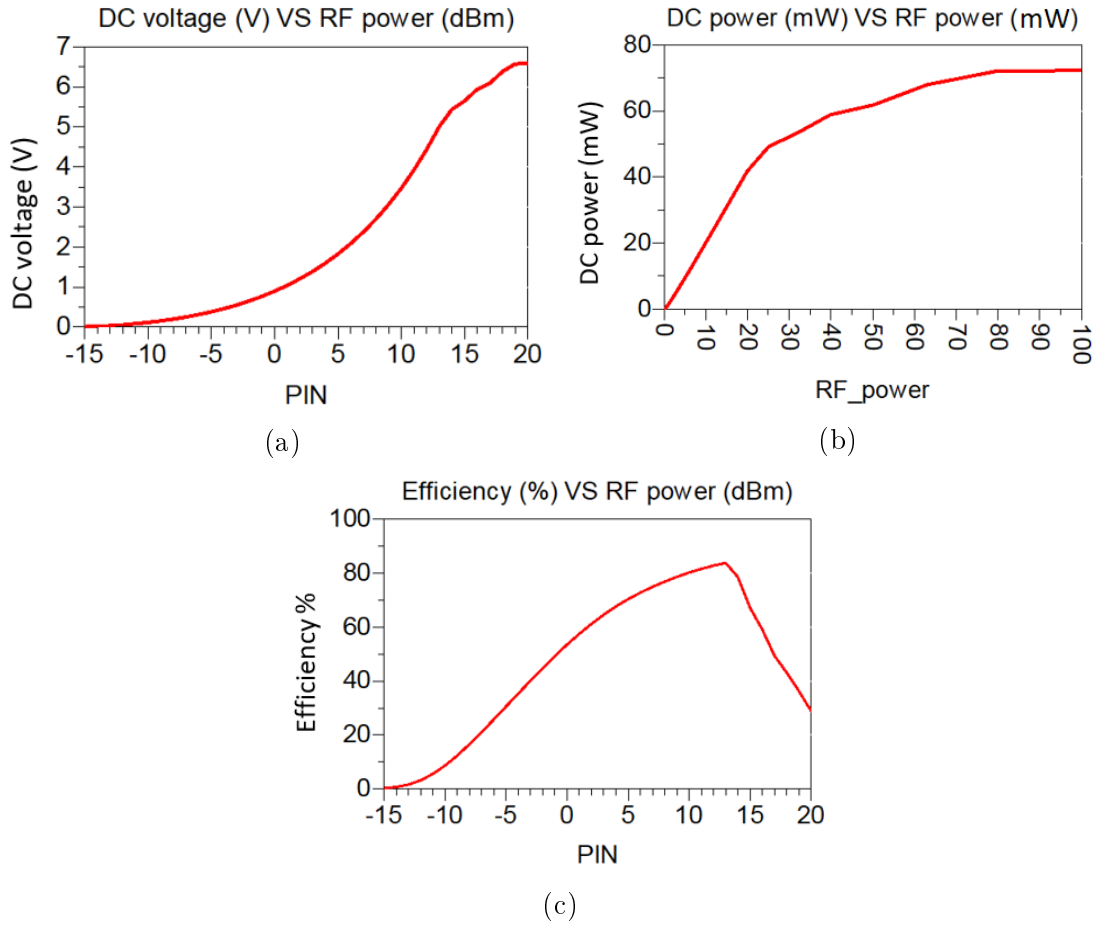
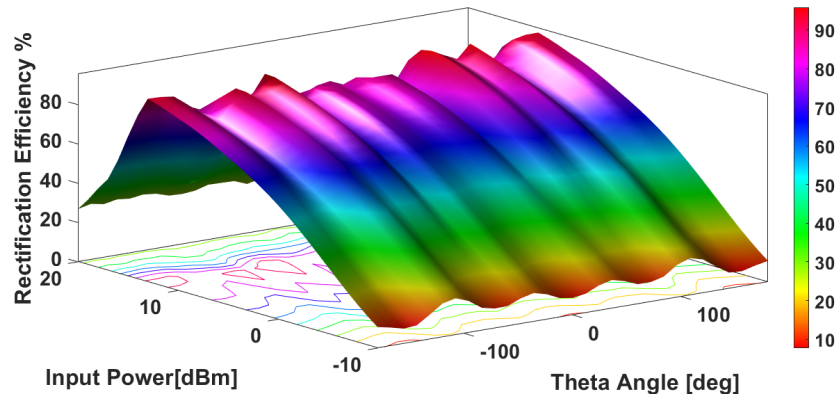
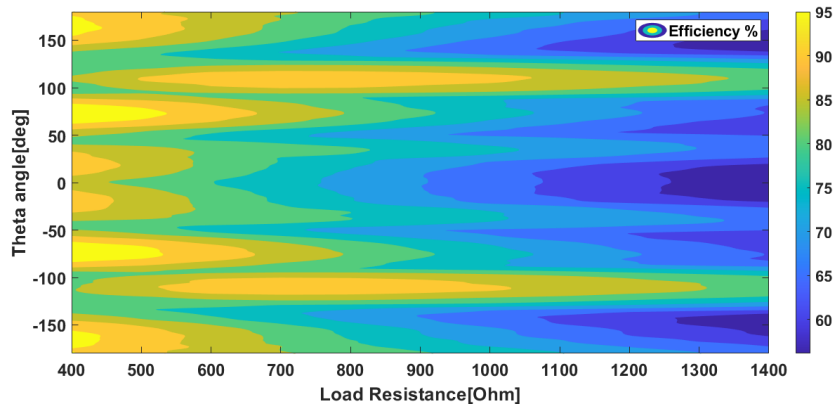


Figure 5.12: The simulated results for rectenna with hybrid combining system (a) the magnitude of output DC signal (V) for rectenna output port VS RF power (dBm) (b) the relationship between the DC power to the RF power (mW) (c) rectification efficiency VS RF power harvested (dBm)

Figure(5.13), as the rectenna can obtain high rectification efficiency along a theta angle with a wide range for RF input power and load resistance. The rectenna design operates with high performance in the case when the load resistance is fixed to one value, which is  $600 \Omega$ , but the efficiency of its performance does not conflict or decrease with dependence on a variable resistance load within a range of  $400 \Omega$  to  $1400 \Omega$ .



(a)



(b)

Figure 5.13: The 3D simulation results for rectenna designed explain the rectification efficiency as a function of Theta angle with wide range of (a) RF power (b) load resistance

## 5.6 A comparison between Power Combining Techniques

The comparison among all types of the power combining techniques mentioned above is provided in this section. From the simulation results, one can infer that the effective way to harvest power or to say which combining technique is the best over others and vice versa. The comparison is introduced according to a rectenna performance at a wide range of incident angles, the input RF power and the variable load resistance.

Figure(5.14) demonstrates the DC harvested output power versus the scan angle and the input RF power for all combining systems. The dot blue line is related

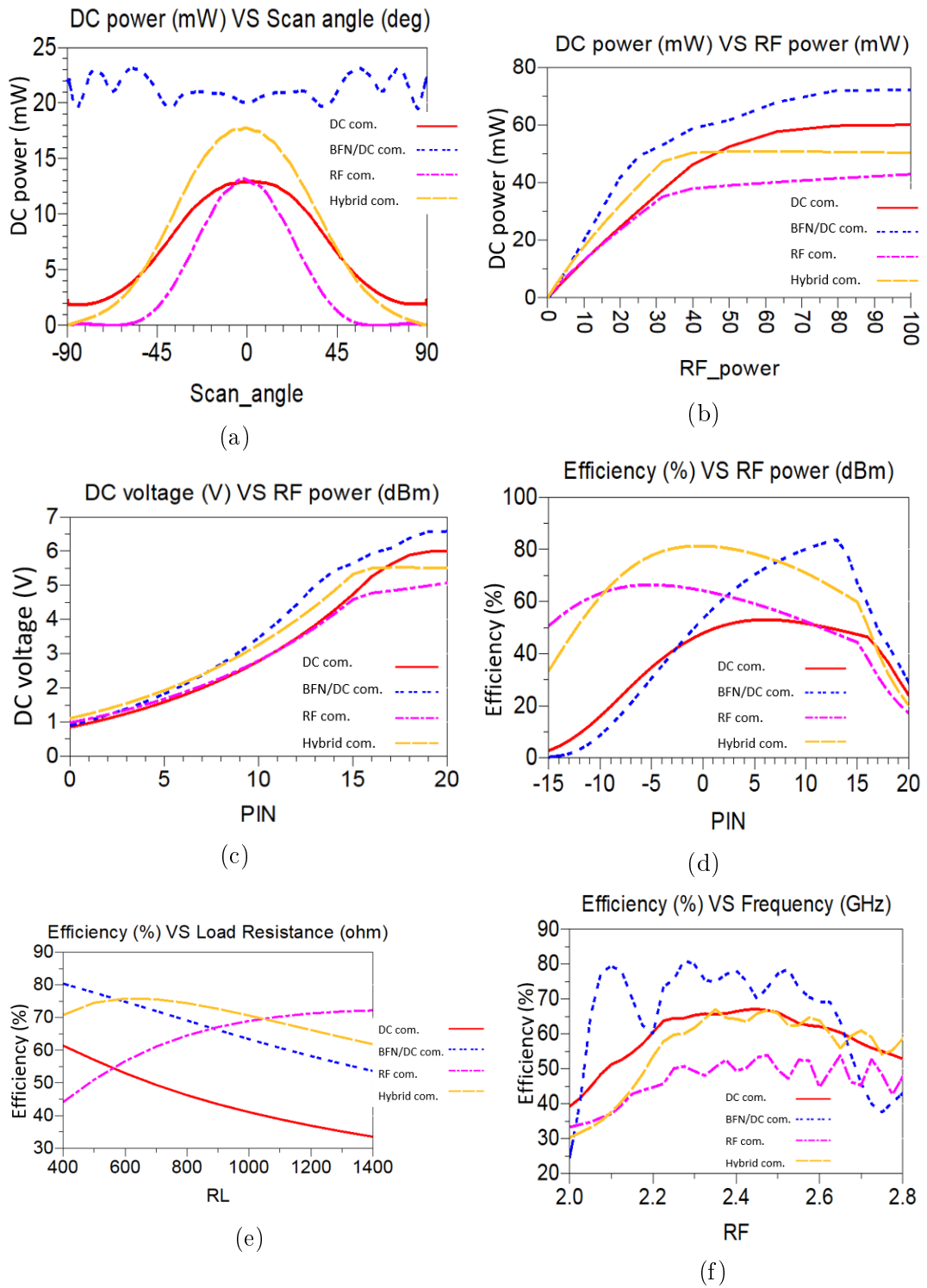


Figure 5.14: The simulated results for (DC combining system (Red, solid line), BFN/DC combining system (Blue, dot dot line), for RF combining system (Pink, short dash dot line ), Hybrid combining system (Yellow, long line)): (a) DC power (mW) VS scan angle (deg) (b) DC power (mW) VS RF power (mW) (c) DC voltage (V) VS RF power (dBm) (d) Rectification efficiency VS RF power (dBm) (e) Rectification efficiency VS load resistance ( $\Omega$ ) (f) Rectification efficiency VS frequency (GHz)

to a scan angle determined using Equation (3.3) of BFN/DC combining system to show the effectiveness of the BFN. As can be seen, the proposed work with the BFN is able to harvest the power from almost all directions and with a wide range of the input RF power. The reason why other systems operate with a limited range of scan angles is that they have only one beam, whereas our proposed work has several beams at the same time. The fluctuations in the DC harvested power belongs to that there are a lot of problem such as the destructive interference at some specific scan angles or the deterioration in the antenna performances because of the increase in the mutual coupling among antenna elements in the array.

Then, the DC combining operates with scan angles from  $-50^\circ$  and  $+50^\circ$ . Hybrid combining has a stable DC power along a wide range of the input RF power, a 50mW dc power has obtained from 40 to 100 mW the input RF power. Since only one rectifier is used in RF combining scenario, the scan angle is limited, thereby resulting in a reduction in the harvested power as compared to other systems. Figure(5.14d) illustrates the rectification efficiency over a wide range of the input RF power in dBm.

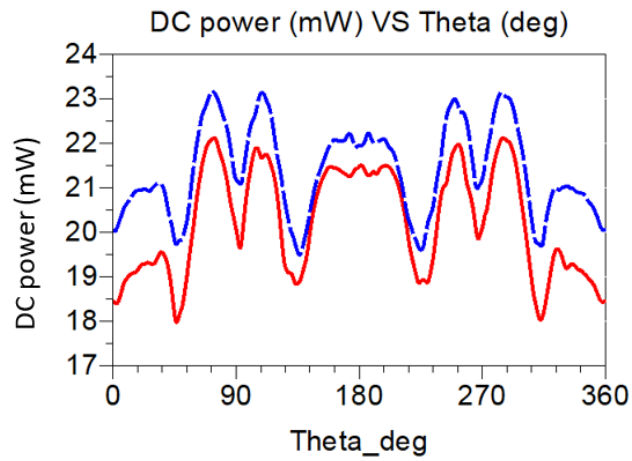
As can be observed, the rectennas implemented by RF and hybrid combining systems have higher efficiency above 40% over a wide range of the input RF power from -3 to 17dBm and above 60% from -10 to 15dBm, for DC and hybrid combining, respectively. However, the BFN/DC combining system has higher efficiency but a little narrower than DC or hybrid system, 1.5 to 16dBm that is 60%. The lower system that has efficiency is RF combining system. Rectennas can work with higher efficiency related to the input RF power is 83.7%, 53%, 66% and 81.3%, for BFN/DC, DC, RF and hybrid combining systems, respectively. The RF-DC effi-

ciency related to range of load resistance and frequency is investigated as shown in Figures (5.14e, 5.14f). In conclusion, the BFN/DC combining system and hybrid power combining system exhibit a great interesting performance to the rectenna circuit design.

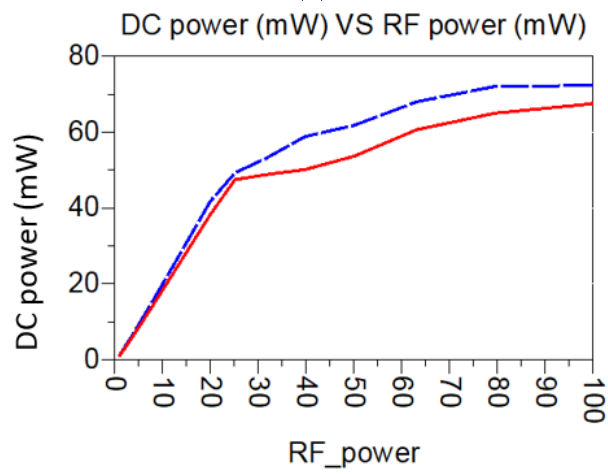
### **5.7 Discussion the Results of the Effectiveness of the PSO Algorithm in the Rectenna Array Design**

The importance of using the PSO algorithm that was employed to obtain an improvement in the performance of the impedance compression circuit to enhance the system performance over wide ranges of the input RF power, load resistances, and frequency. The rectifier circuit used in Figure(4.16) is adopted in Figure(5.11) to fulfill the rectenna design without using the PSO.

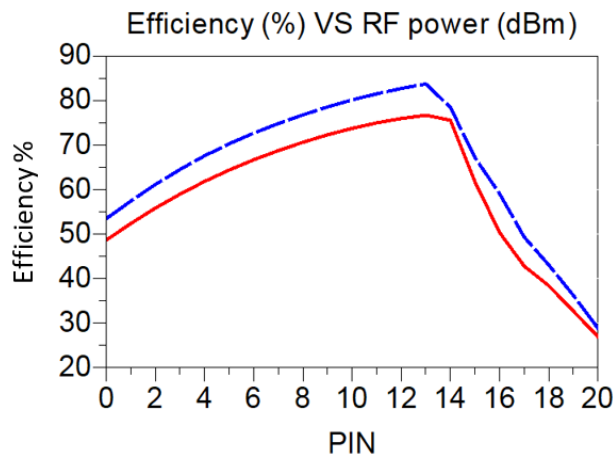
The overall performance of rectenna is illustrated in Figure(5.15). As observed, the rectenna implemented without using the single branch impedance compression network optimized by PSO algorithm, the performance of rectifier to convert the RF power to DC power will not operate well along the scan angle as shown in Figure(5.15a), also with the input RF power as shown in Figure(5.15b). Therefore, the efficiency obtained is lower than the rectenna with the PSO algorithm, as illustrated in Figure(5.15c). A 76.7% which is the maximum efficiency has been obtained by the whole proposed system with the BFN while it is 83.7% when the matching circuit is optimized using the PSO algorithm.



(a)



(b)



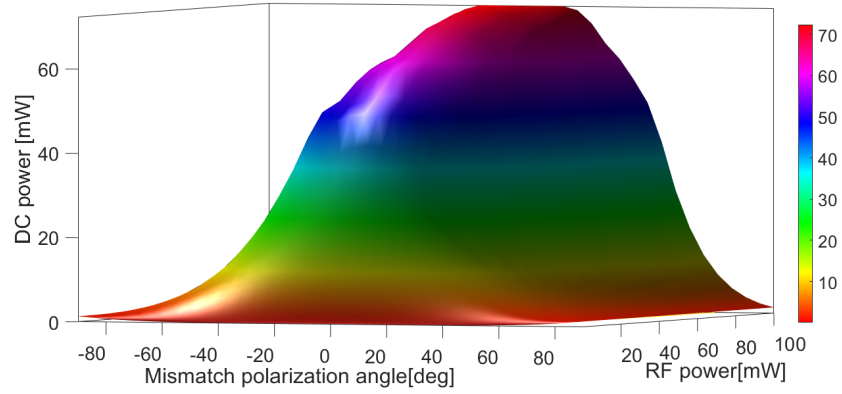
(c)

Figure 5.15: The simulated results for rectenna designed with (Blue, long dash line) and without (Red, solid line) PSO algorithm (a) DC power (mW) VS Theta angle (deg) (b) input to output power (mW) (C) rectification efficiency VS RF power (dBm)

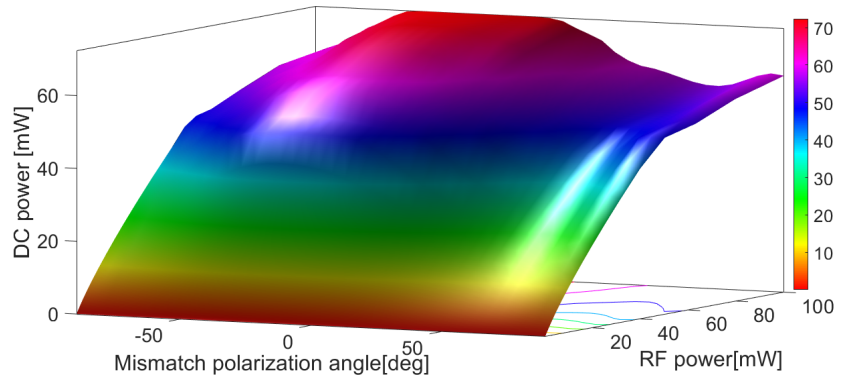
## 5.8 A Comparison between Circular and Linear polarization Rectenna Array Design

As indicated in challenges of the RF energy harvester design, locations of the ambient RF sources are unknown or time-varying. Therefore, the angle of arrival of the RF signals incident on rectennas is random. In order to increase the probability of picking up signals, the mismatch polarization between RF sources and RF energy harvester is removed by employed the circularly polarized rectenna.

A circular polarization antenna has been investigated in the previous chapter. To validate the effectiveness of circularly polarized rectenna in picking up the RF signals, a comparison between linear polarization rectenna and circularly polarization rectenna is preformed. The circular polarization rectenna is adopted in Figure(5.11). The linear polarization rectenna has the same configuration as a circular polarization rectenna, but it has been achieved with a linear polarization antenna. To implement this validation a patch antenna transmitter source were placed away 1 meter from a rectenna utilized. Figure(5.16) illustrates the input power and output power of the rectenna as a function of rotation angle or mismatch polarization angle for the transmitter. As can seen, the rectenna maintains almost the same received harvested power even if the polarization of RF transmitter antenna sources change.



(a)



(b)

Figure 5.16: The 3D simulation results for rectenna designed RF power (mW) VS mismatch polarization angle (deg) VS DC power (mW) (a) linear polarization (b) circular polarization

## 5.9 Related Work

Table 5.1 investigated a comparison with the entire rectenna system with another rectenna in related work. The authors in [57] a 2.45GHz 2x2 rectenna array is proposed with a two combining power system DC and RF power combining, each rectenna element consists of a dual-polarized antenna and simple rectifier circuit. A hybrid coupler has been utilized to connect the antenna and rectifier. The rectifier exhibited wide efficiency over above 50% from -3 to 13 dBm, 3.5 V maximum DC voltage has been obtained. The overall rectenna array design demonstrates a significantly wide and stable rectification efficiency for DC combining systems above 50% for the entire power density range. While in an RF combining system,

the rectification efficiency curve decline at meanwhile increasing the power density.

In addition to that, the RF combining system achieved narrow band efficiency.

Table 5.1: The Comparison of the proposed rectenna and some related designs

Ref.(year)	Freq. [GHz]	Polari.	DC volt (V)	RF power (dBm) >40%	Max Eff. (%)	combining approach
[57] (2020)	2.45	DLP	-	(-5)-15	70,65	DC and RF
[58] (2019)	0.915	CP	7.5	(-5)-15	90.6	directly
[59] (2020)	2.45	LP	16.5	11-27	73	directly
[30] (2018)	at 2.45	LP	-	(-6)-17.5	82.5,80.7	directly
[16] (2020)	at 2.45	CP	-	(-3)-20	50	directly
[60] (2018)	2.45	LP	7,1.8, 3.6	-	70, 73, 75	DC by 3 ways
<b>Our work</b>	<b>2.4</b>	<b>CP</b>	<b>6.6</b> <b>5</b> <b>5.5</b> <b>6</b>	<b>(-3)-18.5</b> <b>, (-18)-16</b> <b>(-14)-17</b> <b>(-3)-17</b>	<b>83.7</b> <b>66</b> <b>81.3</b> <b>53</b>	<b>BFN/DC</b> <b>RF</b> <b>Hybrid</b> <b>DC</b>

Huygens circular polarization rectenna has been introduced in [58], 0.915GHz single rectenna composed of spiral line based on Huygens CP antenna connected directly to a high-efficiency single rectifier circuit. Captured Power range from -15 to 15 dBm. 7.5 V was a maximum DC voltage obtained at 15 dBm. The RF-DC efficiency was above 50% along with the range from -5 to 10 dBm.

A simple rectenna compact was reported in [59] at 2.45 GHz and harvested power range from 0 to 27 dBm. A linear polarization antenna is connected directly to the rectifier circuit through the efficient matching circuit. 4 V has been achieved at 15 dBm RF power and the maximum voltage was 15V at 27 dBm. Rectification efficiency above 50% at an input power range from 13 to 27 dBm, maximum rectification efficiency has been achieved was 75% at 21 dBm.

In [30] the rectenna circuit consists of a microstrip antenna to gathering the RF energy. The antenna is connected to the two rectifier circuits for low and high power, the input power range from -20 to 20 dBm. A selectable frequency design was achieved. At 2.45 GHz the rectenna get an RF-DC conversion efficiency of 60% at 15dBm for high power and 48% at the range from 0 to 11 dBm.

CP rectenna with broadband frequency range is investigated in [16] with wide input power range (-15 to 20) dBm. The rectenna proposed consists of the square loop patch antenna connected to the rectifier circuit through a feeding network. The rectifier circuit was utilized the resistance compression network RCN as a matching network. At a maximum power density employed, the rectenna has been achieved a 50% at 2.4 GHz.

A 2x2 rectenna array was presented in [60]. Also, the three configuration approaches have been investigated in order to implement the DC power combining system series, parallel and series-parallel associations. The rectenna element consists of a fractal patch antenna with a rectifier circuit. 2.45 GHz was the operating frequency, the significantly efficient power captured range (-2 to 8) dBm. Series association achieve above 7 V at 8 dBm and rectification efficiency above 50% over the entire input power range. Parallel association achieve above 1.8 V at 8 dBm and rectification efficiency above 50% also over entire input power range. Series-Parallel association has been achieved above 3.6 V at 8 dBm and rectification efficiency above 50% from 2 dBm to 8 dBm.

In this work, CP multi beams rectenna has been introduced. Four combinations strategies RF, DC, hybrid(RF and DC), BFN/DC power combining have been investigated. The rectenna was composed of a square patch antenna array connected to the rectifier circuit based on a single branch impedance compression network as a matching network. For all combining strategies, the voltage has been achieved closed values of around 6 V, 5 V, 5.5 V and 6.6 V for DC, RF, hybrid and BFN/DC power combining, respectively. The maximum rectification efficiency has been achieved by each one of the strategies that were 53%, 66%, 81.3% and 83.7% for DC, RF, hybrid and BFN/DC power combining, respectively.

## CHAPTER 6

### CONCLUSION AND FUTURE WORK

#### 6.1 Conclusion

This thesis focused on wireless energy harvesting radiated from ambient RF sources and used in charging instead of batteries. Two problem statements have been faced with the RF energy harvesting system, first is the location of RF sources, which are usually unknown and time-varying, furthermore ambient RF signals diversity. The second issue is the low power density for available RF power sources. Both problems have been pointed on in this thesis, as an attempt to introduce a contribution to getting a highly efficient RF energy harvester.

Rectenna is a key component for the harvesting system, composed of an antenna and a rectifier circuit. The linear square patch antenna with circular polarization is what gathers the ambient RF EM energy. Four symmetric CP square patch antenna, 9dB gain has been achieved, an axial ratio was lower than 3dB for the entire array with high matching at resonant frequency 2.4GHz. The beamforming network has been investigated, to increase the scan coverage area by generating multi beams instead of a single beam. So, a butler 4x4 matrix configuration has been designed. Four beams have been generated with scan beam angles  $-82^\circ$ ,  $-21.5^\circ$ ,  $21.5^\circ$  and  $82^\circ$  for output ports 1, 2, 3, and 4, respectively.

A rectifier circuit with voltage doubler Schottky diode has been introduced,

which is based on a single branch impedance compression network as a matching circuit. A compression network has been implemented to be achieved matching and compression for impedance variation range to readable as a single value by diodes. The single branch ICN has been merged with diodes. The simulated results exhibited 73.4% rectification efficiency and good matching at 2.4GHz with a range of large-scale input power (-5 to 20)dBm and (400-1400)  $\Omega$  for load resistance. From 5 to 19dBm have above 50% rectification efficiency. Mathematical models for voltage doubler rectifier circuits and a single branch impedance compression network had been introduced in this thesis. To obtain more enhancement on ICN circuit design. The particle swarm optimization PSO algorithm has been proposed to look forward to maximum leveraging from ICN to get great performance. By using the PSO algorithm the dimension of the ICN implemented have been optimized. As expected, performance after using the ICN optimized, the rectification efficiency reaches 76%, in addition to enhancement in the matching. The Rectifier adopted in this work, has a smaller size, compared to the previous related work, so that it reaches 8.86x4.3x0.15mm<sup>3</sup>.

This thesis introduced four rectenna circuits that are able to harvest RF signals with high gain, circular polarization. To present a completed rectenna design. Various incorporation strategies are appropriated, for different input power range. For instance, rectenna with RF combining strategy and rectenna with hybrid combining strategy exhibited wide rectification efficiency above of > 40% at an input power range from -18 to 17 dBm. While rectenna with DC combining strategy and rectenna with BFN/DC combining strategy suitable for power range from 0 to 20 dBm with rectification efficiency above of > 40% along with the input power range.

## 6.2 Future Work

1. Build single rectifiers with very lower input power less than -10dBm to increase the harvested power.
2. Design single rectifiers with multi band or broadband operating frequency to increase the harvested power.
3. Develop a highly symmetric a passive beam forming network.
4. Miniaturize the butler matrix designed in this work to be low profile.
5. The coverage area can be greater by developing a symmetric 8X8 butler matrix to obtain 8 beams to scan the antenna view angle.
6. Miniaturize the size of the antenna designed or adopting the planar method in the design of the array.
7. Design antenna array with multi-band or broadband operating frequency to increase the harvested power.
8. Adopt the series DC power combining system to arrange the rectenna array.
9. Design multi-substrate rectenna design to build low profile rectenna for RF energy harvesting system.

## BIBLIOGRAPHY

- [1] W. C. Brown. (1977). Electronic and mechanical improvement of the receiving terminal of a free-space microwave power transmission system. *NASA Sti/recon Technical Report N*, vol. 77, p. 31613.
- [2] N. Shinohara. (2011). Power without wires. *IEEE Microwave magazine*, vol. 12, no. 7, pp. S64–S73.
- [3] A. Gulagi, M. Alcanzare, D. Bogdanov, E. Esparcia Jr, J. Ocon, and C. Breyer. (2021). Transition pathway towards 100% renewable energy across the sectors of power, heat, transport, and desalination for the philippines. *Renewable and Sustainable Energy Reviews*, vol. 144, p. 110934.
- [4] A. Triviño, J. González, and J. Aguado. (2021). Wireless power transfer technologies applied to electric vehicles: A review. *energies 2021*, 14, 1547.
- [5] J. Chen, C. W. Yu, and W. Ouyang. (2020). Efficient wireless charging pad deployment in wireless rechargeable sensor networks. *IEEE Access*, vol. 8, pp. 39056–39077.
- [6] C. R. Valenta and G. D. Durgin. (2014). Harvesting wireless power: Survey of energy-harvester conversion efficiency in far-field, wireless power transfer systems. *IEEE Microwave Magazine*, vol. 15, no. 4, pp. 108–120.
- [7] S. Cao and J. Li. (2017). A survey on ambient energy sources and harvesting methods for structural health monitoring applications. *Advances in Mechanical Engineering*, vol. 9, no. 4, p. 1687814017696210.

- [8] M. Piñuela, P. D. Mitcheson, and S. Lucyszyn. (2013). Ambient rf energy harvesting in urban and semi-urban environments. *IEEE Transactions on microwave theory and techniques*, vol. 61, no. 7, pp. 2715–2726.
- [9] V. Talla, B. Kellogg, B. Ransford, S. Naderiparizi, S. Gollakota, and J. R. Smith. (2015). Powering the next billion devices with wi-fi. *Proceedings of the 11th ACM Conference on Emerging Networking Experiments and Technologies*, pp. 1–13.
- [10] Song, C., Huang, Y., Zhou, J., Yuan, S., Xu, Q., and Carter, P. (2015). A broadband efficient rectenna array for wireless energy harvesting. In *2015 9th European Conference on Antennas and Propagation (EuCAP)*, pages 1–5. IEEE.
- [11] Shrestha, S., Noh, S.-K., and Choi, D.-Y. (2013). Comparative study of antenna designs for rf energy harvesting. *International Journal of Antennas and Propagation*, 2013.
- [12] Shi, Y., Fan, Y., Li, Y., Yang, L., and Wang, M. (2018). An efficient broadband slotted rectenna for wireless power transfer at lte band. *IEEE transactions on Antennas and Propagation*, 67(2):814–822.
- [13] Sun, H., Guo, Y.-x., He, M., and Zhong, Z. (2013). A dual-band rectenna using broadband yagi antenna array for ambient rf power harvesting. *IEEE Antennas and Wireless Propagation Letters*, 12:918–921.
- [14] Fakharian, M. M. (2020). A wideband rectenna using high gain fractal planar monopole antenna array for rf energy scavenging. *International Journal of Antennas and Propagation*, 2020.

- [15] Shen, S., Zhang, Y., Chiu, C.-Y., and Murch, R. (2019). A triple-band high-gain multibeam ambient rf energy harvesting system utilizing hybrid combining. *IEEE Transactions on Industrial Electronics*, 67(11):9215–9226.
- [16] Du, Z.-X., Bo, S. F., Cao, Y. F., Ou, J.-H., and Zhang, X. Y. (2020). Broadband circularly polarized rectenna with wide dynamic-power-range for efficient wireless power transfer. *IEEE Access*, 8:80561–80571.
- [17] Maddio, S. (2015). A compact wideband circularly polarized antenna array for *c*-band applications. *IEEE Antennas and Wireless Propagation Letters*, 14:1081–1084.
- [18] Song, C., Huang, Y., Carter, P., Zhou, J., Yuan, S., Xu, Q., and Kod, M. (2016). A novel six-band dual cp rectenna using improved impedance matching technique for ambient rf energy harvesting. *IEEE Transactions on Antennas and Propagation*, 64(7):3160–3171.
- [19] Fabiani, B. and Nascimento, D. (2016). Circularly-polarized antenna array for beam steering. In *2016 IEEE International Symposium on Antennas and Propagation (APSURSI)*, pages 737–738. IEEE.
- [20] Alam, S., Surjati, I., Ningsih, Y. K., Sari, L., Syukriati, E., and Safitri, A. (2019). Design of truncated microstrip antenna with array  $4 \times 2$  for microwave radio communication. In *2019 IEEE Conference on Antenna Measurements & Applications (CAMA)*, pages 1–4. IEEE.
- [21] Zou, Y., Li, H., Xue, Y., and Sun, B. (2019). A high-gain compact circularly polarized microstrip array antenna with simplified feed network. *International Journal of RF and Microwave Computer-Aided Engineering*, 29(12):e21964.

- [22] Ren, H., Li, P., Gu, Y., and Arigong, B. (2020). Phase shifter-relaxed and control-relaxed continuous steering multiple beamforming  $4 \times 4$  butler matrix phased array. *IEEE Transactions on Circuits and Systems I: Regular Papers*, 67(12):5031–5039.
- [23] Vandelle, E., Doan, P. L., Bui, D., Vuong, T., Ardila, G., Wu, K., and Hemour, S. (2017). High gain isotropic rectenna. In *2017 IEEE Wireless Power Transfer Conference (WPTC)*, pages 1–4. IEEE.
- [24] Han, K., Li, W., and Liu, Y. (2019). Flexible phase difference of  $4 \times 4$  butler matrix without phase-shifters and crossovers. *International Journal of Antennas and Propagation*, 2019.
- [25] Ren, H., Shao, J., Zhou, R., Arigong, B., and Zhang, H. (2014). Compact phased array antenna system based on dual-band operations. *Microwave and Optical Technology Letters*, 56(6):1391–1396.
- [26] Shen, S., Chiu, C.-Y., and Murch, R. D. (2017). A dual-port triple-band l-probe microstrip patch rectenna for ambient rf energy harvesting. *IEEE Antennas and Wireless Propagation Letters*, 16:3071–3074.
- [27] He, Z. and Liu, C. (2020). A compact high-efficiency broadband rectifier with a wide dynamic range of input power for energy harvesting. *IEEE Microwave and Wireless Components Letters*, 30(4):433–436.
- [28] Song, C., Huang, Y., Zhou, J., and Carter, P. (2017). Improved ultrawideband rectennas using hybrid resistance compression technique. *IEEE Transactions on Antennas and Propagation*, 65(4):2057–2062.
- [29] Xiao, Y. Y., Du, Z.-X., and Zhang, X. Y. (2018). High-efficiency rectifier

- with wide input power range based on power recycling. *IEEE Transactions on Circuits and Systems II: Express Briefs*, 65(6):744–748.
- [30] Song, C., Huang, Y., Carter, P., Zhou, J., Joseph, S. D., and Li, G. (2018). Novel compact and broadband frequency-selectable rectennas for a wide input-power and load impedance range. *IEEE Transactions on Antennas and Propagation*, 66(7):3306–3316.
- [31] Costantine, J., Eid, A., Abdallah, M., Tawk, Y., and Ramadan, A. (2017). A load independent tapered rf harvester. *IEEE Microwave and Wireless Components Letters*, 27(10):933–935.
- [32] Zheng, S. Y., Wang, S. H., Leung, K. W., Chan, W. S., and Xia, M. H. (2019). A high-efficiency rectifier with ultra-wide input power range based on cooperative structure. *IEEE Transactions on Microwave Theory and Techniques*, 67(11):4524–4533.
- [33] Lu, P., Song, C., and Huang, K. M. (2020). A compact rectenna design with wide input power range for wireless power transfer. *IEEE Transactions on Power Electronics*, 35(7):6705–6710.
- [34] Muhammad, S., Jiat Tiang, J., Kin Wong, S., Iqbal, A., Alibakhshikenari, M., and Limiti, E. (2020). Compact rectifier circuit design for harvesting gsm/900 ambient energy. *Electronics*, 9(10):1614.
- [35] Han, Y., Leitermann, O., Jackson, D. A., Rivas, J. M., and Perreault, D. J. (2007). Resistance compression networks for radio-frequency power conversion. *IEEE Transactions on Power Electronics*, 22(1):41–53.
- [36] Niotaki, K., Georgiadis, A., Collado, A., and Vardakas, J. S. (2014). Dual-

- band resistance compression networks for improved rectifier performance. *IEEE Transactions on Microwave Theory and Techniques*, 62(12):3512–3521.
- [37] Du, Z.-X. and Zhang, X. Y. (2017). High-efficiency single-and dual-band rectifiers using a complex impedance compression network for wireless power transfer. *IEEE Transactions on industrial electronics*, 65(6):5012–5022.
- [38] Nagaveni, S., Kaddi, P., Khandekar, A., and Dutta, A. (2020). Resistance compression dual-band differential cmos rf energy harvester under modulated signal excitation. *IEEE Transactions on Circuits and Systems I: Regular Papers*, 67(11):4053–4062.
- [39] Zhang, X. Y., Ou, J.-H., and Huang, M. (2020). High-efficiency rectifiers with wide input power range and application on powering wireless sensors. In *2020 14th European Conference on Antennas and Propagation (EuCAP)*, pages 1–5. IEEE.
- [40] Li, W. and Zhang, W. (2018). The single-branch resistance compression network based on transmission line. In *2018 International Conference on Microwave and Millimeter Wave Technology (ICMMT)*, pages 1–3. IEEE.
- [41] Xu, J. and Ricketts, D. S. (2013). An efficient, watt-level microwave rectifier using an impedance compression network (icn) with applications in outphasing energy recovery systems. *IEEE microwave and wireless components letters*, 23(10):542–544.
- [42] Xiao, Y. Y., Ou, J.-H., Du, Z.-X., Zhang, X. Y., Che, W., and Xue, Q. (2019). Compact microwave rectifier with wide input power dynamic range based on integrated impedance compression network. *IEEE Access*, 7:151878–151887.

- [43] Balanis, C. A. (2015). *Antenna theory: analysis and design*. John wiley & sons.
- [44] Huang, Y. and Boyle, K. (2008). *Antennas: from theory to practice*. John Wiley & Sons.
- [45] Vallappil, A. K., Rahim, M. K. A., Khawaja, B. A., Murad, N. A., and Gajibo, M. M. (2020). Butler matrix based beamforming networks for phased array antenna systems: A comprehensive review and future directions for 5g applications. *IEEE Access*.
- [46] Pozar, D. M. (2011). *Microwave engineering*. John wiley & sons.
- [47] Gandomi, A. H., Yang, X.-S., Talatahari, S., and Alavi, A. H. (2013). *Meta-heuristic applications in structures and infrastructures*. Newnes.
- [48] Kennedy, J. and Eberhart, R. (1995). Particle swarm optimization. In *Proceedings of ICNN'95-international conference on neural networks*, volume 4, pages 1942–1948. IEEE.
- [49] Jiang, J.-R., Chen, Y.-C., and Lin, T.-Y. (2018). Particle swarm optimization for charger deployment in wireless rechargeable sensor networks. *International Journal of Parallel, Emergent and Distributed Systems*, pages 1–16.
- [50] Mirzaeinia, A., Mirzaeinia, M., Bradfield, Q. A., Bradley, S., and Hassanalian, M. (2019). Particle swarm optimization for wireless charging of swarming drones through ambient radio frequencies. In *AIAA Propulsion and Energy 2019 Forum*, page 4463.
- [51] Ababneh, M. M., Perez, S., and Thomas, S. (2017). Optimized power man-

- agement circuit for rf energy harvesting system. In *2017 IEEE 18th Wireless and Microwave Technology Conference (WAMICON)*, pages 1–4. IEEE.
- [52] Luo, Q., Gao, S. S., Liu, W., and Gu, C. (2019). *Low-cost smart antennas*. John Wiley & Sons.
- [53] Yoo, T.-W. and Chang, K. (1992). Theoretical and experimental development of 10 and 35 ghz rectennas. *IEEE Transactions on Microwave Theory and Techniques*, 40(6):1259–1266.
- [54] Lin, Q. W. and Zhang, X. Y. (2016). Differential rectifier using resistance compression network for improving efficiency over extended input power range. *IEEE Transactions on Microwave Theory and Techniques*, 64(9):2943–2954.
- [55] Waugh, R. W. (1999). Choosing the right diode for your agc detector. *APPLIED MICROWAVE AND WIRELESS*, 11:48–53.
- [56] Lee, D.-J., Lee, S.-J., Hwang, I.-J., Lee, W.-S., and Yu, J.-W. (2017). Hybrid power combining rectenna array for wide incident angle coverage in rf energy transfer. *IEEE Transactions on Microwave Theory and Techniques*, 65(9):3409–3418.
- [57] Sun, H., He, H., and Huang, J. (2020). Polarization-insensitive rectenna arrays with different power combining strategies. *IEEE Antennas and Wireless Propagation Letters*, 19(3):492–496.
- [58] Lin, W. and Ziolkowski, R. W. (2019). Electrically small huygens cp rectenna with a driven loop element maximizes its wireless power transfer efficiency. *IEEE Transactions on Antennas and Propagation*, 68(1):540–545.

- [59] Lin, D.-B., Chou, H.-T., and Chou, J.-H. (2020). Antenna pairing for highly efficient wireless power transmission in the reactive near-field region based on mutual coupled impedance compensation. *IET Microwaves, Antennas & Propagation*, 14(1):60–65.
- [60] Chuma, E. L., Iano, Y., Costa, M. S., Manera, L. T., et al. (2018). A compact-integrated reconfigurable rectenna array for rf power harvesting with a practical physical structure. *Progress in electromagnetics research M*.

## APPENDIX - A

By substitute the equation(4.15) into equations(4.9) and (4.10), and solving the integration for diode1:

$$I_{d1r} = \frac{1}{\pi R_s} \left[ \int_{-(\pi-\theta)}^{\pi-\theta} (-R_s C_j w V_{in}) \sin(\theta) \cos(\theta) d\theta + \int_{\pi-\theta}^{\pi+\theta} (V_{in} + V_f) \cos(\theta) d\theta \right] \quad (6.1)$$

$$I_{d1r} = \frac{C_j w V_{in}}{\pi} [\cos(2\theta)] \quad (6.2)$$

$$I_{d1i} = \frac{1}{\pi R_s} \left[ \int_{-(\pi-\theta)}^{\pi-\theta} (-R_s C_j w V_{in}) \sin(\theta) \sin(\theta) d\theta + \int_{\pi-\theta}^{\pi+\theta} (V_{in} + V_f) \sin(\theta) d\theta \right] \quad (6.3)$$

$$I_{d1i} = \frac{C_j w V_{in}}{\pi} \left[ \pi - \theta + \frac{\sin(2\theta)}{2} \right] \quad (6.4)$$

The current through diode1 given by following equation:

$$I_{d1} = \frac{C_j w V_{in}}{\pi} [\cos(2\theta)] - j \frac{C_j w V_{in}}{\pi} \left[ \pi - \theta + \frac{\sin(2\theta)}{2} \right] \quad (6.5)$$

By substitute the equation(4.15) into equations(4.12) and (4.13), and solving the integration for diode2:

$$I_{d2r} = \frac{1}{\pi R_s} \left[ \int_{\theta}^{2\pi-\theta} (-R_s C_j w V_{in}) \sin(\theta) \cos(\theta) d\theta + \int_{-\theta}^{\theta} (V_{in} - V_f) \cos(\theta) d\theta \right] \quad (6.6)$$

$$I_{d2r} = \frac{(V_{in} - V_f)}{\pi R_s} [2\sin(\theta)] \quad (6.7)$$

$$I_{d2i} = \frac{1}{\pi R_s} \left[ \int_{\theta}^{2\pi-\theta} (-R_s C_j w V_{in}) \sin(\theta) \sin(\theta) d\theta + \int_{-\theta}^{\theta} (V_{in} - V_f) \sin(\theta) d\theta \right] \quad (6.8)$$

$$I_{d2i} = \frac{C_j w V_{in}}{\pi} \left[ \pi - \theta + \frac{\sin(2\theta)}{2} \right] \quad (6.9)$$

The current through diode2 given by following equation:

$$I_{d2} = \frac{(V_{in} - V_f)}{\pi R_s} [2\sin(\theta)] - j \frac{C_j w V_{in}}{\pi} [\pi - \theta + \frac{\sin(2\theta)}{2}] \quad (6.10)$$

When substitution the equations(6.5) and (6.10) into equation(4.8), after that into equation (4.6). The input impedance equation can written as following:

$$Z_D = \frac{\pi R_s}{R_s C_j w \cos(2\theta) + 2\sin(\theta)(1 - \frac{V_f}{V_{in}}) + j(R_s C_j w)(2\pi - 2\theta + \sin(2\theta))} \quad (6.11)$$

Depending on the input voltage, the  $\theta$  is variable and can given by the following equation:

$$\frac{V_f}{V_{in}} = \cos(\theta) + \theta \cos(\theta) - \sin(\theta) \quad (6.12)$$

Now, when substitute the equation(6.12) into equation(6.11) and simplification can obtained the equation(4.16).

## APPENDIX - B

By virtue of equation(4.24) first will be determine the  $Z_1||Z_2$  and given as following:

$$\frac{jZ_{o1}\tan(\theta_2) * (-j)Z_{o2}\tan(\theta_2)}{jZ_{o1}\tan(\theta_2) - jZ_{o2}\tan(\theta_2)} \quad (6.13)$$

With the parallel relation between  $Z_3$  and equation(6.13):

$$Z_{in} = \frac{j * Z_{o1} * Z_{o2} * Z_{o3} * \tan(\theta_2) * (Z_D + Z_{o3} * \tan(\theta_3))}{(Z_{o1} - Z_{o2}) * (Z_{o3} + j * Z_D * \tan(\theta_3)) * \left( \frac{Z_{o3} * (Z_D + Z_{o3} * \tan(\theta_3))}{Z_{o3} + j * Z_D * \tan(\theta_3)} + \frac{j * Z_{o1} * Z_{o2} * \tan(\theta_2)}{Z_{o1} - Z_{o2}} \right)} \quad (6.14)$$

By simplification the above equation can get a equation(4.25)

## APPENDIX - C

Matlab code adopted for the particle swarm optimization algorithm

```

function Zin = Inputimpedance(input)
    M = csvread('zdwithouticn.csv');
    RL=M(1:26,2);
    XL=M(1:26,3);
    zd= RL+1j*XL;
    D2= input(1);
    D3= input(2);
    zo1=input(3);
    zo2=input(4);
    zo3=input(5);
    A= (zo1.*zo2.*zo3.*tan(D2).*(zd + zo3.*tan(D3))*li);
    B= (zo3 + zd.*tan(D3)*li).*(zo1 - zo2);
    C= ((zo3.*(zd + zo3.*tan(D3)))./(zo3 + zd.*tan(D3)*li)...
        +(zo1.*zo2.*tan(D2)*li)./(zo1 - zo2)) ;
    if ((C>= 50-1i*1) && (C<= 50.9+1i*1))
        Zin=A./(B.*C) ;
    else
        Zin=(A)./(1.9.*B.*(C+75));
    end
end

%Problem Definiton
close all
FitnessFunction =@(input) eff(input); % Cost Function
nVar = 5; % Number of Unknown (Decision) Variables
VarSize = [1 nVar]; % Matrix Size of Decision Variables
%Parameters of PSO
MaxIt = 200; % Maximum Number of Iterations
nPop = 50; % Population Size (Swarm Size)
w = 1; % Intertia Coefficient velocity of particals
wdamp = 0.99 ; % Damping Ratio of Inertia Coefficient
c1 =2 ; % Personal Acceleration Coefficient
c2 =2; % Social Acceleration Coefficient
ShowIterInfo =true; % change this value has effect
%Initialization
% The Particle Template
empty_particle.Position = [];
empty_particle.Velocity = [];
empty_particle.Cost = [];
empty_particle.Best.Position= [];
empty_particle.Best.Cost= [];
% Create Population Array
particle = repmat(empty_particle, nPop, 1);
% Initialize Global Best
GlobalBest.Cost = inf;

```

```

% Initialize Population Members
for i=1:nPop
    % Generate Random Solution
    for j = 1:nVar
        if j==1
            varmin=21; varmax=24;
        elseif j==2
            varmin=30; varmax=33.5;
        elseif j==3
            varmin=31.5; varmax=40;
        elseif j==4
            varmin=48.5; varmax=51;
        else
            varmin=18; varmax=19.5;
        end
    end
    Position = unifrnd(varmin,varmax); % particle generator
    r(j)=Position;
end

particle(i).Position = r;
% Initialize Velocity
particle(i).Velocity = zeros(VarSize); % initial velocity
% Evaluation each particle
particle(i).Cost = FitnessFunction(particle(i).Position);
% Update the Personal Best
particle(i).Best.Position = particle(i).Position;
particle(i).Best.Cost = particle(i).Cost;
% Update Global Best
if particle(i).Best.Cost < GlobalBest.Cost
    GlobalBest = particle(i).Best;
end
end
disp(num2str(GlobalBest.Cost(:,1)))
% Array to Hold Best Cost Value on Each Iteration
BestCosts = zeros(MaxIt, 1);

% Main Loop of PSO
for it=1:MaxIt
    for i=1:nPop
        % Update Velocity first equation to update roots
        particle(i).Velocity = w*particle(i).Velocity ...
+ c1*rand(VarSize).*(particle(i).Best.Position - particle(i).Position) ...
+ c2*rand(VarSize).*(GlobalBest.Position - particle(i).Position);
        %Apply Lower and Upper Bound Limits
        for j = 1:nVar
            if j==1
                varmin=21; varmax=24;
            elseif j==2
                varmin=30; varmax=33.5;
            elseif j==3
                varmin=31; varmax=40;
            elseif j==4
                varmin=48.5; varmax=51;
            else
                varmin=18; varmax=19.5;
            end
            %Apply Bound Limits
            MaxVelocity(j) = 0.2*(varmax-varmin);
            MinVelocity(j) = -MaxVelocity(j);
        end
    end
end

```

```

% Apply Velocity Limits
particle(i).Velocity = max(particle(i).Velocity, MinVelocity);
particle(i).Velocity = min(particle(i).Velocity, MaxVelocity);
% Update Position
particle(i).Position = particle(i).Position + particle(i).Velocity;
for j = 1:nVar
    if j==1
        varmin=21; varmax=24;
    elseif j==2
        varmin=30; varmax=33.5;
    elseif j==3
        varmin=31; varmax=40;
    elseif j==4
        varmin=48.5; varmax=51;
    else
        varmin=18; varmax=19.5;
    end
    in(j)=varmin;
    ax(j)= varmax;
end
particle(i).Position = max(particle(i).Position, in);
particle(i).Position = min(particle(i).Position, ax);
% Evaluation
particle(i).Cost = FitnessFunction(particle(i).Position);

% Update Personal Best
if particle(i).Cost > particle(i).Best.Cost
    particle(i).Best.Position = particle(i).Position;
    particle(i).Best.Cost = particle(i).Cost;
% Update Global Best
    if particle(i).Best.Cost > GlobalBest.Cost
        GlobalBest = particle(i).Best;
    end
end
end

end
% Store the Best Cost Value
BestCosts(it,1:29)= GlobalBest.Cost;
if it == 10
    figure
    hold on
    plot( particle(i).Cost)
    legend('1')
end
if it == 30
    figure
    plot( particle(i).Cost)
end
if it == 50
    figure
    plot( particle(i).Cost)
end
end

```

```

        if it == 70
            figure
            plot( particle(i).Cost)
        end
        if it == 100
            figure(2)
            plot( particle(i).Cost)
        end
        if it == 200
            figure(2)
            plot( particle(i).Cost)
        end
        grid on
        end
        % Display Iteration Information
        if ShowIterInfo
            disp(['Iteration ' num2str(it) ': Best Cost = ' num2str(BestCosts(it))]);
        end
        % Damping Inertia Coefficient
        w = w* wdamp;
    end
    out.pop = particle;
    out.BestSol = GlobalBest;
    out.BestCosts =BestCosts;
    disp(num2str(GlobalBest.Cost(1:29,1)))

```

## LIST OF PUBLICATIONS

1. Aliwi, S., Al-Khafaji, N., Al-Battat, H. (2021, August). a single-branch impedance compression network (icn) optimized by particle swarm optimization algorithm for rf energy harvesting system. In Journal of Physics: Conference Series (Vol. 1973, No. 1, p. 012080). IOP Publishing.
2. Sarah Aliwi, Nasr Al-Khafaji, Hayder Al-Battat. "A Rectifier Circuit Design Based on a Single Branch ICN Optimized by Particle Swarm Optimization Algorithm for RF Energy Harvesting Systems ". The manuscript was accepted in the Al-Furat Journal of Innovation in Electronic and Computer Engineering (FJIECE).
3. Sarah Aliwi, Nasr Al-Khafaji, Hayder Al-Battat. "Multi Beams Circular Polarization Antenna Array for RF Energy Harvesting System ". The manuscript was accepted for Possible publication in AIP Conference Proceedings (ISSN: 0094-243X, 1551-7616, SCOPUS, WOS, Indexed).

## الخلاصة

زيادة عدد الأجهزة الإلكترونية المتصلة بالإنترنت أو تلك التي سيتم توصيلها في المستقبل تفرض قيودًا وتحديات عندما يرغب المصممون في تطوير البنية التحتية. أحد هذه التحديات المهمة هو كيفية تشغيل كل هذه الأجهزة. في الوقت الحاضر ، يبذل الباحثون قصارى جهدهم لجعل الأجهزة الإلكترونية تعمل باستهلاك أقل للطاقة وبتكلفة منخفضة. يعد نظام حصاد الطاقة تقنية واعدة لتحقيق أجهزة بدون بطارية، مما يعني تمكين الأجهزة من أن تكون أكثر إحكاما عند إزالة ضرورة البطاريات التي يجب صيانتها أو استبدالها بشكل دوري. يعتمد حصاد طاقة الترددات اللاسلكية المحيطة على جمع الطاقة من مصادر طاقة الترددات اللاسلكية المحيطة (الخارجية). مع هذا النوع من الطاقة ، يكون موقع مصدر الطاقة غير معروف و مقدار هذه الطاقة في الفضاء منخفضًا جدًا. وبالتالي ، لتصميم حصادات طاقة RF ذات كفاءة ، يجب أخذ هذين التحديين في الاعتبار. التحدي الأول، موقع مصادر طاقة التردد اللاسلكي واتجاهها. تم اعتماد شبكات RF متعددة الحزم (أي نوع من تشكيل الحزمة) BFNs لتغطية معظم الاتجاهات في الفضاء ، بينما تُستخدم الهوائيات ذات إمكانات الاستقطاب الدائري للتغلب على اتجاهات مصادر طاقة التردد اللاسلكي. بعد ذلك ، تركز هذه الرسالة على حل المشكلة الثانية وهي استخدام العديد من حصادات طاقة التردد اللاسلكي في شكل مصفوفة تسمى مصفوفة الريكتينا الحل للتحدي الثاني. يؤدي هذا إلى زيادة مقدار الطاقة المسلمة إلى كل مقوم واحد ، حيث تهيمن مشاكل اللاخطية لذلك قام المؤلفون بحل هذه المشكلة باستخدام شبكة ضغط المعاوقة ICN ، يؤدي ICN الخاص بنا وظيفتين ليس فقط ضغط المعاوقة ولكن أيضًا مطابقة المعاوقة. تم تصميم المقومات المزودة بشبكات ICN وتحليلها وتحسينها باستخدام خوارزمية PSO لتحسين حشد الجسيمات. وسيتم توصيل المقومات بـ منافذ الإخراج للهوائي. نتيجة لذلك ، سيكون هناك العديد من مصادر طاقة التيار المستمر. لتجميع قوى التيار المستمر من تلك المنافذ المتعددة ، هناك العديد من الطرق للقيام بذلك مثل تقنيات تجميع الطاقة DC و RF و Hybrid(RF/DC) و BFNs/DC. تقدم كل تقنية دمج العديد من الفوائد على غيرها.



نهج جديد لنظام حصاد الاشارات الراديوية عالية القدرة بالاعتماد على تقنية تشكيل  
الحزم

الرسالة  
مقدمه الى قسم هندسة تقنيات الاتصالات كجزء من متطلبات نيل درجه الماجستير في  
هندسة الاتصالات

تقدمت بها  
سارة محمد عليوي

أشرف  
الأستاذ المساعد الدكتور

حيدر جواد محمد

2021





جمهورية العراق  
وزارة التعليم العالي والبحث العلمي  
جامعة الفرات الاوسط التقنية  
الكلية التقنية الهندسية نجف

نهج جديد لنظام حصاد الاشارات الراديوية عالية القدرة  
بالاعتماد على تقنية تشكيل الحزم

سارة محمد عليوي

ماجستير في هندسة تقنيات الاتصالات

2021